Site Specific Radar Coverage and Land Clutter Modelling

Prepared by:

Sulayman Salie

SLXSUL003

Prepared for:

Professor Michael Raymond Inggs

Department of Electrical Engineering

University of Cape Town

April 2016

A minor dissertation submitted to the Department of Electrical Engineering, University of Cape Town, in partial fulfilment of the requirements for the degree of

Master of Engineering Specialising in *Radar and Electronic Defence*

Declaration

I know the meaning of plagiarism and declare that all the work in the document, save for that which is properly acknowledged, is my own. It is being submitted for the degree of Master of Engineering Specialising in Radar and Electronic Defence in the University of Cape Town. It has not been submitted before for any degree or examination in any other university.

Signature of Author ..... signature removed .....

Cape Town

April 2016

Abstract

The objectives of this minor dissertation were to investigate relevant theory, models and processes required for the development of a site specific radar coverage and land clutter modelling tool.

Various sources of digital elevation model (DEM) and land cover (LC) data were investigated. It was found that the ASTER GDEM and SRTM 30 m DEM datasets can be used to characterise land topography for all intended areas of interest. It was also found that two LC datasets, namely the National Land Cover 2009, and GlobeLand30 m data sources can be used to characterise land cover for all intended areas of interest. For each terrain type found in the GlobeLand30 or NLC 2009 datasets, a decision was made as to which of the terrain types for each land clutter model matches the land cover data terrain type the closest. These classifications were presented in the form of tables. It was concluded that the SRTM 30 m DEM dataset and the GlobeLand30 LC dataset should be used as they are currently the highest quality DEM and LC datasets that are freely available that covers all intended areas of interest.

Numerous monostatic land clutter models exist in literature that address specific cases of clutter types and behaviours. Nine such land clutter models were investigated. Measured land clutter data collected over various terrain types in the Western Cape region of South Africa are compared to simulated backscatter data from these land clutter models. From insights gained from the literature study as well as the analysis of these comparisons, a classification was made on each model's compatibility and validity for different grazing angles and frequency ranges. A classification table was presented indicating the appropriate land clutter models to use in order of their validity, with respect to different grazing angle regions and frequency ranges. It was found that out of the nine models investigated, only the land clutter models developed by Billingsley, Ulaby and Dobson and Mediavalli

can be classified and used as a high validity model. This investigation identified that for many grazing angle and frequency ranges of interest, only lower validity models exist, and in some cases no appropriate model exists.

It was concluded that the validity of such a tool is highly dependent on the validity of the data and specific elements of the land clutter model used.

Acknowledgements

First of all, I thank Allah S.W.T for giving me the strength and ability to complete this research study.

I would like to thank ARMSCOR for funding the larger part of this research study.

CSIR for providing me with the time to work on my research and use of their resources.

My supervisor and co-supervisor Professor Michael Inggs and Johan Smit for their excellent assistance and guidance throughout my research.

My wonderful wife Ameera Gangat, family, and friends for their belief in me, encouragement and support.

Contents

Declaration i

Abstract ii

Acknowledgements iv

List of Symbols xv

Nomenclature xviii

1 Introduction 1

1.1 Subject and Motivation 1

1.2 Background to the Study 2

1.3 Objectives and Aim 4

1.4 Scope and Limitations 5

1.5 Document Outline and Overview 5

2 Theoretical Overview 8

2.1 Radar Propagation 8

2.1.1 Wave Propagation Through the Earth's Atmosphere and Atmospheric Propagation Effects 8

2.1.2 Refraction 10

2.1.2.1 Refractive Conditions 11
2.1.2.2 Standard and Normal Conditions 12
2.1.2.3 Subrefractive Conditions 12
2.1.2.4 Superrefractive Conditions 12
2.1.2.5 Trapping Conditions 12
2.1.2.6 Diffraction 13
2.1.3 Radar Horizon and Earth Curvature Effects 13
2.2 Radar Coverage 16
2.2.1 Flat Earth and Spherical Earth 16
2.2.2 Shadowing Effects by Land Terrain and Cover 17
2.2.3 Optimisation of Radar Deployment Sites 17
2.3 Pattern Propagation Factor, F 18
2.4 Radar Clutter 19
2.4.1 Radar Land Clutter 19
2.4.2 Backscatter Coefficient σ° 20
2.4.3 Backscatter Coefficient σ° Dependencies 21
2.4.3.1 Frequency / Wavelength 22
2.4.3.2 Incident, Depression and Grazing Angle 22
2.4.3.3 Polarisation 24
2.4.3.4 Resolution 25
2.4.3.5 Surface Roughness and Moisture Content 26
2.4.3.6 Land Topography and Relief 26
2.4.3.7 Complex Dielectric Constant 27
2.4.3.8 Type of Terrain / Land Cover 27

2.4.3.9 Spatial and Temporal Statistics 27
2.4.4 Land Clutter Modeling 29
2.4.4.1 Standard PDF's Used to Model Land Clutter Variation . 29
2.4.4.2 Empirically Derived Land Clutter Models 32
2.4.4.3 Mathematically Derived Land Clutter Models 33
2.5 GIS Data 33
2.5.1 Digital Elevation Model Data 33
2.5.2 Earth References, Geoids and Ellipsoids 34
2.5.2.1 WGS84 Reference Ellipsoid Model 35
2.5.2.2 EGM96 Reference Geoid Model 35
2.5.2.3 Mean Sea Level (MSL) and Height Above Mean Sea Level (AMSL) 35
2.5.3 Land Cover Data 36
2.6 Chapter Summary 37

3 System Models, Processes and Data **40**

3.1 Land Clutter / Backscatter Coefficient Models 40
3.1.1 Constant Gamma Land Clutter Model 42
3.1.2 Morchin Land Clutter Model 44
3.1.3 Kulemin Land Clutter Model 46
3.1.4 Nathanson Land Clutter Model Tables 47
3.1.5 Georgia Tech Research Institute (GTRI) Land Clutter Model . . . 49
3.1.6 Ulaby and Dobson Land Clutter Model 50
3.1.7 σ° Generating Function Land Clutter Model 55
3.1.8 Adapted GTRI Sea Clutter Model 58

3.1.9 Billingsley Land Clutter Model 61
3.1.10 Land Clutter Models Discussion and Summary 66
3.2 GIS Data 71
3.2.1 Digital Elevation Model Data 71
3.2.1.1 Shuttle Radar Topography Mission (SRTM) Digital Elevation Model Data 71
3.2.1.2 Advanced Spaceborne Thermal Emission and Reflection Radiometer (ASTER) Global Digital Elevation Model (GDEM) Data 74
3.2.1.3 Digital Terrain Elevation Data (DTED) 75
3.2.1.4 Astrium Data 76
3.2.2 Land Cover Data 77
3.2.2.1 Global Land Cover Data (GlobeLand30) 78
3.2.2.2 South African National Land Cover 1994 (NLC 1994) . 80
3.2.2.3 South African National Land Cover 2000 (NLC 2000) . 80
3.2.2.4 South African National Land Cover 2005 (NLC 2005) . 81
3.2.2.5 South African National Land Cover 2009 (NLC 2009) . 81
3.2.2.6 Global Land Cover (GLC) 2000 83
3.2.2.7 Global Land Cover by National Mapping Organisations (GLCNMO) 84
3.2.2.8 Global Land Cover Share (GLC-Share) 85
3.2.3 GIS Data Discussion and Summary 86
3.3 Simulating the Clutter Scene 87
3.3.1 Clutter Patch Grid Method 87
3.3.2 Radar Coverage 91

3.3.3 Clutter Cell Size, DEM Resolution, and DEM Height Accuracy . 91
3.3.4 Simulating Coherent Radar Returns 94
3.4 Chapter Summary 95

4 Analysis and Results **97**

4.1 Analysis of Land Clutter Models 97
4.1.1 Low Grazing Angle Region 98
4.1.2 Plateau and High Grazing Angle Region 99
4.1.3 Discussion and Summary 104
4.2 Grazing Angle and Frequency Ranges Considered by Land Clutter Models 105
4.2.1 Low Grazing Angle Region 106
4.2.2 Plateau Grazing Angle Region 109
4.2.3 High Grazing Angle Region 109
4.2.4 Discussion and Summary 109
4.3 Linking Land Clutter Models to Land Cover Data 110
4.4 Proposed Site Specific Radar Coverage and Land Clutter Modelling Tool Program Flow 110
4.5 Chapter Summary 114

5 Conclusions, Recommendations and Future Work **116**

5.1 Conclusions and Recommendations 116
5.2 Future Work 122

A Source Code **124**

Bibliography **125**

List of Figures

2.1 Geometry of the earth's atmosphere. 9

2.2 Atmospheric attenuation due to water vapor and gaseous content of the air. 10

2.3 Depiction of the four different types of refractive conditions. 11

2.4 Radar horizon and dead zone. 14

2.5 Grazing angle as a function of range near the horizon for two different effective earth radii values. 15

2.6 Radar horizon for different tower heights, and target heights. 16

2.7 Shadowing effects by land terrain. 17

2.8 Spatial resolution cell for a radar looking at the surface of the earth. . . . 21

2.9 Diagram of : incident, local incident, depression and grazing angle. 23

2.10 General behaviour of σ° as a function of grazing angle. 23

2.11 Theoretical polarisation dependence of the backscatter coefficient for different changing grazing angles. 25

2.12 Forms of surface roughness 26

2.13 Land clutter measurements showing varying values. 28

2.14 Digital elevation model for Setif region in Algeria. 34

2.15 EGM geoid height for earth in metres. 35

2.16 Reference geoid and ellipsoid earth model. 36

2.17 Land cover dataset for Africa developed in the year 2000. 37

3.1 Backscatter coefficient at 10 GHz using the constant gamma land clutter model. 43

3.2 Backscatter coefficient in dB for the various terrain types at 13.8 GHz using the Morchin land clutter model. 45

3.3 Backscatter coefficient at 10 GHz using the Kulemin land clutter model. . 47

3.4 Backscatter coefficient at 10 GHz using the GTRI land clutter model. . . 51

3.5 Backscatter coefficient in dBs for the various terrain types at 10 GHz using the Ulaby and Dobson land clutter model. 54

3.6 Mean reflected energy σ^0 in dBs for the various terrain types at 10 GHz, polarisation HH, using the generating function. 57

3.7 Backscatter at X-band, Polarisation HH, Using the Adapted GTRI Sea Clutter Model. 60

3.8 Spatial resolution cell area, A, from the geometry of land clutter for a surface radar: (a) elevation view, (b) plan view. 63

3.9 Reflected energy $\sigma^0 F^4$ in dBs for the various terrain types at 10 GHz using the Billingsley angle specific land clutter model. 65

3.10 Mean clutter strength versus frequency for all measured terrain types. . . 66

3.11 Interferometric process from the SRTM space shuttle. 72

3.12 NLC 1994 five terrain class land cover map. 80

3.13 NLC 2000 five terrain class land cover map. 81

3.14 NLC 2005 five terrain class land cover map. 82

3.15 NLC 2009 five terrain class land cover map. 83

3.16 GLCNMO land cover map. 85

3.17 GLC-Share land cover map. 86

3.18 DEM for simulated mountainous terrain. 90

3.19 Triangulation process. 90

3.20 Radar coverage using ray tracing process. 92

4.1 Comparison of measured and simulated land clutter map at Brazeau, Alberta Canada. 99

4.2 Average backscatter coefficient $\sigma^{\circ}F^4$ for various terrain types. 100

4.3 Average backscatter coefficient $\sigma^{\circ}F^4$ for terrain types farmland and fynbos compared to land clutter models. 101

4.4 Average backscatter coefficient $\sigma^{\circ}F^4$ for all urban terrain types compared to land clutter models. 102

4.5 RMSE of the measured average backscatter $\sigma^{\circ}F^4$ for and simulated data from land clutter models. 103

4.6 Radar land clutter models frequency and grazing angle ranges and validity. 107

4.7 Radar land clutter models frequency and grazing angle ranges and validity (log scale). 108

List of Tables

2.1 Refractive gradients for the different types of refractive conditions. 13

2.2 Backscatter coefficient σ° dependencies. 22

2.3 Radar frequency bands. 22

3.1 The value of γ for various terrain types. 43

3.2 Morchin land clutter model constant values for various terrains. 45

3.3 Terrain types and constants values for Kulemin land clutter model. 46

3.4 Nathanson land clutter model tables. 48

3.5 Constant values for GTRI Land Clutter model for various terrain types and frequencies. 50

3.6 Valid grazing angle ranges of each terrain type category, for the various frequency bands and polarisations. 55

3.7 GTRI sea state for wind speed and wave height descriptor values. 60

3.8 Billingsley's angle specific land clutter model. 64

3.9 Land clutter models summary. 69

3.10 SRTM dataset characteristics. 73

3.11 Format information for ASTER GDEM DEM and QA files. 74

3.12 DTED levels description. 75

3.13 Elevation datasets currently available from Astrium. 77

3.14 Digital Elevation Model summary. 88

3.15 Land Cover data summary. 89

3.16 Clutter cell sizes and computation times for different DEM data resolutions for 9 km radius coverage area. 93

3.17 Statistics of the calculated grazing angle for each DEM set of different RMSE values. 93

4.1 Land clutter models to use for low, plateau and high grazing angle regions in order of model compatibility and validity. 106

4.2 Linking GlobeLand30 terrain types to Land Clutter model terrain types. . 111

4.3 Linking NLC 2009 terrain types to Land Clutter model terrain types. . . . 112

List of Symbols

A	—	Spatial resolution cell area; Morchin land clutter model constant 1; GTRI land clutter model constant 1
$A_1 - A_3$	—	Kulemin land clutter model constant 1 to 3
A_i	—	Interference factor
A_u	—	Upwind-downwind factor
a_w	—	Weibull shape parameter
A_w	—	Wind speed factor
b	—	Scale parameter for Weibull PDF
B	—	Morchin land clutter model constant 2; GTRI land clutter model constant 2
c	—	Speed of light
C	—	GTRI land clutter model constant 3
D	—	GTRI land clutter model constant 4
D_0	—	Distance from reference point
e^s	—	Partial pressure of water vapor
f	—	Frequency
$f_\circ$	—	Base frequency
F	—	Pattern propagation factor
G	—	Antenna gain
h	—	Height above sea level
h_{av}	—	Average wave height
h_r	—	Tower height
h_t	—	Target height
HH	—	Horizontal-Horizontal polarisation
H_2O	—	Water vapour

HV	—	Horizontal-Vertical polarisation
k	—	Effective earth radius constant; Shape parameter for Weibull PDF
LC	—	Left-hand circular polarisation
L_s	—	System losses
M	—	Modified refractivity; Number of columns
$M_1 - M_3$	—	Ulaby and Dobson land clutter model resultant coefficients for SD function
n	—	Index of refraction
N	—	Refractivity index; Number of samples; Vector length; North; Number of rows
$N''(f)$	—	Imaginary part of the frequency dependent complex refractivity
O_2	—	Oxygen
p	—	Atmosphere's barometric pressure
$P_1 - P_6$	—	Ulaby and Dobson land clutter model constants 1 to 6
P_t	—	Transmit power
P_r	—	Receive power
qw	—	Power factor
r_e,R_e	—	Earth radius
R	—	Target range
R_{eff}	—	Effective earth radius
R_h	—	Distance to radar horizon
RC	—	Right-hand circular polarisation
s	—	Scale parameter for Rayleigh and Log-normal PDF's
S	—	Nathanson land clutter model statistics variable; South
SD	—	Standard deviation
T	—	Absolute temperature
VH	—	Vertical-Horizontal polarisation
v	—	Velocity
VV	—	Vertical-Vertical polarisation
V_w	—	Wind velocity
x	—	longitude; General vector of variables
y	—	latitude
α	—	One way attenuation coefficient; Skewness parameter

β	—	Amplitude term
β_0	—	Morchin land clutter model constant 3
γ	—	Gamma constant for CG specific terrain types; Distribution adjustment term
δ	—	Grazing angle
δ_c	—	Critical grazing angle
$\delta R, \triangle r$	—	Range resolution
$\triangle\theta, \Theta_{3dB}$	—	3 dB azimuth beamwidth
$\triangle E$	—	Elevation drop
θ, Θ	—	Incidence angle
Θ_L	—	Local incident angle
κ	—	Two-way signal attenuation
κ_o	—	Specific attenuation constant for oxygen
κ_w	—	Specific attenuation constant for water
λ	—	Wavelength
μ	—	Shape parameter for Log-normal PDF; Morchin land clutter model surface roughness
σ	—	Radar cross section
σ°	—	Backscatter coefficient
σ_c	—	Critical angle
σ_h	—	RMS height of surface irregularities; RMS surface roughness
$\overline{\sigma^\circ_W}$	—	Weibull mean clutter strength
σ°_ϕ	—	Calculated backscatter
τ	—	Pulsewidth
Φ_{3dB}	—	3 dB elevation beamwidth
ψ	—	Depression angle

Nomenclature and Abbreviations

1-D—One dimensional

2-D—Two dimensional

3-D—Three dimensional

AD—Air Defence

AMSL—Above Mean Sea Level

AREPS—Advanced Refractive Effects Prediction System

ARMSCOR—Armaments Corporation of South Africa

ASTER—Advanced Spaceborne Thermal Emission and Reflection Radiometer

ATC—Air Traffic Control

Azimuth—Angle in a horizontal plane, relative to a fixed reference, usually north or the longitudinal reference axis of an aircraft or satellite.

Beamwidth—The angular width of a slice through the mainlobe of the radiation pattern of an antenna in the horizontal, vertical or other plane.

BIL—Band Interleaved by Line

CARPET—Computer Aided Radar Prediction and Evaluation Tool

CG—Constant Gamma

CLT—Central Limit Theorem

cm—Centimetre

CSIR—Council of Scientific and Industrial Research

dB—Decibel

DEM—Digital Elevation Model

DLR—Deutsches Zentrum für Luft- und Raumfahrt (German Aerospace Centre)

DOD—Department of Defence

DTED—Digital Terrain Elevation Data

EGM96—Earth Gravitational Model 1996

EM—Electromagnetic

EOS—Earth Observing System

FAO—Food and Agriculture Organisation

GDEM—Global Digital Elevation Model

GeoTIFF—Georeferenced Tagged Image File Format

GHz—Gigahertz

GIS—Geographic Information System

GLC—Global Land Cover

GLCD—Global Land Cover Data

GLCNMO—Global Land Cover by National Mapping Organisations

GPS—Global Positioning System

GSFC—Goddard Space Flight Centre

GTRI—Georgia Tech Research Institute

HDF—Hierarchical Data Format

Hz—Hertz (cycles per second)

IES—Institute of Environment and Sustainability

IfSAR—Interferometric Synthetic Aperture Radar

JPL—Jet Propulsion Laboratory

km—Kilometre

Kw—Kilo-Watt

LC—Land Cover

LiDAR—Light Detection and Ranging

LOS—Line of Sight

m—Meter

METI—Ministry of Economy Trade and Industry

MHz—Megahertz

MIT/LL—Massachusetts Institute of Technology/Lincoln Labs

MODIS—Moderate Resolution Imaging Spectroradiometer

MSL—Mean Sea Level

NASA—National Aeronautics and Space Administration

NASU—National Academy of Sciences of Ukraine

NIMA—National Imagery and Mapping Agency

PDF's—Probability Density / Distribution Functions

PRF—Pulse Repetition Frequency

QA—Quality Assessment

Radar—Radio Detection and Ranging

RCS—Radar Cross Section

RMSE—Root Mean Squared Error

RMS—Root Mean Square

RSA—Republic of South Africa

s—Second

SADC—Southern African Development Community

SANBI—South African National Biodiversity Institute

SAR—Synthetic Aperture Radar

SPOT—Satellite Pour l'Observation de la Terre, (Earth-Observing Satellite)

SRTM—Shuttle Radar Topography Mission

TIN—Triangular Irregular Networks

UHF—Ultra High Frequency

US—United States

VHF—Very High Frequency

W—Watt

WGS84—World Geodetic System 1984

WGS—World Geodetic System

X-SAR—X-band Synthetic Aperture Radar

Chapter 1

Introduction

1.1 Subject and Motivation

This minor dissertation describes the related theoretical information, models and processes required for the development of a site specific radar coverage and land clutter modelling tool. The scope of the investigation involved a theoretical overview and investigation of radar propagation, radar coverage, geographic information systems (GIS) related data and radar land clutter models.

Due to the complex nature of clutter, radar land clutter models are difficult to characterise with consistency and accuracy. No land clutter model will therefore represent the exact clutter returns from a specific site. However these models can be used to predict typical conditions. The nature of land clutter models can be determined from how they were derived, and their relationship with clutter returns seen on specific sites or trials.

Different land clutter models can be used for different clutter conditions and scenarios, thus existing land clutter model's validity are based on different underlying assumptions and dependencies. In the context of this dissertation, land clutter model validity will be defined as the extent to which the model corresponds to different simulated clutter conditions and characteristics. Some of the different land clutter simulation conditions can be summarised as the dependence that the model has on:

1. Grazing, incidence or depression angle of the simulated clutter patch area.

2. Surface roughness of the simulated clutter patch area.

3. Surface moisture of the simulated clutter patch area.

4. Radar waveform transmitted and received frequencies.

5. Radar waveform transmitted and received polarisation.

6. Type of terrain (land cover) of the simulated clutter patch area.

7. Topography and relief of the simulated clutter patch area.

8. Spatial and temporal statistics of the simulated clutter patch area.

These are therefore some of the significant characteristics that affect clutter returns. Given the review of some of the existing monostatic radar land clutter models, the purpose of the investigation is to determine the most appropriate land clutter models and processes to use for different clutter conditions which significantly affect the clutter returns, such as those listed above, in order to aid clutter model decisions required for the development of a site specific radar coverage and land clutter modelling tool.

1.2 Background to the Study

Radio Detection and Ranging (radar), is a remote sensing device that uses electromagnetic waveforms for the purpose of detecting, ranging and tracking of targets of interest. It can also be used for imaging and remote sensing purposes [1]. A radar operates by transmitting an electromagnetic wave, and the echo that is reflected back to the radar is used to determine the target's range. In addition to target range, a radar can also be used to determine target location, direction, and speed. The return signal is comprised of the direct return path as well as other artefacts such as, multipath returns, echoes from other targets, thermal noise and jammers if present [2]. Clutter can thus be defined as unwanted radar return echoes, typically from the ground, sea, rain or other precipitation, chaff, birds, insects, meteors, and aurora [3]. Specifically, all echoes besides that of the target of interest, noise and jammer can be considered to be radar clutter [2].

The determination of a radar's direct line of sight (LOS) coverage and clutter performance in a specific area of interest is required for optimal radar placement, optimisation and

performance analysis. The ability to be able to model the radar observed environment, coverage and clutter contributions, in site specific areas of interest, are of value to the effective development, placement and deployment of medium to long range surveillance radar systems. This capability is required for air traffic control (ATC), as well as air defence (AD) radar purposes.

As part of the design or acquisition of radar systems, modelling and simulation of the radar system performances can be used to facilitate project planning, development, system engineering processes, and to reduce project risk and costs.

There have been a number of studies and investigations into characterising the spatial and temporal statistics of radar land clutter over various sites [4, 5, 6, 7, 8, 9, 10, 11]. These types of models accurately reproduce the patchiness of land clutter, but the modelling results are not relevant to the specific geographic region, terrain topography, terrain type, and radar position. In the case of determining the radar coverage and clutter performance in a complex environment, a more site specific approach is required in order to effectively characterise the radar observed terrain and target visibility, as well as the terrain clutter. This characterisation is important for modelling purposes due to the complications that terrain and terrain clutter pose to the radars performance. These complications include terrain shadowing over the land and the effects of clutter returns from the terrain [12]. Terrain shadowing results in decreased coverage performance due to masking or ghost areas within the operating range of the radar. Terrain clutter returns result in dynamic range and radar receiver saturation issues. In order to accurately model the performance of a radar system in a specific radar deployment site, terrain obscuration's and environment effects (clutter contributions) need to be taken into account [13].

This requirement would necessitate accurate and relevant (GIS) data as well. The increasing quality and availability of digital terrain elevation data and advancements in computer technology have led to a significant increase in the need to effectively model the coverage capabilities and clutter performance of a radar system in a complex environment.

In order to develop such a tool, related theoretical information, relevant clutter model's and processes required for the development of a site specific radar coverage and land clutter modelling tool needs to be investigated. The validity of such a modelling tool is greatly dependent on the clutter modelling approach used.

For successful modelling of site specific radar coverage, the terrain topography properties of the intended simulated area of interest needs to be known. Similarly for successful characterisation of the clutter performance, land cover data of the intended simulated area needs to be taken into account. The clutter performance can be modelled by implementing an appropriate land clutter model for the particular area of interest. Numerous land clutter models exist in literature that address specific cases of clutter types and behaviors [14, 15, 9, 16, 7, 17, 18, 19, 6]. Land clutter models in most cases are described in terms of the backscattering coefficient (σ°), which is the normalised measure of electromagnetic energy return from a distributed target [3]. For a radar site specific case, appropriate land clutter models need to be identified and chosen to cater for the varying types of clutter that can exist in particular areas of interest. The purpose is thus to investigate and examine existing monostatic land clutter models in order to identify the appropriate models to use for the varying land clutter simulation cases that can arise which significantly affects clutter returns.

1.3 Objectives and Aim

The aim of this project is to bring together the models and processes needed to start the development of a site specific radar coverage and land clutter modelling tool. The objectives of this project are therefore to investigate the related theoretical information and intended models and processes required for the development of a site specific radar coverage and land clutter modelling tool. These include:

1. Review of radar propagation, land clutter, coverage and GIS related information.
2. Investigation and review of appropriate land clutter models, and related digital elevation and land cover data.
3. Investigation of which are the most appropriate land clutter models to use for varying terrain types, range of frequencies and significant characteristics which affect clutter returns. This will include a comparison of measured backscatter data with simulated backscatter data calculated from these land clutter models.
4. To provide a classification table in terms of each model's validity for different grazing angles and frequency ranges.

5. Highlight grazing angle and frequency ranges where low validity or no land clutter models are available, such that recommendations can be made on where future studies on land clutter modelling can be focused on.

1.4 Scope and Limitations

The scope of this investigation is limited to the review, description and analysis of radar propagation, radar coverage, GIS related data and existing monostatic radar land clutter models appropriate for modelling the clutter behaviour and strength from any specified site specific areas within the Southern African Development Community (SADC) region. A review and description of the processes, models and data required for a simulation of this nature will be conducted. The main focus of this investigation will be to determine the most appropriate monostatic land clutter models to use for the varying land clutter simulation cases that can arise. The development and implementation of a site specific radar coverage and clutter simulation modelling tool is not within the scope of this investigation. The development of new land clutter models is also not within the scope of this investigation and the focus will remain on the use of existing models, data and processes.

The author notes that all measures of clutter strength, or measures of backscatter coefficient σ° in this dissertation , both in the representation of measured data as well as in predictive modelling of σ°, do not attempt to separate the effects of propagation (in terms of F^4), over the terrain between the radar and the clutter cell from the intrinsic terrain backscatter $\sigma^\circ$from the clutter cell itself. Thus terms such as the clutter strength, σ or σ° as used in this dissertation is defined as the product of the backscatter coefficient σ° and the patter propagation factor to the fourth power, F^4, where F is assumed to include all propagation effects, including multipath and diffraction, between the radar and the clutter cell.

1.5 Document Outline and Overview

The structure and layout of this dissertation mirrors the approach taken during the course of research. Chapter 2 gives an overview of some of the relevant theory from literature

that provides context to the investigation. Although much of this chapter is derived from standard text book material, it highlights important information and considerations required for the development of a site specific radar coverage and land clutter modelling tool. It describes relevant topics of radar propagation, radar coverage, radar clutter and GIS related information.

Due to the nature of the objectives and scope of this dissertation, much of the literature review of current land clutter models, GIS data / sources and other topics required for the development of a site specific radar coverage and land clutter modelling tool is given in Chapter 3.

In Chapter 3, a description of the models and processes of the different topics covered in the Chapter 2 is given. Firstly it describes appropriate existing statistical and empirical monostatic radar land clutter models. Several clutter (backscatter coefficient) models are discussed in this section in order to determine the appropriate clutter models to use for a particular clutter scene and radar setup. Based on the information gathered, the models investigated will be classified as either a weak, strong, or excellent land clutter model to use for site specific radar land clutter modelling purposes. The classification will be based upon the model's validity, parameters taken into account, terrain types, angular and frequency ranges. It should be noted that a particular model can be considered valid and classified as an excellent model to use when restricted to certain grazing angle or frequency range, however the aim is to base the classification not only on specific ranges but as a general classification which takes into account all ranges of grazing angle and radar related frequencies of interests as well. This concept of results will be illustrated as well as tabulated in aid of developing algorithms for use in a site specific radar coverage and land clutter modelling tool. It follows on by providing a description and overview of relevant digital elevation and land cover data sources that can be considered in simulation for areas within the SADC region. It then ends by describing the methods and processes used to simulate the clutter scene as well as a discussion on the required simulated clutter cell size, DEM resolution, and DEM height accuracy. This includes the description of proposed creation of clutter patches using meshing and grid methods, radar coverage using LOS ray tracing algorithms, and a method of simulating coherent clutter returns.

Chapter 4 provides a discussion of the land clutter models in the context of use in a site specific radar clutter modelling tool. It aims to determine which of the existing models

are the most appropriate to use for the varying simulation cases, as well as to identify categories of land clutter models where little or insufficient models are available, such that recommendations can be made on where future studies on land clutter modelling can be focused on. The aim is to determine how well simulated site specific clutter using the land clutter models agree with measured data, and which models are best suited to use for the various grazing angle and frequency ranges. The process will be based on information gathered from literature for low grazing angles, and from comparing simulated clutter using the land clutter models with measured data for angles in the plateau and high grazing angle region. It also aims to provide the link between the different terrain classes described in land cover data compared to those in land clutter models. As with the land clutter models, link results for land cover data will be illustrated and tabulated in aid of developing algorithms for use in a site specific radar coverage and land clutter modelling tool. It ends by proposing a guide on the process to follow for the development of a site specific radar coverage and land clutter modelling tool.

Chapter 5 provides a discussion of the information and results obtained during this research. It then provides conclusions based on the foregoing information in the report, and then ends by providing recommendations and discussions for future work.

Chapter 2

Theoretical Overview

This chapter gives an overview of some of the relevant theory from literature that provides context to the investigation. It describes radar propagation, radar coverage, radar clutter and GIS related information considered necessary for the development of a site specific radar coverage and land clutter modelling tool.

2.1 Radar Propagation

The atmosphere of the earth and the surrounding environment has a considerable effect on propagating electromagnetic waves. In order to predict the performance of the radar system, the signal distortions due to the earth's surface and the atmosphere needs to be taken into account. These effects include diffraction of electromagnetic waves, refraction of radar waves caused by the atmosphere, and the absorption or attenuation of radar wave energy due to the gases in the atmosphere [20].

2.1.1 Wave Propagation Through the Earth's Atmosphere and Atmospheric Propagation Effects

The earth's atmosphere constitutes several different layers, as shown in Figure 2.1. The first layer up to an altitude of about 20 km is known as the troposphere. The layer between 20 km and 50 km is known as the interference zone and the layer between altitudes 50 km and 600 km is known as the ionosphere. The section below the troposphere and horizon,

close to the earth's surface as shown in Figure 2.1 is known as the diffraction zone.

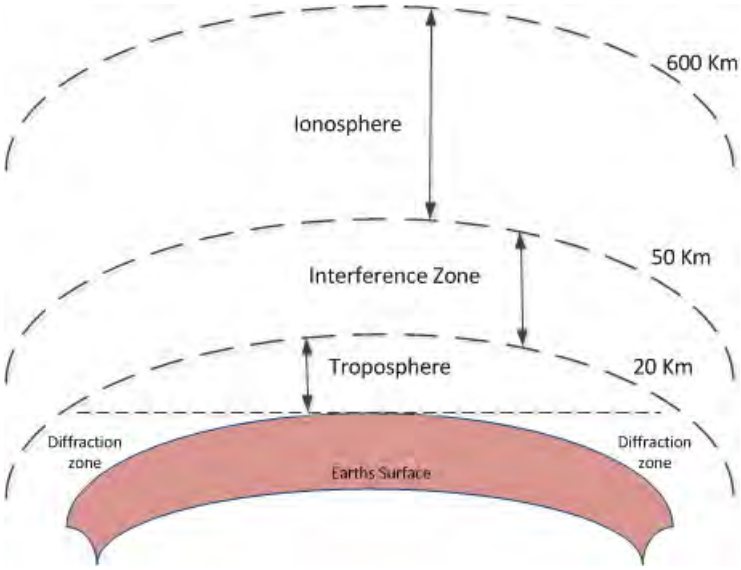

Figure 2.1: Geometry of the earth's atmosphere [21].

Electromagnetic waves behave differently in these different atmospheric zones. In the troposphere, electromagnetic waves refract (bend) as they propagate through. This refraction effect is due to the dielectric constant, which is a function of the temperature, pressure, water vapor, and the gaseous content of the air. The water vapor and gaseous content of the air also results in a loss of electromagnetic energy. This loss is known as atmospheric attenuation. The two gas compounds in the atmosphere that are responsible for the majority of electromagnetic signal attenuation are oxygen (O_2), and water vapor (H_2O). Atmospheric attenuation due to oxygen and water vapor in the air depends on the operating frequency of the propagating electromagnetic wave, as shown in Figure 2.2, as well as range and elevation angle.

From Figure 2.2, it can be seen that at lower frequencies, atmospheric attenuation is not very significant. However at operating frequencies above 23 GHz, in the millimetre wave region, signal attenuation significantly increases due to the presence of oxygen and water vapor peaks. The signal attenuation also increases significantly due to the presence of rain, fog, dust and clouds [23]. The specific gaseous attenuation in $^{dB}/_{km}$ can be expressed as shown in Equation 2.1.

$$\kappa = \kappa_o + \kappa_w = 0.1820 \times f \times N^{''}(f) \tag{2.1}$$

where κ_o and κ_w are the specific attenuation due to oxygen and water vapour respectively,

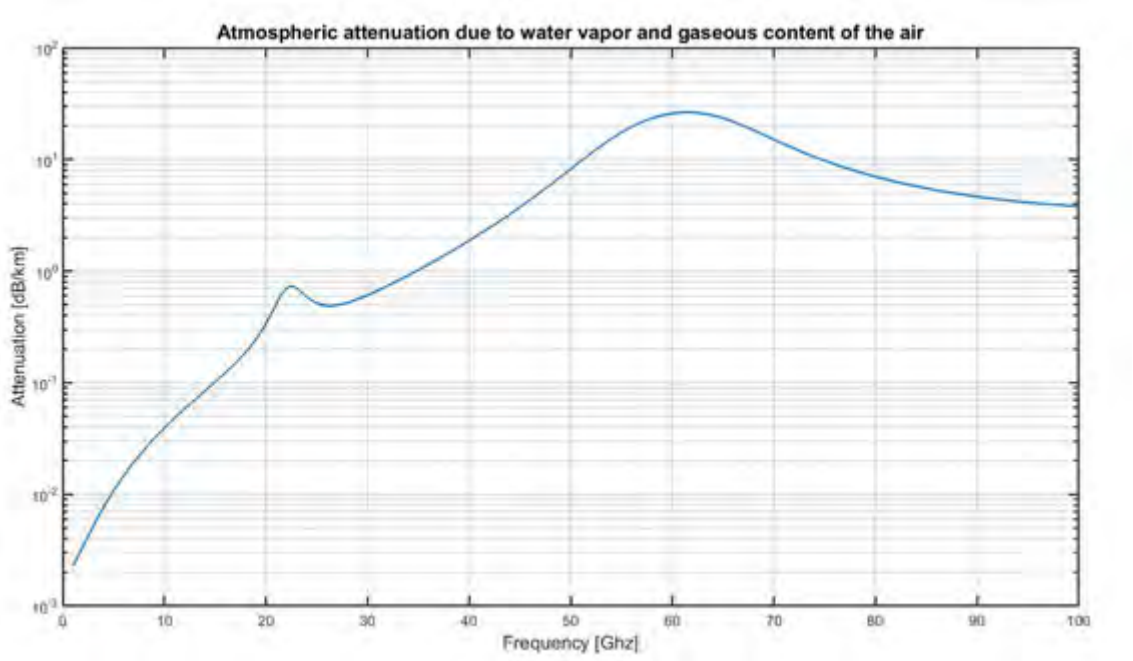

Figure 2.2: Atmospheric attenuation due to water vapor and gaseous content of the air [22].

and where f is the frequency in GHz and $N''(f)$ is the imaginary part of the frequency dependent complex refractivity [22].

The interference zone behaves much like free space where little refraction or atmospheric attenuation occurs [23]. The effects of the ionosphere are considered not relevant to the nature of this work.

2.1.2 Refraction

Refraction refers to the property that causes deviation of electromagnetic waves from a straight line as they propagate through the earth's atmosphere [20]. The index of refraction n is defined as,

$$n = \frac{c}{v} \tag{2.2}$$

where c and v are the velocity in m/s, of the electromagnetic wave in free space and through the medium respectively. A more convenient scaled index for refraction is used in electromagnetic propagation studies called the refractivity index N. For microwave frequencies the refractive index, n, and refractivity index, N, for air containing oxygen

and water vapor is given by,

$$N = (n-1) \times 10^6 = \frac{77.6p}{T} + \frac{e^s \times 3.73 \times 10^5}{T^2} \tag{2.3}$$

where e^s is the partial pressure of water vapor in millibars, p is the atmosphere's barometric pressure in millibars and T is the absolute temperature in Kelvin. For practical purposes in propagation modelling, a modified refractivity that includes the effects of the earth's curvature is used. The modified refractivity M is given by,

$$M = N + \frac{h}{r_e \times 10^{-6}} = N + 0.157h. \tag{2.4}$$

Where r_e is the radius of the earth in metres and h is the height above sea level in metres.

2.1.2.1 Refractive Conditions

There are four types of refractive conditions, namely:

1. Standard, normal conditions,
2. Subrefractive conditions,
3. Superrefractive conditions,
4. Trapping conditions.

Figure 2.3 depicts the four refractive conditions.

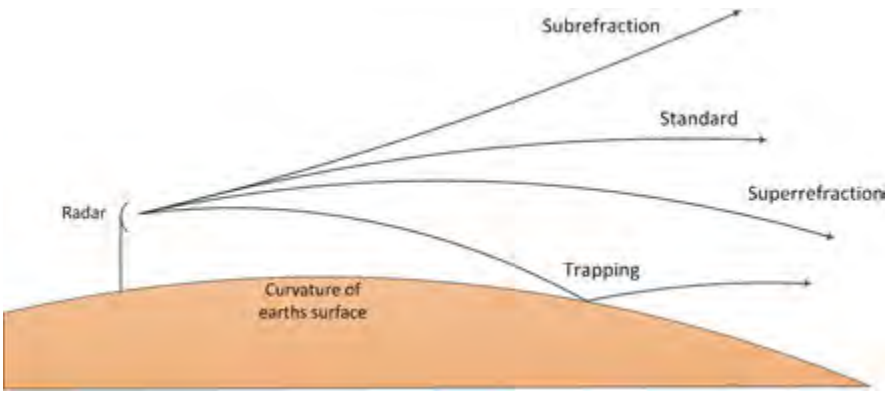

Figure 2.3: Depiction of the four different types of refractive conditions.

2.1.2.2 Standard and Normal Conditions

A normal refractivity gradient may vary between 0 N/km and -79 N/km, or between 79 M/km and 157 M/km. Such a gradient will cause EM waves to bend slightly downward from a straight line. This results in an increase in detection range and a further radar horizon. The actual refractivity distribution in the troposphere is approximately exponential. However for altitudes below 1 km, the distribution can be approximated by a linear gradient. The standard gradient is characterised by a linear decrease of 39 N/km or an increase of 118 M/km [20].

2.1.2.3 Subrefractive Conditions

A subrefractive gradient is greater than 0 N/km, or greater than 157 M/km. This gradient will cause the EM wave to bend upwards causing the energy to travel away from the earth. This results in decreased detection ranges and a shorter radar horizon [20].

2.1.2.4 Superrefractive Conditions

As the refractivity gradient decreases below the normal refractive gradient, the EM wave will bend towards the earth more than normal. At the critical gradient, the EM wave will bend with a radius of curvature equal to that of the earth. Under this condition, the EM wave will travel parallel to the earth at a fixed height above the surface. A superrefractive gradient refers to refraction conditions between the normal and critical gradients. This corresponds to gradients between -157 N/km and -79 N/km, or between 0 M/km and 79 M/km [20].

2.1.2.5 Trapping Conditions

A trapping refractive condition occurs when the refractive gradient is less than 157 N/km or 0 M/km. Such conditions occur for only a limited altitude extent in the troposphere. Since the refractive gradient in this layer is greater than the critical gradient, the EM wave will bend towards the earth with a curvature smaller than that of the earth. The EM wave will then encounter a layer of normal gradients and get refracted upwards or hit the surface and get reflected upwards. Thereafter the EM wave will re-enter the same region of the

atmosphere causing a downward refraction again. Hence this condition is called trapping, as the EM wave tends to be confined in a narrow region of the troposphere [20].

The various refractive conditions and associated refractive gradients are summarised in Table 2.1.

Table 2.1: Refractive gradients for the different types of refractive conditions.

Refractive Condition	**N-Gradient [N/km]**	**M-Gradient [M/km]**
Standard	-39	118
Normal	-79 to 0	79 to 157
Subrefraction	> 0	> 157
Superrefraction	-157 to -79	0 to 79
Trapping	< 157	< 0

2.1.2.6 Diffraction

Diffraction occurs when electromagnetic waves bend around physical objects. When electromagnetic waves meet with physical objects in the diffraction zone, the wave has a natural tendency to bend around the obstacle and results in part of the wave energy changing direction from its normal line of sight path. Diffraction thus allows wave energy to be present around the edges of objects. Radars operating at lower frequencies tend to illuminate more of the shadow region around an obstacle as compared to radars operating at higher frequencies. There are two types of diffraction, these are knife edge and cylinder edge diffraction [24]. The principal effect of diffraction causes the propagating electromagnetic wave to extend to ranges beyond that of the radar horizon, and at low operating frequencies, can even cause electromagnetic waves to encircle the earth due to diffraction effects.

2.1.3 Radar Horizon and Earth Curvature Effects

Assuming optical line of sight, due to the spherical nature of the earth, EM waves are subjected to geometrical limiting effects that prevent radar detections due to the target being below the tangent line that the radar makes with the earth. This maximum line of sight range is known as the radar horizon as shown in Figure 2.4. Targets beyond this range are known to be in the radar's dead zone.

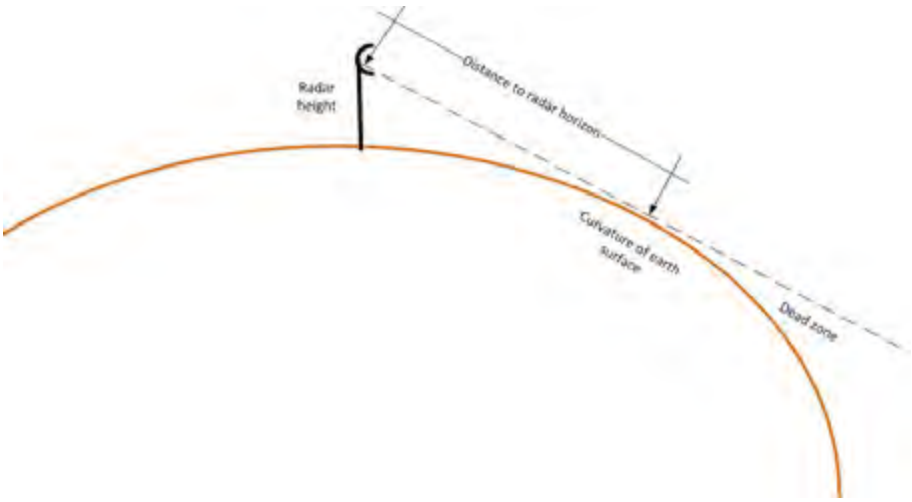

Figure 2.4: Radar horizon and dead zone.

The radar horizon is thus one of the contributing factors that limits the maximum range of long range radars. The radar horizon to a target is approximately proportional to the height of the radar and target above the surface. For a radar at a tower height of h_r and a target height of h_t in metres, the radar horizon can be expressed as,

$$R_h = \sqrt{2 \times R_e \times h_r} + \sqrt{2 \times R_e \times h_t} \tag{2.5}$$

Where R_h is the distance to the radar horizon in kilometres, R_e is the earth's radius in kilometres and h_r and h_t are the radar tower and target heights in metres.

The above discussion on radar horizon neglects the effects of the earth's atmosphere. As discussed in section 2.1.1 and 2.1.2, a radar's EM waves that are propagating within the earth's atmosphere are subject to refraction, and thus do not travel in straight lines but bend slightly. One of the effects of refraction of radar EM waves is that the distance to the horizon is extended, thus increasing radar coverage. Another effect is that refraction introduces errors in the measurement of elevation angle. A simple and effective method used by the radar community to account for this atmospheric refraction effect is to replace the actual atmosphere by a homogeneous atmosphere in which waves propagate in straight lines. This is done by replacing the earth radius term $R_e \approx 6.4 \times 10^3 km$ in equation 2.5 with an effective earth radius term $R_{eff} \approx 8.5 \times 10^3 km$. The ratio of the actual to effective earth radius can be shown to be $\frac{4}{3}$, thus this correction model is know as the $\frac{4}{3}$ Earth Model [25]. By using the effective earth radius, the effects of the earth's curvature and refraction in the atmosphere are approximated by assuming that propagation of EM waves are along

straight lines.

Because of it's simplicity and convenience, the $\frac{4}{3}$ earth model has been a trusted model to use to account for the effects of atmospheric refraction. The model does however have limitations. The model assumes standard atmospheric conditions throughout altitudes and uses a constant value for $k = \frac{4}{3}$. In reality, the value for k will change as a function of altitude, atmospheric conditions, frequency, etc [1]. Atmospheric refraction not only causes bending of EM waves, but produces errors in radar measurements of range and elevation as well. These errors decrease with elevation angle, and are generally independent for frequencies below $\sim$20 GHz [10, 26]. By assuming standard atmospheric conditions, these measurement errors can be corrected to an accuracy of approximately 15% by using error curves as those found in [26] (Figure 4.9, and Figure 4.10, p75).

According to Blake [27], the $\frac{4}{3}$ earth model is reasonably accurate up to altitudes of approximately 4 km, but at higher altitudes it predicts too much ray bending. Using a constant value of $k = \frac{4}{3}$ could also lead to errors at very small grazing angles. Figure 2.5 shows the calculated grazing angle as a function of range near the horizon for two effective earth radii, $R_{eff} = \frac{4}{3} \times R_e$, and $10R_{eff}$ respectively. From Figure 2.5, it can be seen that at small grazing angles, changes in σ° with range may be caused by differences in the calculated grazing angle as a function of range resulting from using different values for k. Very small grazing angles are thus highly sensitive to the assumed atmosphere [10].

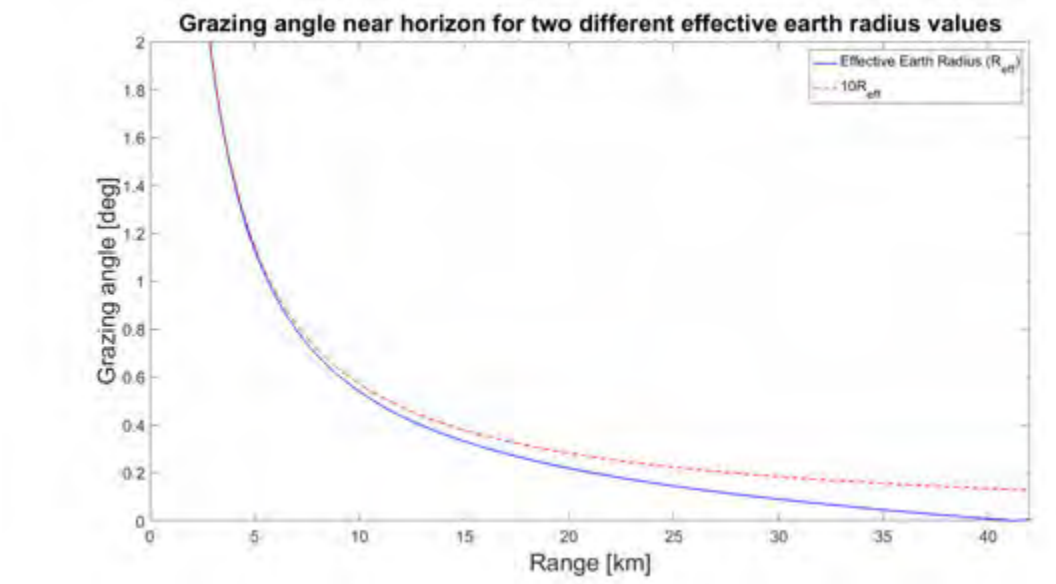

Figure 2.5: Grazing angle as a function of range near the horizon for two different effective earth radii values [10].

Figure 2.6 shows the radar horizon using the $\frac{4}{3}$ Earth Model as described above for different tower heights, and target heights. From this figure it can be seen that the radar horizon is proportional to the square root of the height of the radar and target above the surface, h_r and h_t respectively.

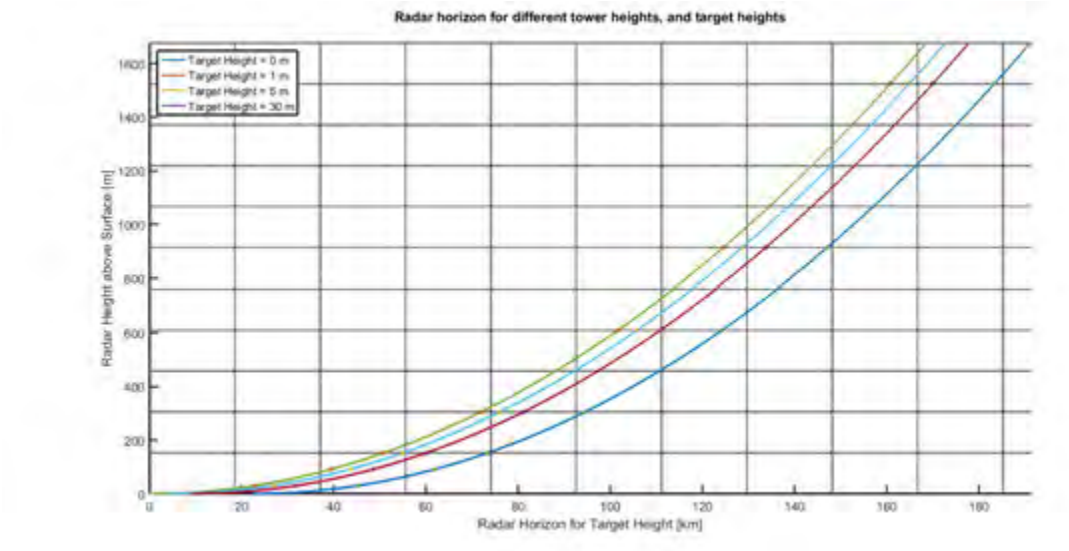

Figure 2.6: Radar horizon for different tower heights, and target heights.

2.2 Radar Coverage

The coverage of a radar system refers to the volume around the system in which targets can be detected. The prediction and visualisation of radar coverage thus plays a significant role in determining the performance of a particular radar system.

2.2.1 Flat Earth and Spherical Earth

Typically in radar systems and propagation modelling, the assumption is made that the earth is sufficiently flat such that the depression angle ψ, at the target is the same as the grazing angle δ at the target. For short range over relatively flat terrain and for low altitude targets this assumption holds. However at longer ranges and higher flying targets the spherical curvature of the earth needs to be taken into account. In order to effectively model land clutter contributions, the effects of the earth's curvature needs to be taken into account as well.

2.2.2 Shadowing Effects by Land Terrain and Cover

The local terrain and land cover in the radar observed area creates undesirable interference effects that decrease radar coverage detection performance. These effects include terrain obscuration, which causes shadowing effects, as well as land clutter, which is the unwanted reflectivity from the local terrain and land cover [28]. Targets that are masked by terrain due to terrain obscuration are known to be within the radars shadow zone as illustrated in Figure 2.7. Due to diffraction effects as discussed above, it is possible for the radar beam to illuminate parts of the region around an obstacle not within direct LOS of the radar as shown by the black arrows in Figure 2.7.

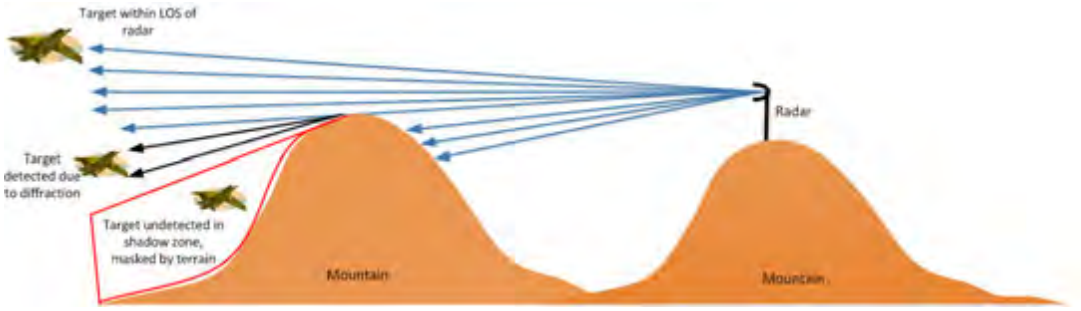

Figure 2.7: Shadowing effects by land terrain.

The radar system will thus be unable to detect targets that are masked by the terrain. It is of significant importance to characterise the topography of the land around the radar such that these shadow zones can be known. It is also important to determine which areas of the land are visible to the radar system and which are not, in order to effectively model the land clutter returns. Only the areas that are not masked by the terrain, will cause a significant clutter return.

2.2.3 Optimisation of Radar Deployment Sites

The optimal radar deployment site, where the radar should have the optimal radar coverage performance, can be selected by calculating the maximum terrain LOS coverage in a particular area of interest. Radar equation formulas and modelling tools such as CARPET (Computer Aided Radar Prediction and Evaluation Tool) [29], and AREPS (Advanced Refractive Effects Prediction System) [30], can be used to predict the maximum range and coverage capabilities of a radar system given the necessary system parameters. The problem is that when the location of the radar is selected, the surrounding terrain within

the proposed coverage of the radar could potentially reduce the coverage performance of the radar due to effects such as shadowing by the topography and masking by clutter. It is thus important to determine which parts of the surrounding observed terrain is within the radar's LOS and which areas are blinded, as well as to be able to determine the clutter contributions from the area of interest.

2.3 Pattern Propagation Factor, F

The pattern propagation factor (F), is defined in [3], as the ratio of the field strength that is actually present at a point in space to that which would have been present if free-space propagation had occurred with the antenna beam directed toward the point in question. This factor is used in the radar equation to modify the strength of the transmitted or received signal to account for the changes in field strength caused by multipath propagation, diffraction, refraction, and the antenna beam pattern..

The effects of the environment are included in the radar equation via means of the pattern propagation factor F. As a consequence of the definition of F, the power at a point is F^2 times its value if the propagation medium is a vacuum, for one-way propagation. Thus for monostatic radars, the received power is proportional to F^4 [10].

For a fixed resolution cell with area A, the echo strength is thus proportional to $\sigma^\circ F^4$. For measurement data, the effects of F^4 are due to environmental factors and are therefore necessarily included in the measurement. Determining F^4 accurately is extremely complex and in most cases cannot be separated from the echo strength measurement. Thus from measurement data reflecting the echo strength, the investigator can determine σF^4 or $\sigma^\circ F^4$, and not σ or σ°. The effects of F^4 are thus inherently included in the measurement [10]. Existing empirically derived land clutter / backscatter coefficient models may express backscatter data in terms of σ or σ°, but it should be noted that the pattern propagation factor to the fourth power F^4 is inherently included [10]. This is especially true for low grazing angles less than 10°where the effect of F is generally different in each resolution cell and thus impractical to determine. For microwave and millimetre wave frequencies, and for grazing angles greater than 10°, it is found that F^4 can often be approximated by unity and therefore σF^4 or $\sigma^\circ F^4$ might be reasonably represented by σ or σ° [6]. This is found to be the case for most land clutter models which focuses on

grazing angles in the plateau or high grazing angle regions.

For the purposes of the models and work presented in this dissertation, it is assumed that the effects of the propagation factor are necessarily included in RCS (σ) or backscatter coefficient (σ°) values. If they are expressed without F^4, it is assumed to be inherently included and are in fact, averages of either σF^4 or $\sigma^\circ F^4$ [10].

2.4 Radar Clutter

The term radar clutter is used to describe echoes that are of no interest to the radar. Radar clutter takes on different forms depending on the type of radar system. For ground based radars in which targets of interest are man made objects such as aircraft, ships or ground targets, clutter would then be all unwanted returns from naturally occurring objects such as echo reflections from land terrain and the sea. However for earth imaging radars for remote sensing purposes, reflections from natural land objects and terrain are of interest, and man made objects are considered clutter. The primary focus of this dissertation will be radar land clutter.

2.4.1 Radar Land Clutter

Radar land clutter can be caused by terrain, vegetation and man made structures. All natural and man made objects on the ground that are of no interest to the function or role of a radar system constitute radar land clutter. This section focuses on radar land clutter and discusses the most important characteristics of land clutter necessary for the development of a site specific radar coverage and land clutter modelling tool. Due to many distributed scatterers found over land terrain, land clutter is generally described and modelled by the RCS per unit area of the clutter surface, called the backscatter coefficient, σ° [1, 31]. The backscatter coefficient is described and discussed further in the section to follow.

2.4.2 Backscatter Coefficient σ°

For a given wavelength λ , the radar equation for a monostatic radar system can be written as,

$$P_r = \frac{P_t G^2 \lambda^2 \sigma_{RCS} F^4}{(4\pi)^3 L_s R^4} \tag{2.6}$$

where P_r and P_t are the received and transmitted power in Watts respectively, G is the antenna gain, λ is the wavelength, L_s is the system losses, σ is the RCS, F is the pattern propagation factor, and R is the target range. This form of the radar equation is suitable for point scatterers but not for distributed targets such as land clutter, where many scatterers contribute to the total echo power. The equation should therefore be modified to account for the area defined by the beamwidths and range resolution of the radar [2].

The backscatter coefficient, σ°, is a measure of the electromagnetic wave energy reflected back to the receiver of a radar system and defined in Equation 2.7 [10], as,

$$\sigma^\circ = \frac{\sigma}{A} \tag{2.7}$$

where σ is the total RCS, and A is the total area of the contributing clutter that is defined by the intersecting radar beam with the surface [2]. By describing σ as the RCS per unit area, σ° now becomes independent of the radars geometric parameters.

The clutter surface area A can take on two forms. Firstly if the range resolution of the radar is large in comparison to the projection of the vertical beam onto the surface (pulse limited case), and secondly where the range resolution is smaller than the projection of the vertical beam onto the surface (beamwidth limited case) [2]. These two cases are depicted in Figure 2.8.

For the pulse limited case, the resolution cell is proportional to the range , R, and thus the area , A, defined by the beam and pulse width is given by,

$$A = c\tau R \tan(\frac{\Theta_{3dB}}{2}) \sec \delta \tag{2.8}$$

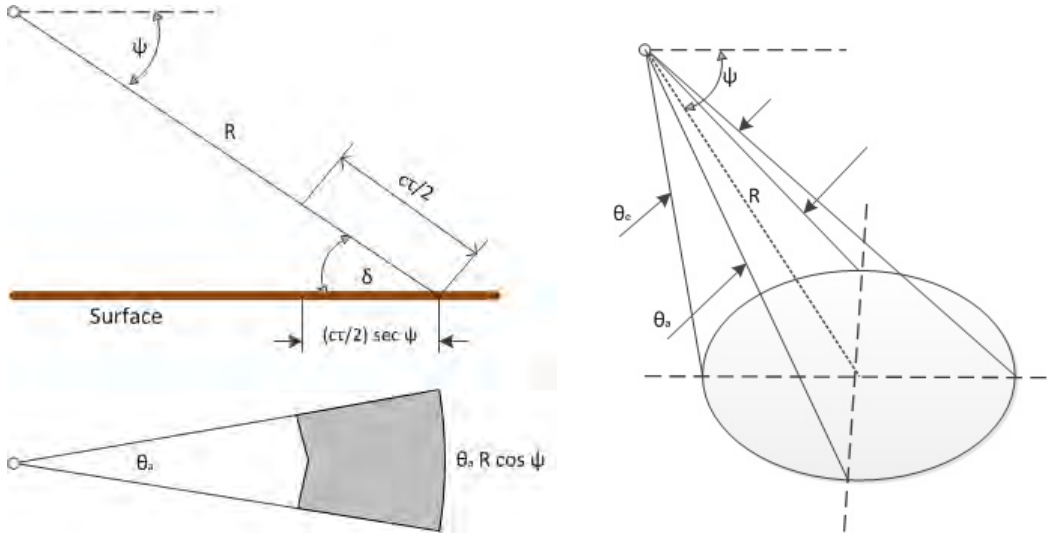

(a) (b)

Figure 2.8: Spatial resolution cell for a radar looking at the surface of the earth [10]: (a) pulse limited case, (b) beamwidth limited case.

where R is the range to the target, Θ_{3dB} is the 3dB beamwidth, τ is the pulsewidth and δ is the grazing angle. If the beamwidth is less than 10°, the following approximation holds,

$$A \approx (\frac{c\tau R\Theta_{3dB}}{2}) \sec\delta. \tag{2.9}$$

The echo power is thus inversely proportional to R^3 for the pulse limited case [10].

For the beamwidth limited case, the resolution cell is proportional to R^2, and the area , A, is defined by both elevation and azimuth angles and given by,

$$A = \pi R^2 \tan(\frac{\Theta_{3dB}}{2}) \tan(\frac{\Phi_{3dB}}{2}) \csc\delta. \tag{2.10}$$

Where Φ_{3dB} is the elevation beamwidth. In this case the echo power is thus inversely proportional to R^2 [10].

2.4.3 Backscatter Coefficient σ° Dependencies

Various radar and environment parameters influence the reflected backscatter coefficient, σ°. These dependencies are listed in Table 2.2.

The dependencies listed in Table 2.2 are described and discussed in the section to follow.

Table 2.2: Backscatter coefficient σ° dependencies.

Radar Parameters	Environment Parameters
Incident / Grazing / Depression Angle	Surface Roughness and Moisture Content
Frequency / Wavelength	Land Topography and Relief
Polarisation	Complex Dielectric Constant
Resolution	Type of Terrain / Land Cover
-	Spatial and Temporal Statistics

2.4.3.1 Frequency / Wavelength

Radar operating frequencies are divided into different frequency / wavelength bands as shown in Table 2.3.

Table 2.3: Radar frequency bands.

Radar Band	Frequency	Wavelength
UHF	300-1000 MHz	100-30 cm
L	1-2 GHz	30-15 cm
S	2-4 GHz	7.5-15 cm
C	4-8 GHz	7.5-3.75 cm
X	8-12 GHz	3.75-2.4 cm
Ku	12-18 GHz	2.4-1.7 cm
K	18-27 GHz	1.7-1.1 cm
Ka	27-40 GHz	1.1-0.75 cm
V	40-75 GHz	0.75-0.4 cm
W	75-110 GHz	0.4-0.27 cm

The wavelength of radar systems has a strong influence on the backscattered energy that is received at the receiver. Longer wavelengths have greater penetration depths through land objects that are small in comparison to the length of the wave as compared to shorter wavelengths. Different wavelengths will therefore reflect different properties of the land and thus significantly influences the backscattered energy received [2, 32].

2.4.3.2 Incident, Depression and Grazing Angle

The incident angle, θ, is described as the angle between the radar line of sight and the vertical with respect to the earth geoid. The incident angle does not take into account the terrain slope. The angle with respect to the slope is known as the local incident angle θ_L. The local incident angle accounts for the variation in the slope of the terrain at the point of illumination. The look or elevation angle is defined as the angle between the

antenna and the vertical, and the depression angle, ψ, is defined as the angle between the horizontal line of the antenna and the radar line of sight [33]. The grazing angle, δ, is defined as the angle between the horizontal line relative to the slope and the radar line of sight (compliment of the local incident angle). The depression angle and grazing angle are closely related and are identical for flat horizontal surfaces [2]. These angles are depicted in Figure 2.9.

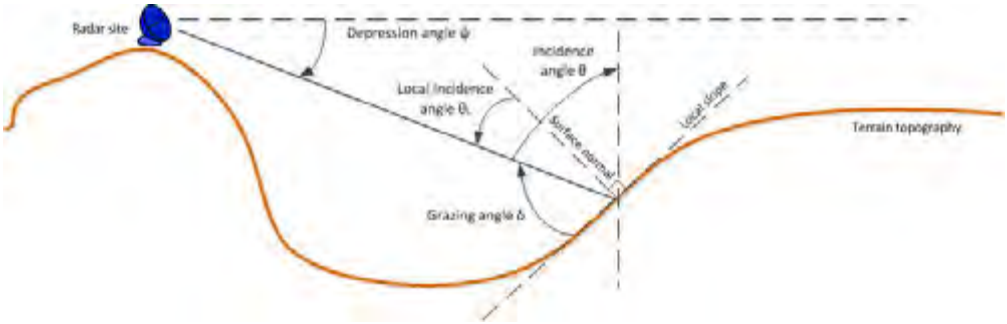

Figure 2.9: Diagram of : incident, local incident, depression and grazing angle.

There is a strong backscatter coefficient dependency to the radar viewing geometry. The grazing angle is the most important viewing angle that explains scattering mechanisms and will be used throughout this dissertation unless otherwise stated. Some backscatter datasets and models are published as a function of depression or incident angle because the grazing angle could not be precisely known [2].

From radar measurements it was observed that in general, the backscatter coefficient changes with respect to grazing angle, as depicted in Figure 2.10.

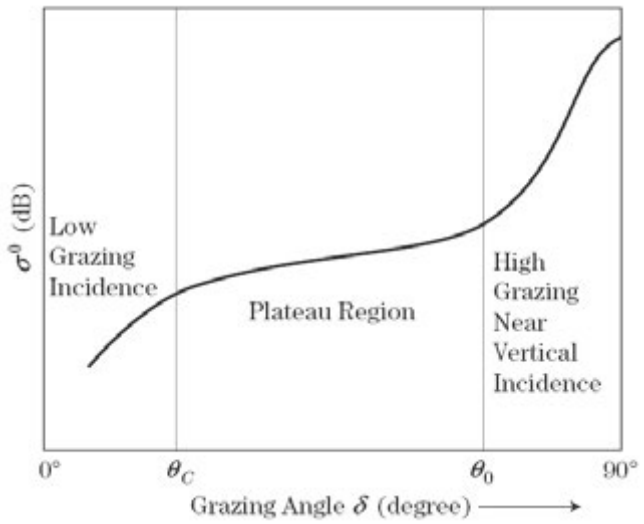

Figure 2.10: General behaviour of σ° as a function of grazing angle [2].

There are three distinct grazing angle regions to be considered:

1. **Low Grazing Angle Region:** At low grazing angles, the backscatter coefficient decreases significantly with decreasing grazing angle [19]. This region extends from 0 to critical grazing angle σ_c. The critical angle is the angle below which the surface remains smooth with respect to Rayleigh's definition. This condition is defined by,

$$\sigma_h \sin\delta < \frac{\lambda}{8} \tag{2.11}$$

   The critical angle is thus given by,

$$\sin\delta_c = \frac{\lambda}{8\sigma_h} \tag{2.12}$$

   where σ_h is the RMS height of the surface irregularities, δ is the grazing angle, and λ is the wavelength [2]. In general, rough surfaces have a larger σ° than smooth surfaces for low grazing angles (conversely, at very high grazing angles (near 90°), smooth surfaces exhibit a higher σ° than rough ones).

2. **The Plateau Region:** At medium to high grazing angles the backscatter coefficient changes linearly with grazing angle with a dependence much less than at lower grazing angles [34]. The clutter power in the plateau grazing angle region seems to increase relative to $1/R^3$. It follows then that σ° would vary as $1/R$ due to the resolution cell area A that increases with R^2.

3. **High Grazing Angle Region:** At high grazing angles the backscatter coefficient increases rapidly with grazing angle to maximum value. In this grazing angle region, smooth surfaces exhibit a higher σ° compared to rough surfaces.

2.4.3.3 Polarisation

The EM wave energy that is transmitted or received by a radar can be either horizontally, vertically or circularly polarised. A radar can thus operate in four linear polarisation modes, namely HH, VV, HV or VH, where the first letter is the transmitted waveform polarisation and second the received waveform polarisation, or two circular polarisation modes, namely right hand circular (RC) or left hand circular (LC) [33, 35]. The theoretical

vertical and horizontal polarisation dependence of the backscatter coefficient σ° for a relatively smooth surface is shown in Figure 2.11.

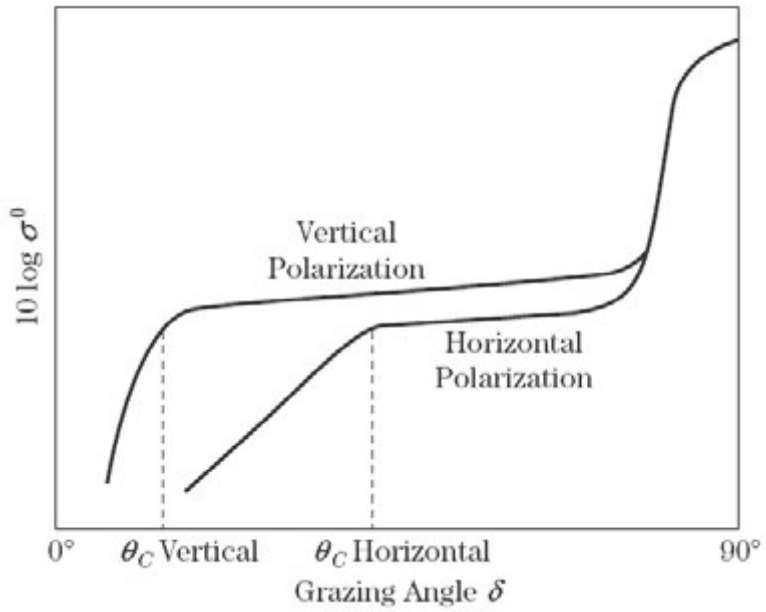

Figure 2.11: Theoretical polarisation dependence of the backscatter coefficient for different changing grazing angles [2].

From Figure 2.11, it can be seen that the critical angle for horizontal and vertical polarisations are different. This is due to multipath effects. At lower grazing angles, the difference between the backscatter coefficient for horizontal and vertical polarisations can be quite large, but at higher grazing angles the backscatter coefficient for horizontal polarisation is only a few dB lower than vertical polarisation [2].

Considering the theoretical behaviour of reflections of circular polarisations, both RC and LC polarisations behave similarly, i.e. the backscatter coefficient decreases with increasing grazing angle [36, 2]. It should be noted that in the case that a circular polarised wave is reflected off a relatively flat conducting plate, the backscatter coefficient subsequently increases with increasing grazing angle [36].

2.4.3.4 Resolution

Range resolution, δR, of a radar is defined as the ability of the radar system to distinguish between two or more targets on the same bearing but different ranges. Conversely angular resolution is the ability for a radar to distinguish between two or more targets at the same range but different bearing. As defined previously, σ° can be described as the mean

clutter strength over the illuminated scene with area A. Resolution therefore does not directly affect σ°, but both resolutions would therefore affect the amplitude statistics or fluctuations about the mean defined by σ° [2].

2.4.3.5 Surface Roughness and Moisture Content

The size of the land particles on a micro composition scale relative to the radar wavelength determines the surface roughness. Rough terrain will reflect stronger backscatter energy as compared to smooth terrain surfaces [33]. Rayleigh's condition's to determine surface roughness is explained in section 2.4.3.2 above. The relationship between surface roughness and surface scattering can take on three forms, as shown in Figure 2.12.

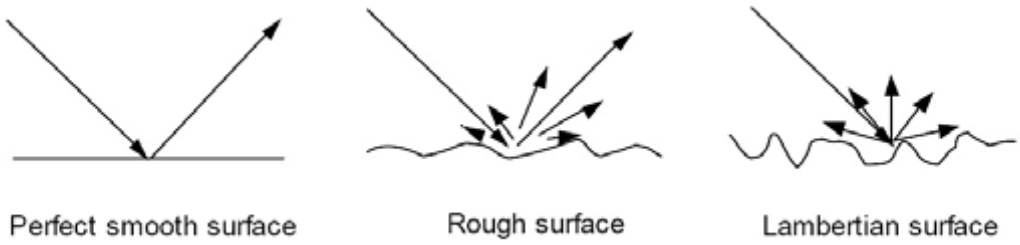

Figure 2.12: Forms of surface roughness [31, 17].

For a perfectly smooth surface, the surface behaves like a mirror and the incident wave is reflected. For rough surfaces, the reflections has two components. The reflected component in the specular direction and the scattered component in all directions. As the surface becomes more rough, the reflected component disappears and the scattered field is equally radiated in all directions and is then known as a Lambertian surface [17, 37].

The reflected energy is also significantly dependent on the surface moisture. Even if the surface roughness remains constant, the backscatter coefficient of land may change by as much as 10 dB from very dry to very wet conditions [17]. Increasing amounts of moisture content in terrain surfaces result's in a reduction of penetration of the radar signal, thus increasing the reflected backscatter coefficient energy [17].

2.4.3.6 Land Topography and Relief

Land topography refers to the arrangement of natural and artificial physical features of a particular area. Land relief refers to the vertical elevation change of a particular area of

interest (related to the slopes / gradients of surfaces). Relative to the area that radar energy is illuminating, both land topography and land relief influence the backscatter coefficient. The differences and dependence that backscatter energy has on land topography and relief will be investigated further in subsequent sections of this dissertation.

2.4.3.7 Complex Dielectric Constant

The electric characteristics of terrain surfaces influences the reflected backscatter energy of the returned radar signal. These characteristics are denoted by the complex dielectric constant which is the ratio of the permittivity of a substance to the permittivity of free space. The complex dielectric constant is an indicator of the intrinsic ability of a substance / terrain surface to store charge and transmit energy [38, 32]. Dry surface areas will contain low dielectric constant, and wet surfaces a high dielectric constant (typically >80), due to the presence of water [39]. Surface areas with a low dielectric constant that are illuminated by radar energy will reflect less backscatter energy than surface areas with a high dielectric constant [40]. Thus with constant surface roughness, the reflected backscatter coefficient energy increases with increasing dielectric constant (surface moisture) [17].

2.4.3.8 Type of Terrain / Land Cover

The type of terrain being illuminated vastly influences the reflected backscatter energy. Different types of terrain will present different backscatter coefficients due to its particular surface properties. The differences and dependence that backscatter energy has on different types of terrain will be investigated further in subsequent sections of this dissertation.

2.4.3.9 Spatial and Temporal Statistics

The reflected backscatter energy as seen by the radar system varies from one region to another. Given a certain land type, the reflected energy is not a constant value over time and space. This is shown in Figure 2.13, which represents the mean backscatter coefficient as a function of various radar frequencies and range resolutions, as measured at 35 sites

of similar land type. These measurements as collected by Billingsley and represented in [6], show broad and decreasing variability with increasing frequency. As these are measurement backscatter data, the pattern propagation factor to the fourth power is explicitly included, as represented by F^4.

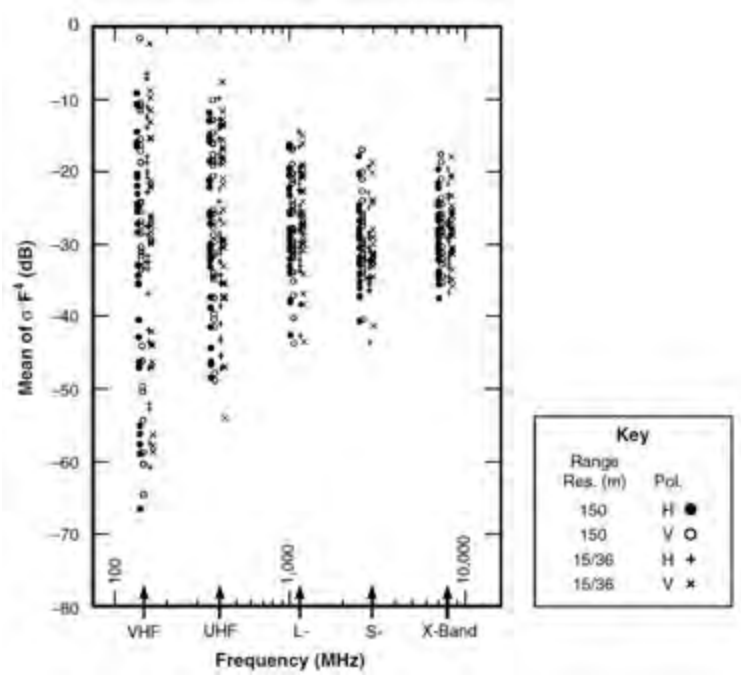

Figure 2.13: Land clutter measurements showing varying values, as collected and analysed by Billingsley in [6], from terrain type "general rural".

The way in which the reflected energy changes from one range cell to another is known as the spatial distribution of clutter. The way in which clutter changes within a range cell over time is known as the temporal distribution (corresponding doppler spectrum in the frequency domain) of clutter. Both the spatial and temporal variations of the clutter of an area of interest influences the backscatter coefficient [6]. The spatial variations of the backscatter coefficient are associated with the type of land cover, and layout of scatterers within the illuminated area of the range cells. The spatial behaviour of clutter is mainly dependent upon the range resolution of the radar system. The temporal behaviour of clutter is mainly dependent on the fluctuations of scatterers within a range cell over time. These fluctuations within a range cell are caused mainly by weather conditions, for example, wind changes the reflected backscatter energy from grass filled areas over time [6]. However, particularly for land based radars which utilises moving target indication (MTI) to separate weak moving targets from strong clutter returns, the corresponding variation in the frequency domain (doppler spectrum) of these fluctuations within a range cell is of greater significance. Different statistical models are used to describe the spatial

and temporal statistics of land clutter. These models are described in the section to follow.

2.4.4 Land Clutter Modeling

In order to estimate radar system performance in land clutter, clutter models are required. Standard probability density functions (PDF's) models can be used to describe the variation of different types of land clutter. From measurement data, statistical parameters required by these PDF models for different types of land clutter can be defined empirically. Empirical models that describe the mean backscatter reflectivity σ° for various types of land terrain as a function of frequency, grazing angle and polarisation can also be developed from measurement data. The type of existing land clutter models that can be used to characterise σ° for use in a site specific radar coverage and land clutter modelling tool is dependent on the nature of how the model was developed. Mathematical models can also be developed that provide an estimation to the the general shape of the backscatter coefficient.

2.4.4.1 Standard PDF's Used to Model Land Clutter Variation

PDF's are used to describe and characterise the statistics of land clutter in space and time. In the past, most radars operated with inherently low range resolution capabilities such that reflected clutter echoes were thought to be comprised of a sum of responses from a very large number of individual scatterers. From the central limit theorem (CLT), it was concluded that the appropriate statistical model to describe the in-phase and quadrature components of reflected backscatter energy was the Gaussian PDF [41]. The amplitude of the clutter is thus Rayleigh distributed. The theoretical PDF for Rayleigh distribution is defined by Equation 2.13,

$$PDF_{Rayleigh} = \frac{x}{s^2}\exp(\frac{-x^2}{2s^2}) \tag{2.13}$$

where x is the amplitude of the return signals, and s is the scale parameter of the distribution which determines the statistical dispersion of the distribution.

As the range resolution improves, the CLT begins to fail and the subsequent in-phase and

quadrature components of clutter can no longer be considered Gaussian distributed. This is due to the number of scatterers in a resolution cell becoming finite or due to individual dominating scatterers. The improved range resolution results in the radar being more sensitive to spatial variations in the clutter which makes the distribution more spiky [42, 43]. The amplitude statistics thus deviates from Rayleigh as well. The spiky characteristic of high range resolution clutter causes the tail of the amplitude distribution to rise. The amplitude distributions considered to best fit this situation for land clutter are the Log-normal and Weibull PDF's [16, 10, 42]. The theoretical PDF for Log-normal distribution is defined by two parameters (shape and scale), and shown in Equation 2.14,

$$PDF_{Log-normal} = \frac{1}{xs\sqrt{2\pi}} \exp\left(\frac{-(\ln x - \mu)^2}{2s^2}\right) \tag{2.14}$$

where μ is the shape parameter, and s is the scale parameter. The shape and scale parameters μ and s represents the mean and standard deviation, respectively, of the clutter intensity expressed in dB having a Gaussian PDF.

In some cases the tail of the Log-normal PDF is too long for the clutter amplitude data to fit. In this case, the Weibull PDF is considered as it's tail is shorter than that of the Log-normal PDF but still longer than that of the Rayleigh PDF [44]. The Weibull PDF is also defined by two parameters (shape and scale), and shown in equation 2.15.

$$PDF_{Weibull} = \frac{k}{b}\left(\frac{x}{b}\right)^{k-1} \exp\left(-\left(\frac{x}{b}\right)^k\right) \tag{2.15}$$

where k is the shape parameter, and b is the scale parameter. For $k = 2$, the Weibull PDF is identical to that of the Rayleigh PDF.

The above distributions describe the spatial behaviour of land clutter, i.e., the variation of land clutter from one range cell to another. These spatial variations are associated with the layout of the backscatterers in the range cells that are illuminated. Thus the spatial behaviour of land clutter is related to the land cover and the radar range resolution.

For temporal variations in land clutter, the return from scatterers within a range cell can be classified as either a steady component, or diffuse component. The steady component is a result of return from fixed discrete scatterers that do not change in time, such as

buildings. Diffuse components is a result of discrete scatterers that can move and change in time, such as wind-blown foliage due to weather conditions. The temporal variations of land clutter mainly depends on the fluctuations of backscatterers within a range cell over time, however it is important to note the indirect effect land cover and range resolution plays on the temporal variations of clutter as well. For example, clutter within a range cell that is dominated by a strong stationary scatterer, such as a building, exhibits little or no fluctuation in time, whereas clutter within a range cell that is dominated by foliage would exhibit more fluctuations in time. The radar range resolution therefore affects the temporal statistics of land clutter by changing the contents within range cells [45].

The Ricean PDF was derived from the analysis of the statistical properties of a sine wave in additive noise, as described and discussed in [46]. H.C Chan describes in [45] that through the analyses of radar land clutter, it was found that the coherent component of land clutter can be considered a constant or slow varying signal, and thus can be modelled as a sine wave with zero frequency. It was further found that if the corresponding diffuse components is describable by complex Gaussian distributions. Thus for a case where a range cell consists of both a strong steady component as well as a diffuse component, the distribution that can be used to model this situation is the Ricean PDF. The diffuse component can be modelled using the Rayleigh PDF, which is a special case of the Ricean PDF [47, 45, 46].

For clutter that changes both in space and in time, a compound clutter model is required. A compound clutter model that is widely used is the K-Distribution. This distribution enables both spatial and temporal correlation properties to be taken into account [48, 49]. The K-Distribution is a widely used model for sea clutter, but can be applied to other types of clutter as well. The K-Distribution is also a two parameter (shape and scale) PDF. Further information of the K-Distribution as used for radar clutter can be found in [50, 51, 8].

The different grazing angle regions as discussed in section 2.4.3.2 affect the amplitude statistics of land clutter as well. Clutter at low grazing angles are characterised by patchiness / lack of uniformity in spatial extent, due to shadowing, and / or extreme resolution dependencies leading to large resolution cell-to-cell variability. Clutter amplitude statistics in the low-grazing angle region are characterised by distributions with long tails (spiky clutter), making Weibull and Log-Normal distributions suitable choices to model

their probability density functions (PDF's). The long tails of the distributions are due to the prevalence of terrain shadowing and multipath at these low grazing angles. The amplitude statistics for clutter in the plateau grazing angle region tend to be more consistent and less spiky than those at lower grazing angles, since terrain shadowing and multipath effects are of less concern. In general, the Rayleigh PDF is a good distribution to use to fit the clutter amplitude statistics observed in the plateau grazing angle region.

2.4.4.2 Empirically Derived Land Clutter Models

Empirical and semi-empirical land clutter models are developed by using radar measurement data. Measurement trials are performed over different terrain surfaces, at varying grazing angles and frequencies. The measurement data collected from these trials are then used to develop empirical land clutter models that describe the average or statistical behaviour of the backscatter coefficient. These models provide an estimation of the backscatter coefficient of different terrain surfaces, at varying grazing angles and frequencies. These models are dependent upon the type of terrain, frequency of operation and grazing angle. To describe the statistical behaviour, the measurement data is fit to common PDF models. The PDF parameters are then empirically derived. These types of models would require large amounts of computer resources for use in a site specific radar coverage and land clutter modelling tool described in this study.

The measurement data can also be used to develop semi-empirical models. Instead of describing the statistical behaviour of the clutter, these models often describe the average backscatter coefficient given by simple formulas containing several parameters (e.g. grazing angle, frequency, polarisation, terrain type, etc). These provide a quick and simple estimation of the backscatter coefficient. It is important to remember that these models are based upon experimental data and include a pattern propagation factor F to the 4^{th} power. Other influences of the environment may also be included that is not taken into account by these models. Some of these models may also only be valid for certain terrain types, grazing angles and frequencies. Despite the limitations, the simplicity and lower computational resources required to simulate these models make semi-empirical land clutter models more suited to be used for developing a site specific radar coverage and land clutter modelling tool. The limitations and validity of some of these models will be discussed and compared to each other in this dissertation in order to determine the appropriate land

clutter / backscatter coefficient models to use for the varying land clutter simulation cases that can arise.

2.4.4.3 Mathematically Derived Land Clutter Models

Rather than using empirical models which are based on observations, mathematical models can be derived which mathematically describe relationships of land clutter. Simple mathematical formulas are thus developed that provide an estimation to the the general shape of the backscatter coefficient for different terrain types and frequencies. Mathematical models are usually evaluated by validating the model against experimental measurements or other empirical data.

2.5 GIS Data

In order to develop a site specific radar coverage and land clutter modelling tool, models of real world terrain surfaces, terrain classification and terrain characteristics are required. The GIS data products that are considered are real world digital elevation model (DEM) data, and land cover (LC) data.

2.5.1 Digital Elevation Model Data

DEM data is defined as a digital model, or 3-D representation of a terrain's surface that is created from terrain elevation data. An example of DEM data is shown in Figure 2.14. The figure represents a digital elevation model for Setif region in Algeria.

Available DEM data products vary in quality, arc spacing (resolution), accuracy, availability and cost. The DEM data can either be represented by digital raster / height maps, or by vector based triangular irregular networks (TIN). The TIN dataset can be considered the primary raw measured dataset whereas the digital raster / height map dataset considered being the secondary computed DEM dataset. Early digital elevation model data were a product of photogrammetric data capture. These relied on interpretation of aerial photographs or satellite imagery. This can also be done by digitising contour lines on topographic maps. Present DEM data is acquired and produced by mappers and na-

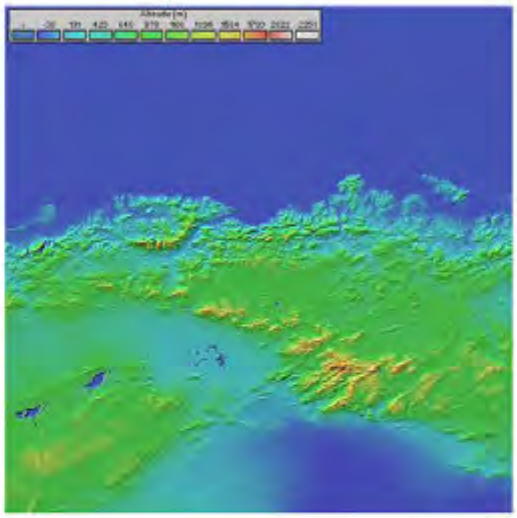

Figure 2.14: Digital elevation model for Setif region in Algeria [52].

tional agencies through remote sensing and land surveying techniques such as photogrammetry, LiDAR (Light Detection and Ranging), IfSAR (Interferometric Synthetic Aperture Radar), and land surveying [53]. There are different types and sources of real world DEM data available, varying in quality, accuracy, availability and methods of production. A number of data sources are considered and discussed in sections to follow. The discussion will provide an analysis on available DEM datasets, their resolutions and height accuracies, as well as the resolutions and height accuracies that would be required for use in a site specific radar coverage and land clutter modelling tool. These DEM elevation heights need to be referenced to a specific earth ellipsoid or geoid.

2.5.2 Earth References, Geoids and Ellipsoids

In geodesy, an earth reference geoid is considered a model of the shape that the earth's oceans would take under the influence of earth's gravitational fields and rotation alone. An earth reference ellipsoid is a mathematically-defined surface model that approximates the shape of the earth [54]. There are many different geoids and ellipsoid models available. Considered here, are the EGM96 reference geoid model, and the WGS84 reference ellipsoid model.

2.5.2.1 WGS84 Reference Ellipsoid Model

The world geodetic system (WGS) is a standard reference ellipsoid derived mathematically, which provides a standard co-ordinate system for the earth's surface. The latest model is the WGS84, and is stated to have an error of less than 2 cm [55]. WGS84 is currently the reference system being used by Global Positioning Systems (GPS).

2.5.2.2 EGM96 Reference Geoid Model

The Earth Gravitational Model 1996 (EGM96) is a geoid model of the earth developed through a collaboration between the National Imagery and Mapping Agency (NIMA), the NASA Goddard Space Flight Centre (GSFC) and the Ohio State University. This spherical harmonic model is complete to degree and order of 360. The EGM96 geoid height model is shown in Figure 2.15. The EGM96 geoid height file provides the height above the WGS84 ellipsoid [56], as illustrated below in Figure 2.16. The EGM96 geoid height file is freely available for download from a number of different sources.

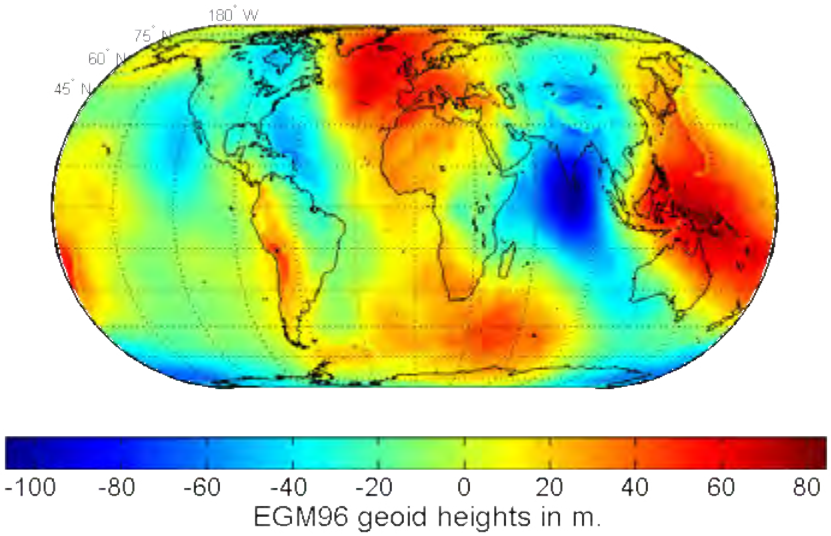

Figure 2.15: EGM geoid height for earth in metres [56].

2.5.2.3 Mean Sea Level (MSL) and Height Above Mean Sea Level (AMSL)

The mean sea level (MSL) is a datum that represents the average height of the ocean's surface [55]. It is important to note that the MSL is considered to coincide with the geoid model; i.e. the geoid model approximates the mean sea level. This is shown in Figure

2.16. The height above mean sea level (AMSL) is considered the elevation height of an object above the average sea level datum, thus it is important to note that the height AMSL is referenced to the earth geoid and not the earth ellipsoid. With this in mind, it is important to note that because GPS systems provide the height above a reference ellipsoid (in this case WGS84), to obtain the height AMSL, the geoid height needs to be taken into account and subtracted from the GPS measurement. These are illustrated in Figure 2.16.

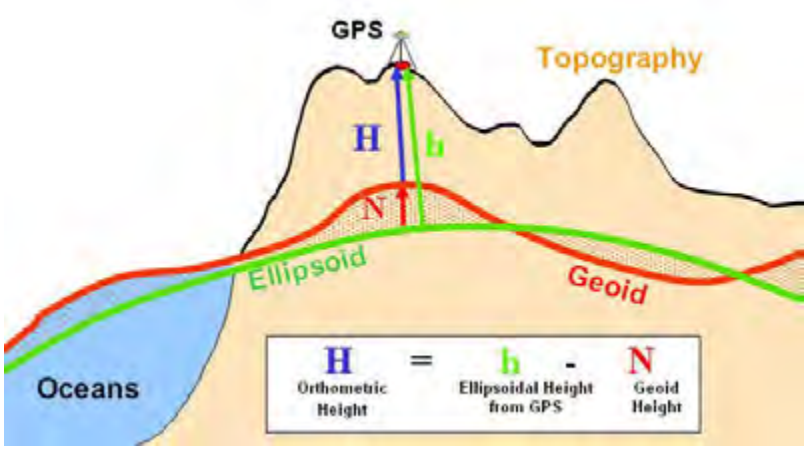

Figure 2.16: Reference geoid and ellipsoid earth model[56].

2.5.3 Land Cover Data

Land cover is defined as the observed physical cover on the earth's surface [57]. Whereas the DEM data provides a representation of the earth's physical terrain surface, land cover data provides a digital representation of the type of terrain surfaces. Land cover datasets are produced and provided by various agencies and organisations throughout the world. Datasets vary by the number of terrain classes defined, accuracy, quality and availability. There has not been a standard classification system used to describe land classes, thus some land cover dataset classes vary significantly and are inappropriate for particular purposes [57]. The datasets are also provided in different formats. There are two primary methods used to produce digital land cover datasets. These are by capturing land cover information via field surveys, or analysis of remotely sensed imagery. An example of a land cover dataset for Africa developed in the year 2000 is shown in Figure 2.17. A number of land cover data sources are considered and discussed in sections to follow.

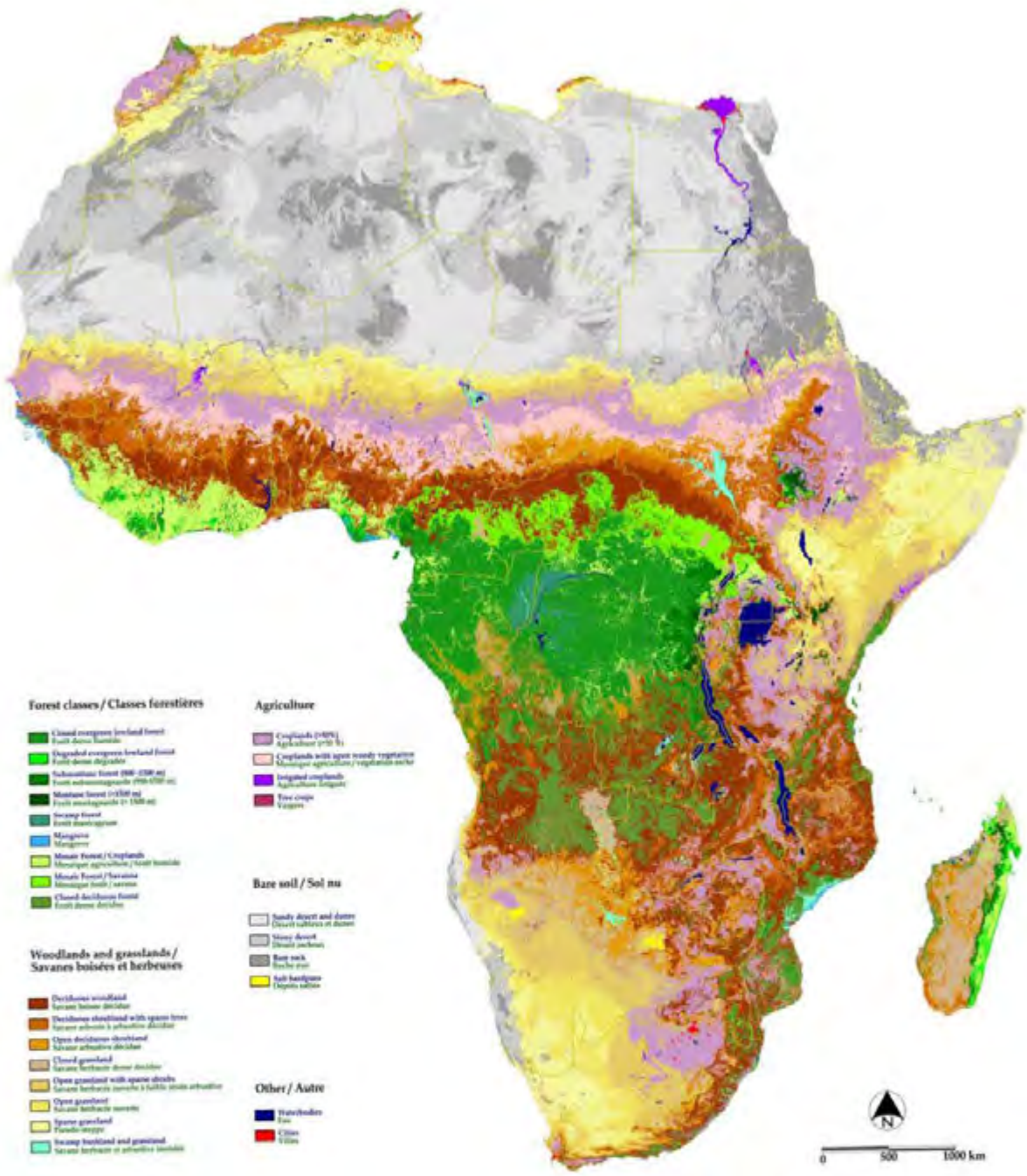

Figure 2.17: Land cover dataset for Africa developed in the year 2000 [58].

2.6 Chapter Summary

In this chapter, an overview of radar propagation, radar coverage, radar clutter and GIS related information were presented. These fields are aspects that are considered important for the development of a site specific radar coverage and land clutter modelling tool.

An overview of radar propagation is presented in section 2.1. Radar waves propagating through the atmosphere are subjected to signal distortions. These distortions need to be taken into account in a site specific radar coverage and land clutter modelling tool. These effects include diffraction of electromagnetic waves, refraction of electromagnetic waves caused by the atmosphere, the absorption or attenuation of radar wave energy due to the gases in the atmosphere, and earth curvature effects.

An overview of radar coverage is presented in section 2.2. It was found that for short range propagation modelling, the flat earth approximation holds. However for longer ranges and higher flying targets the spherical curvature of the earth needs to be taken into account. The radar horizon is a geometrical limiting effect that prevent radar detection's due to the target being below the tangent line that the radar makes with the earth. The radar horizon is thus one of the contributing factors that limits the maximum range of long range radars. Terrain obscuration, causes shadowing effects, as well as land clutter. Optimisation of radar deployment sites requires knowledge of which parts of the surrounding observed terrain is within the LOS and which areas are blinded, as well as to be able to determine the clutter contributions from the area of interest. It is important to model the terrain to determine shadow regions, and to characterise the land cover for land clutter modelling purposes.

An overview of the pattern propagation factor, F, is presented in section 2.3. The effects of the environment are included in the radar equation via means of the pattern propagation factor F. For monostatic radars, the received power is proportional to F^4. It has been noted that F^4 is inherently included in the measurement and modelling of the backscatter coefficient and attempts to separate it is not within the scope of this dissertation. F is assumed to include all propagation effects, including multipath and diffraction, between the radar and the clutter cell.

An overview of radar clutter is presented in section 2.4. Radar land clutter can be caused by terrain, vegetation and man made structures. Due to many distributed scatterers found over land terrain, land clutter is generally described and modelled by the radar cross section (RCS) per unit area of the clutter surface, called the backscatter coefficient, σ°. It was found that the backscatter coefficient is dependent on a number of factors, these include both radar and environment parameters. One of the most important factors that influences σ° is the grazing angle. Three grazing angle regions exist and reflectivity behave differ-

ently in these three regions. Standard probability density functions (PDF's) models can be used to describe the variation of different types of land clutter. From measurement data, statistical parameters required by these PDF models for different types of land clutter can be defined empirically. Empirical and semi-empirical models that describe the mean backscatter reflectivity σ° for various types of land terrain as a function of frequency, grazing angle and polarisation can also be developed from measurement data. Empirically derived PDF models would require large amounts of computer resources for use in a site specific radar coverage and land clutter modelling tool described in this study. Semi-empirical models describe the average backscatter coefficient given by simple formulas containing several parameters. These provide a quick and simple estimation of the backscatter coefficient and considered more suited to be used for developing a site specific radar coverage and land clutter modelling tool. Mathematical models can also be developed that provide an estimation to the the general shape of the backscatter coefficient. The nature of how a land clutter model was derived is thus an important factor to consider when determining the appropriate model to use for particular cases. Several existing land clutter models are investigated in sections to follow.

An overview of GIS data is presented in section 2.5. The types of GIS data considered important for site specific radar coverage and land clutter modelling are DEM and LC data. DEM data is required for determining land topography and LC data is required for characterising land cover. Several DEM and LC data sources are investigated in sections to follow.

Chapter 3

System Models, Processes and Data

This chapter provides a description of the models and processes of the different topics covered in the literature review. First it describes appropriate existing statistical and empirical monostatic radar land clutter / backscatter coefficient models, which is considered the main focus of this minor dissertation. It follows on by providing a description and overview of relevant digital elevation and land cover data sources that can be considered in simulation for areas within the SADC region. It then ends by describing the methods and processes used to simulate the clutter scene as well as a discussion on the required simulated clutter cell size, DEM resolution, and DEM height accuracy. This includes the description of proposed creation of clutter patches using meshing and grid methods, radar coverage using LOS ray tracing algorithms, and methods of simulating coherent clutter returns. As discussed in section 2.3, for the purposes of the land clutter / backscatter coefficient models and work presented below, it is assumed that the effects of propagation are necessarily included in RCS (σ) or backscatter coefficient (σ°) values by the pattern propagation factor F^4. If they are expressed without F^4, it is assumed to be inherently included and are in fact, averages of either σF^4 or $\sigma^\circ F^4$.

3.1 Land Clutter / Backscatter Coefficient Models

One of the fundamental procedures in developing a site specific radar land clutter modelling simulation, is to estimate the clutter strength from the area of interest. The land clutter strength can be characterised by a land clutter map. In order to estimate the clutter

strength from a particular area of interest, an appropriate land clutter model is required. Different clutter models are used for different clutter scenes, depending on the scene characteristics. The clutter strength received is determined by the backscatter coefficient from the land surface. Several clutter (backscatter coefficient) models are discussed in this section in order to determine the appropriate clutter models to use for a particular clutter scene and radar setup.

The reflectivity strength from land is a difficult phenomenon to document due to the wide variety of land types, surface roughness's, and describing area with specificity [10]. The backscatter coefficient is a useful parameter to use to for describing extended areas of various terrain types. There are hundreds of papers and texts on land clutter modelling in literature today. For the evaluation of clutter models for the purpose of site specific radar land clutter modelling, it was decided to only consider those models which appeared to the author as being well referenced and documented, and those that consider the varying grazing angles, terrain types, and frequencies of interest. Nine land clutter models are considered, namely:

1. Constant Gamma Land Clutter Model [14].
2. Morchin Land Clutter Model [15].
3. Kulemin Land Clutter Model [9].
4. Nathanson Land Clutter Model Tables [16].
5. Georgia Tech Research Institute (GTRI) Land Clutter Model [7].
6. Ulaby and Dobson Land Clutter Model [17].
7. σ° Generating Function Land Clutter Model [18].
8. Adapted Georgia Tech Research Institute (GTRI) Sea Clutter Model [19].
9. Billingsley Land Clutter Model [6].

Based on the information gathered, the above models will be classified as either a weak, strong, or excellent land clutter model to use for site specific radar land clutter modelling purposes. The classification will be based upon the model's validity, parameters taken into account, terrain types, angular and frequency ranges. This classification aims to represent

the extent to which a model agrees to real world land clutter situations, such that the most appropriate available model can be used for particular simulation and radar characteristics. It should be noted that a particular model can be considered valid and classified as an excellent model to use when restricted to certain grazing angle or frequency ranges, however the aim is to base the classification not only on specific ranges but as a general classification which takes into account all ranges of grazing angles and radar related frequencies of interests as well. This concept of results will be illustrated as well as tabulated in aid of developing algorithms for use in a site specific radar coverage and land clutter modelling tool.

3.1.1 Constant Gamma Land Clutter Model

Based on land clutter measurement data, Clapp [14], developed a simple model to characterise the backscatter from rough surfaces known as the constant gamma model, shown in Equation 3.1.

$$\sigma^{\circ} = \gamma \sin \delta \tag{3.1}$$

where δ is the grazing angle, and γ is a constant for specific terrain types. This model was found to be a reasonably good fit for uniformly, electromagnetically rough surfaces in the plateau region of grazing angles, approximately between 20° and 60° [16]. To account for different operating frequencies, a correction to the constant γ is performed, as shown in Equation 3.2 [16]. For a given terrain type, γ will vary with frequency. This is valid for operating frequencies from 1-10 GHz [10].

$$\gamma_{corrected} = \gamma + 5 \log(\frac{f}{f_0}) \tag{3.2}$$

where f is the operating frequency and f_0 is the base frequency of 10 GHz. Eight terrain classes are associated with the constant gamma land clutter model. The types of terrain classes and their associated γ value is shown in Table 3.1. The γ value is almost constant with different frequencies for rough terrain and increases slightly with frequency for smooth terrain.

Table 3.1: The value of γ for various terrain types.

Terrain Type	**Gamma γ [dB]**
Sea State 3	-40
Sea State 5	-30
Woods	-15
Metropolitan	0
Rugged Mountain	0
Farmland	-15
Wooded Hill	-10
Flatland	-20

Figure 3.1 shows the backscatter coefficient σ° in decibels for grazing angles ranging from 20° and 60°, for the various terrain types at 10 GHz using the constant gamma land clutter model.

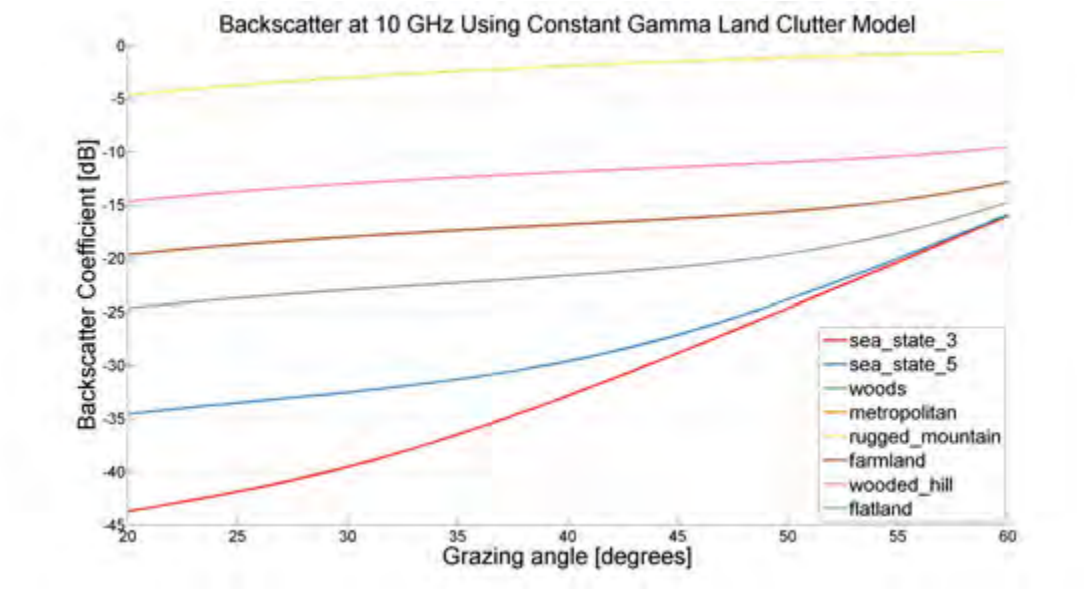

Figure 3.1: Backscatter coefficient at 10 GHz using the constant gamma land clutter model.

From Figure 3.1 it can be seen that there is a general increase in backscatter strength with the increase in grazing angle. There is also as much as 40 dB difference between terrain types at low grazing angles, which decreases to less than 10 dB as the grazing angle increases. This suggests that at extremely high grazing angles, the backscatter strength difference between terrain types are far lower than at grazing angles in the plateau region. The constant gamma model is a basic land clutter model that has been used to model backscatter coefficient values by a number of researchers and simulation tool developers for plateau grazing angles [59, 60, 61, 12]. The drawbacks of this model are the

limited grazing angle range, frequency range, and restrictions on the terrain classes and surface characteristics. It also does not take into account polarisation. Based on these, the constant gamma land clutter model can successfully be used to represent typical average backscatter coefficient values for plateau grazing angle regions for which the required frequency is limited to the valid frequencies of the model. In general, taking into account all regions of the identified parameters, and given the subsequent drawbacks discussed, the constant gamma land clutter model can be generally classified as a strong model to use for site specific radar land clutter modelling purposes.

3.1.2 Morchin Land Clutter Model

Morchin, in [15], presents a land clutter model that considers more parameters than the constant gamma land clutter model, for example, terrain type, radar wavelength (frequency), grazing angle, critical angle, surface roughness, and absorption in the altitude line clutter region. There is no mention of the specific grazing angle region that this model is valid for, but from information found in [62, 59], it is assumed that the model is valid for high grazing angle regions (70° to 90°). The Morchin land clutter model takes the form shown in Equation 3.3 [15].

$$\begin{aligned} \sigma^{\circ} &= A - 10\log\lambda + 10\log(\sin\delta) + 10\log[\cot^2\beta_0 \\ &\quad \exp(-\tan^2(B-\delta)/\tan^2\beta_0)] + \mu + \sigma_c \end{aligned} \tag{3.3}$$

$$\begin{aligned} where\ \sigma_c &= -10\log(\frac{\delta}{\delta_c}),\ \delta < \delta_c\ for\ desert \\ &\quad where\ \delta_c = \arcsin(\frac{\lambda}{4\pi h_e}); \\ &\quad where\ h_e \approx 9.3B_0^{2.2},\ \mu = \frac{\sqrt{f}}{4.7} \end{aligned}$$

where λ is the wavelength, δ is the grazing angle in degrees, σ_c is the critical angle, u is the surface roughness, and f is the frequency. A, B and β_0 are constants that were de-

rived from experiments. The Morchin land clutter model considers four terrain types and operating frequencies from $3-100$ GHz. The various terrain types, and corresponding constant values for each terrain type is shown in Table 3.2.

Table 3.2: Morchin land clutter model constant values for various terrains [59].

Terrain	A	B	β_0	σ_c
Desert	0.00126	$\pi/2$	0.14	δ/δ_c
Farmland	0.00400	$\pi/2$	0.2	1
Woodland	0.01260	$\pi/2$	0.4	1
Mountain	0.04000	1.24	0.5	1

Figure 3.2 shows the backscatter coefficient in dB for the various terrain types at 13.8 GHz using the Morchin land clutter model.

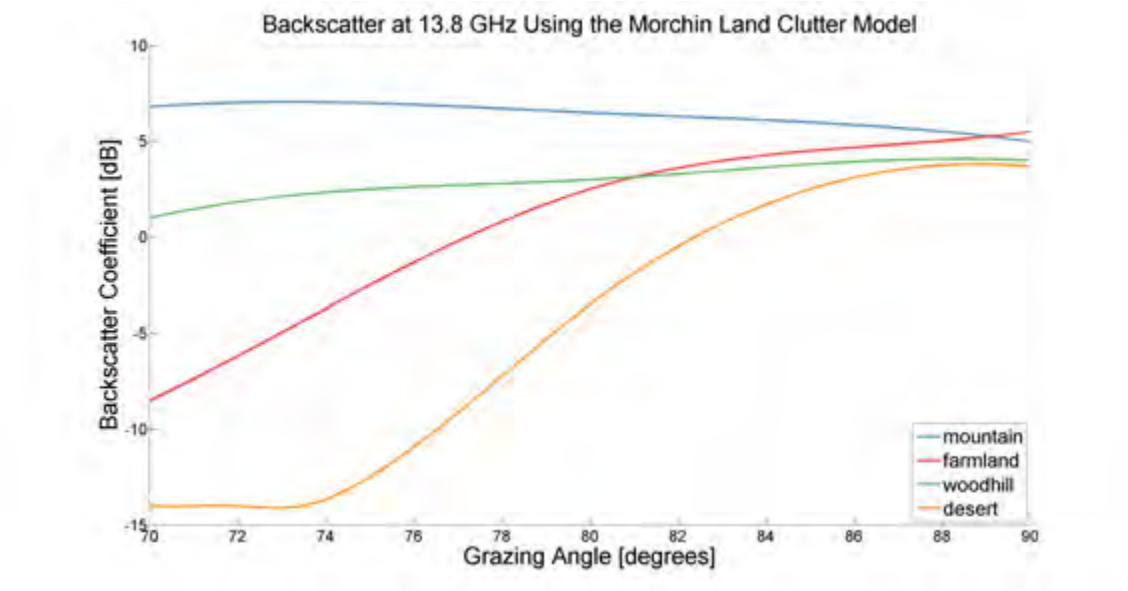

Figure 3.2: Backscatter coefficient in dB for the various terrain types at 13.8 GHz using the Morchin land clutter model [62].

The Morchin land clutter model is simple and considers many parameters not taken into account by others. However, the model does not take into account polarisation and works for only a limited range of grazing angles and terrain types. Generally for land based radars, the high grazing angle range is not of great significance as compared to low and plateau regions. Due to the limitations, the Morchin land clutter model would generally be classified as a weak model to use for site specific radar land clutter modelling purposes.

3.1.3 Kulemin Land Clutter Model

An empirical land clutter model was developed by the Institute for Radiophysics and Electronics of Nasu and takes on the form shown in Equation 3.4 [9].

$$\sigma^{\circ}(dB) = A_1 + A_2 \log \frac{\delta}{20} + A_3 \log \frac{f}{10} \tag{3.4}$$

where f is the frequency in GHz and δ is the grazing angle in degrees. $A_1 - A_3$ are constants for various terrain types as shown in Table 3.3.

Table 3.3: Terrain types and constants values for Kulemin land clutter model [9].

Terrain Type	A_1	A_2	A_3
Concrete	-49	32	20
Arable Land	-37	18	15
Snow	-34	25	15
Deciduous forests in summer	-20	10	6
Deciduous forests in winter	-40	10	6
Grass, height > 0.5 m	-21	10	6
Grass, height < 0.5 m	-25	10	6
Urban Territories	-8.5	5	2

This model is suitable for plane homogeneous, quasi smooth and rough land surfaces for a range of frequencies from 3-100 GHz and a limited grazing angle range from 15° to 30°. This model is quite limited as it does not give the full picture of the clutter distributions both for range and azimuth. An essential feature of this model is that it replaces the real variety of terrains in the observed radar environment, with a limited number of land surface types [9]. These limited number of terrain are sufficient for land clutter estimations in typical radar operation conditions.

Figure 3.3 shows the backscatter coefficient in decibels for grazing angles ranging from 15° to 30° for the various terrain types using the Kulemin land clutter model.

From Figure 3.3 it can be seen that the Kulemin land clutter model changes by less than 10dB over all characterised terrain types. The Kulemin model is a simple model to determine the backscatter coefficient for a large range of frequencies. However the grazing angle range is limited and lacks validation of the model for the full frequency range. One advantage however is that the model's terrain classes are classified in such a way that they encompass most of the terrain types seen in an operational radar environment. It also

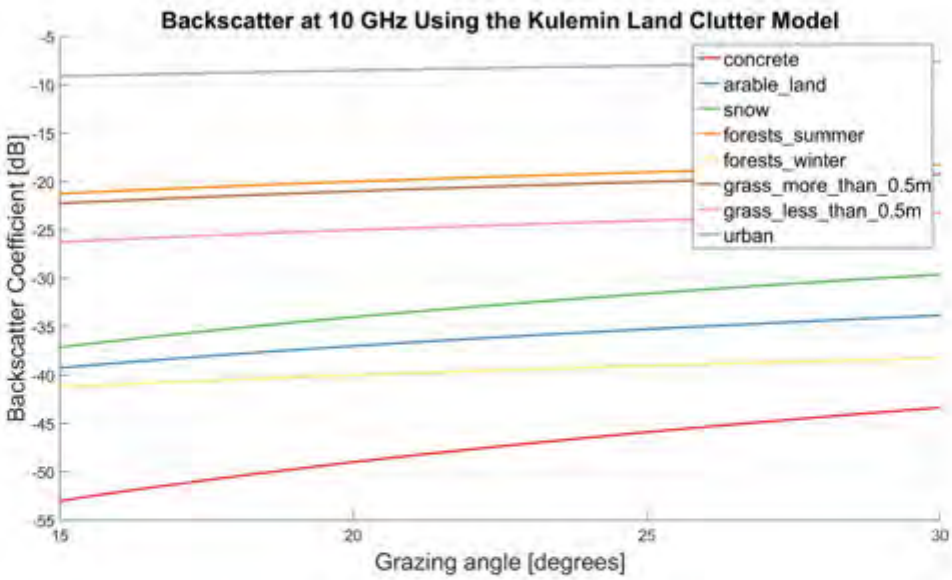

Figure 3.3: Backscatter coefficient at 10 GHz using the Kulemin land clutter model.

does not take into account polarisation effects. Based on the models limitations, and lack of validations, this model in general would be classified as a weak model to use for site specific radar land clutter modelling purposes.

3.1.4 Nathanson Land Clutter Model Tables

Nathanson, [16], provides a summary of the backscatter coefficient values from more than 50 investigators for various terrains and frequencies, at discrete grazing angles, namely $0° - 1.5°$, $3°$, $10°$, $30°$and $60°$. The tables provide the mean $\sigma°$ value, which is the average of horizontal and vertical polarisations. In some cases, it also attempts to define the statistics of the backscatter coefficient by S, which is the dB difference between the median value and 84^{th} percentile. This provides an indication of whether the distribution can be approximated by a Rayleigh distribution or not, but no further statistical information is provided [16]. The terrain types covered are deserts, farmlands, heavy woods / jungle and urban. The frequency bands covered are L, S, C, X, K_u and K_a bands. The Nathanson land clutter model tables are shown in Table 3.4.

Table 3.4: Nathanson land clutter model tables: (a) $0^\circ - 1.5^\circ$, (b) 3°, (c) 10°, (d)30°, (e) 60° [16].

(a)

Grazing angle $0^\circ - 1.5^\circ$	**Frequency Band**											
	L-band		**S-band**		**C-band**		**X-band**		K_u		K_a	
	σ_0	S	σ_0	S	σ_0	S	σ_0	S	σ_0	S	σ_0	S
Deserts	-44	-	-45	-	-39	-	-39	-7	-	-	-	-
Farmlands	-35	-9	-33	-9	-32	-7	-32	-12	-22	-12	-17	-
Heavy woods / jungle	-27	-7	-27	-12	-26	-12	-25	-12	-	-12	-20	-
Urban	-24	-	-22	-	-20	-	-19	>-12	-	-	-	-

(b)

Grazing angle 3°	**Frequency Band**											
	L-band		**S-band**		**C-band**		**X-band**		K_u		K_a	
	σ_0	S	σ_0	S	σ_0	S	σ_0	S	σ_0	S	σ_0	S
Deserts	-42	-	-37	-	-34	-	-31	-	-29	-	-	-
Farmlands	-31	-	-30	-	-29	-	-27	-7	-24	-7	-17	-
Heavy woods / jungle	-23	-	-24	-	-24	-	-23	-7	-23	-7	-18	-
Urban	-19	-	-18	-	-18	-	-17	-	-11	-	-	-

(c)

Grazing angle 10°	**Frequency Band**											
	L-band		**S-band**		**C-band**		**X-band**		K_u		K_a	
	σ_0	S	σ_0	S	σ_0	S	σ_0	S	σ_0	S	σ_0	S
Deserts	-37	-	-35	-	-32	-	-29	-	-27	-	-24	-
Farmlands	-29	-	-27	-	-25	-	-25	-	-21	-	-17	-
Heavy woods / jungle	-25	-	-23	-	-22	-	-22	-	-19	-	-18	-
Urban	-17	-	-17	-	-17	-	-15	-	-	-	-	-

(d)

Grazing angle 30°	**Frequency Band**											
	L-band		**S-band**		**C-band**		**X-band**		K_u		K_a	
	σ_0	S	σ_0	S	σ_0	S	σ_0	S	σ_0	S	σ_0	S
deserts	-27	-	-24	-	-22	-	-20	-	-18	-	-17	-
Farmlands	-19	-	-17	-	-15	-	-15	-	-15	-	-14	-
Heavy woods / jungle	-17	-	-15	-	-15	-	-13	-	-13	-	-11	-
Urban	-14	-	-12	-	-10	-	-9	-	-	-	-	-

(e)

Grazing angle 60°	**Frequency Band**											
	L-band		**S-band**		**C-band**		**X-band**		K_u		K_a	
	σ_0	S	σ_0	S	σ_0	S	σ_0	S	σ_0	S	σ_0	S
Deserts	-20	-	-16	-	-15	-	-13	-	-12	-	-12	-
Farmlands	-14	-	-15	-	-14	-	-13	-	-12	-	-12	-
Heavy woods / jungle	-18	-	-14	-	-14	-	-13	-	-11	-	-10	-
Urban	-11	-	-10	-	-9	-	-9	-	-	-	-	-

Due to the crude nature of the above model and severe limitations with regards to supported grazing angle ranges, Nathanson's land clutter model tables would in general be classified as a weak model to use for for site specific radar land clutter modelling purposes.

3.1.5 Georgia Tech Research Institute (GTRI) Land Clutter Model

In the late 1970's researchers at the Georgia Tech Research Institute (GTRI) conducted a number of radar land clutter measurement campaigns for various terrain types. During the 1980's they extended these measurement campaigns to include a range of frequencies. From these measurements they developed an empirical model that reflects the backscatter coefficient for various terrain types and frequencies at grazing angles in the plateau region between 20° and 65° [2]. The model takes into account the terrain type (seven classes), RMS surface roughness, wavelength / frequency (3-95 GHz) and grazing angle. This model is known as the GTRI land clutter model and takes the form shown in Equation 3.5 [7].

$$\sigma^{\circ}(dB) = A(\delta + C)^{B} \exp\left(\frac{-D}{1+\frac{0.1\sigma_h}{\lambda}}\right) \tag{3.5}$$

where σ_h is the RMS surface roughness, δ is the grazing angle in radians, and A, B, C and D are empirically derived constants for various terrain types and frequencies as shown in Table 3.5.

From Table 3.5 it can be seen that the GTRI land clutter model can be used for a number of terrain types and frequencies, however no data is available for L-band and for a few terrain types at certain frequencies. These are mainly for high frequencies between 35 GHz and 95 GHz for all terrain types, as well as lower frequencies between 3 GHz and 15 GHz for wet and dry snow terrain types. Figure 3.4 shows the backscatter coefficient in dBs for grazing angles ranging from 20°to 65°, for the various terrain types at 10 GHz using the GTRI land clutter model.

The GTRI land clutter model presents the mean σ° value. Different polarisations are not taken into account in this model. To improve the realism of this model, contributions from discrete scatterers need to be added. It should be noted that even though the GTRI

Table 3.5: Constant values for GTRI Land Clutter model for various terrain types and frequencies [2].

Constant	Frequency [GHz]	Soil / Sand	Grass	Tall Grass Crops	Trees	Urban	Wet Snow	Dry Snow
A	3	0.0045	0.0071	0.071	0.00054	0.362	-	-
	5	0.0096	0.015	0.015	0.0012	0.779	-	-
	10	0.25	0.023	0.006	0.002	2.0	0.0246	0.195
	15	0.05	0.079	0.079	0.019	2.0	-	-
	35	-	0.125	0.301	0.036	n/a	0.195	2.45
	95	-	-	-	3.6	n/a	1.138	3.6
B	3	0.83	1.5	1.5	0.64	1.8	-	-
	5	0.83	1.5	1.5	0.64	1.8	-	-
	10	0.83	1.5	1.5	0.64	1.8	1.7	1.7
	15	0.83	1.5	1.5	0.64	1.8	-	-
	35	-	1.5	1.5	0.64	-	1.7	1.7
	95	-	1.5	1.5	0.64	-	0.83	0.83
C	3	0.0013	0.012	0.012	0.002	0.015	-	-
	5	0.0013	0.012	0.012	0.002	0.015	-	-
	10	0.0013	0.012	0.012	0.002	0.015	0.0016	0.0016
	15	0.0013	0.012	0.012	0.002	0.015	-	-
	35	-	0.012	0.012	0.012	-	0.008	0.0016
	95	-	0.012	0.012	0.012	-	0.008	0.0016
D	3	2.3	0	0	0	0	-	-
	5	2.3	0	0	0	0	-	-
	10	2.3	0	0	0	0	0	0
	15	2.3	0	0	0	0	-	-
	35	-	0	0	0	-	0	0
	95	-	0	0	0	-	0	0

land clutter model can be used for grazing angles in all regions, there is no indication whether the values at low or high grazing angles are valid. The model should thus be used cautiously for low and high grazing angles [10]. The model has been used successfully by a number of researchers to predict the backscatter from terrains in the plateau grazing angle range. Further information on the use of the model and applications can be found in [34, 31, 63, 12].

Due to the model's versatility and use in many past applications, the GTRI land clutter model would be classified as a strong model to use for site specific radar land clutter modelling in the valid grazing angle, terrain types, and frequency ranges.

3.1.6 Ulaby and Dobson Land Clutter Model

Ulaby and Dobson [17] present a comprehensive set of land clutter models that have been derived from a number of measurement campaigns conducted by amongst others, Ohio State University, the US Naval Research Laboratory, NASA, University of Kansas and the University of Michigan. The set of models present average σ° data versus terrain type and incidence angle with respect to nadir, polarisation and carrier frequency. Their

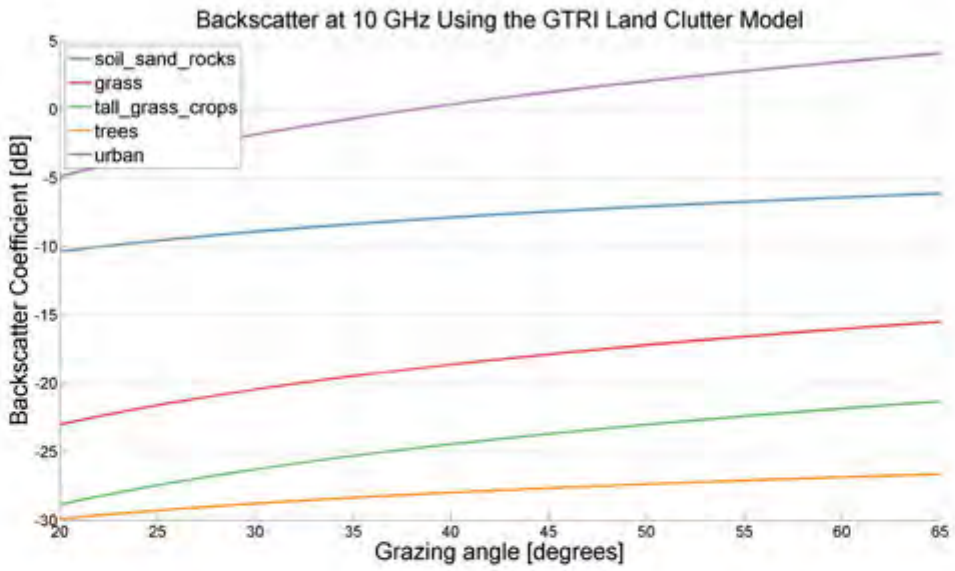

Figure 3.4: Backscatter coefficient at 10 GHz using the GTRI land clutter model.

model covers a range of terrain types, frequencies and angles in the plateau and high grazing angle region (10° to 90°). The Ulaby and Dobson set of models include tabulated data and graphs on the mean, standard deviation, median, 5^{th}, 25^{th},75^{th}, 95^{th} and most extreme percentile values of the distribution as a function of terrain type, incidence angle, polarisation and carrier frequency. In addition it also provides probabilities of occurrence of average σ° [17].

The model takes into account nine terrain types that are characterised as follows:

1. Barren and sparsely vegetated land. Classified in the model as “Soil and rock surfaces”.

2. Forests and orchids. Classified in the model as “Trees”.

3. Grasses. Classified in the model as “Grasses”.

4. Shrubs, bushy plants, and other crops. Classified in the model as “Shrubs”.

5. Grass, shrubs and wetlands. Classified in the model as “Short vegetation”.

6. Man-made surface. Classified in the model as “Road surfaces”.

7. Residential, commercial and industrial areas. Classified in the model as “Urban”.

8. Dry snow. Classified in the model as “Dry snow”.

9. Wet snow. Classified in the model as “Wet snow”.

The data for the nine terrain types are grouped to their corresponding frequency bands. The range of frequencies included in this model are L, S, C, X, K_u, K_a and W bands. Then for each terrain category and frequency band, the data are arranged by polarisation and valid incidence angles. Three polarisation types are included, namely HH, VV, and HV [10]. The data for each category can be found in the appendix section of [17]. It should be noted that the validity of the data provided is not the same for all categories. They differ by the valid incidence angle ranges and number of observations taken. Some categories can be classified as having insufficient data due to the low number of observations taken. An overview of the source data in terms of number of observations and the range of valid incidence angles is given in Tables 6.6 through to 6.8, from [17].

From the datasets provided, Ulaby and Dobson derived an empirical model for the mean value as a function of incidence angle, for each terrain category, frequency band and polarisation. The model takes the form shown in Equation 3.6. This relationship between the mean value of σ° was calculated by a least squares curve fitting process for each terrain type [10].

$$\sigma^\circ_{mean}(dB) = P_1 + P_2 \exp(-P_3\theta) + P_4 \cos(P_5\theta + P_6) \tag{3.6}$$

where θ is the incidence angle expressed in radians and P_1 through to P_6 are empirically derived constants which differ for each category type. This model is only valid for the categories with sufficient data. Expressions to compute the standard deviation SD is also given, as shown in equation 3.7.

$$SD(dB) = M_1 + M_2 \exp(-M_3\theta) \tag{3.7}$$

where M_1through to M_3 are resultant coefficients used for the standard deviation function. For instances where the sample space is small, (i.e. N<6), the values for M are statistically insignificant and are therefore not included [17]. From computed values for the σ°_{mean} and SD, the 5^{th} and 95^{th} percentile values are then given as shown in Equation 3.8 and 3.9. These are based upon the assumption of Gaussian distributions.

$$\sigma^{\circ}_{5\%}(dB) = \sigma^{\circ}_{mean} + 1.645 \times SD \tag{3.8}$$

and

$$\sigma^{\circ}_{95\%}(dB) = \sigma^{\circ}_{mean} - 1.645 \times SD \tag{3.9}$$

By taking the compliment of the incidence angle, the above models can easily be expressed in terms of the grazing angle instead. The values for P and M can be found in the appendix section of [17] for each category. Table 3.6 provides a summary of the valid grazing angle ranges of each terrain type category, for the various frequency bands and polarisations. The categories with a null, indicates insufficient data where equations 3.6 to 3.9 can not be used. Ulaby and Dobson do however provide mean values for a limited range of discrete grazing angles for categories that are classified as having insufficient data. These values should be used with caution. As shown in Table 3.6, the urban terrain type has no sufficient data for all frequency ranges and polarisations.

Figure 3.5 shows the backscatter coefficient in dBs for the various terrain types at 10 GHz using the Ulaby and Dobson land clutter model for polarisations HH, HV and VV.

These plots agree with the valid grazing angle ranges and terrain types as shown in Table 3.6. Snow terrain types were purposefully excluded from the plot as snow rarely falls within the SADC region. It is assumed that a Log-normal distribution is generally accepted to provide a good fit to the measured data [17].

The Ulaby and Dobson land clutter model provides valid data for a range of terrain types, frequencies and polarisations at grazing angles in the plateau and high region. Caution should be taken when using the Ulaby and Dobson model for categories which has insufficient data, especially for urban terrain which has no sufficient data for all categories. Caution should also be taken when using the model for certain grazing angle ranges, as many of the categories valid range differs from the assumed 10° to 90° as shown in Table 3.6. Due to the many advantages and extra information given for the Ulaby and Dobson model as compared to others, this model would in general be classified as an excellent model to use for site specific radar land clutter modelling for grazing angles ranging in

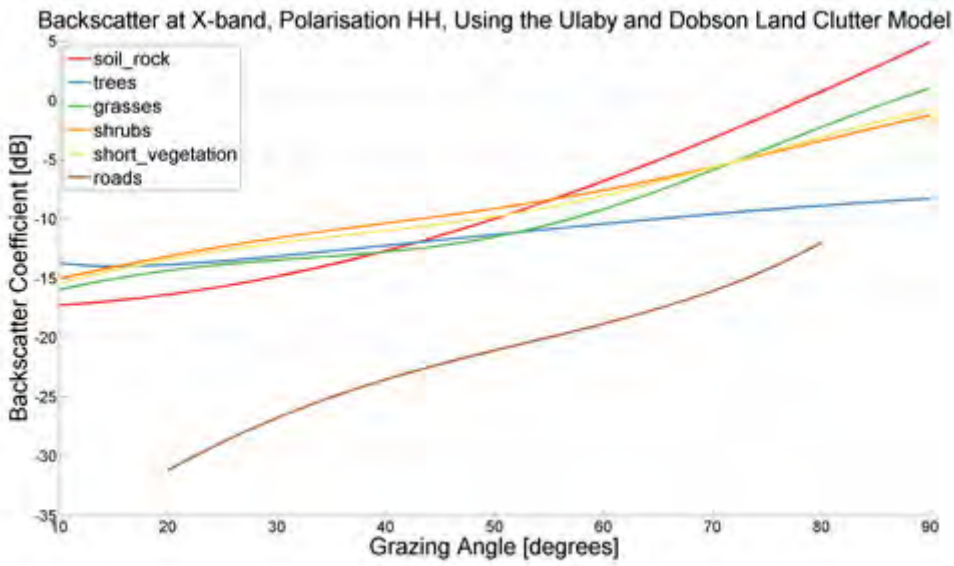

(a)

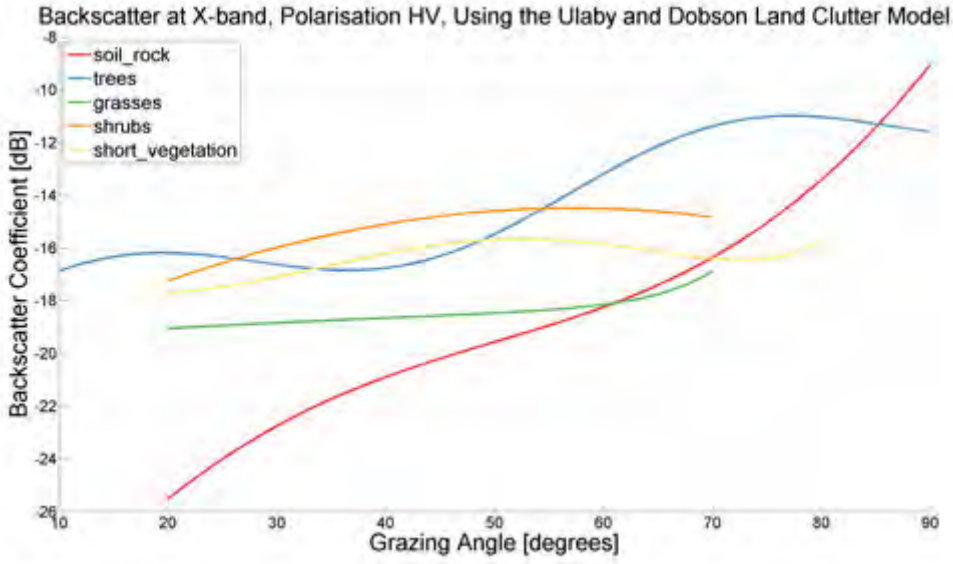

(b)

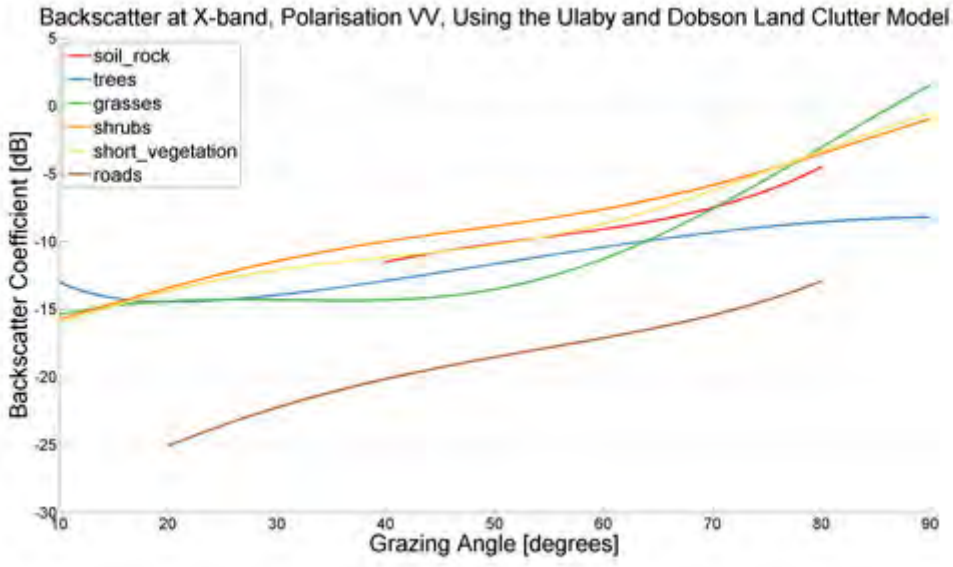

(c)

Figure 3.5: Backscatter coefficient in dBs for the various terrain types at 10 GHz using the Ulaby and Dobson land clutter model for polarisations (a) HH, (b) HV and (c) VV.

Table 3.6: Valid grazing angle ranges of each terrain type category, for the various frequency bands and polarisations: (a) HH polarisation, (b) HV polarisation, (c) VV polarisation.

(a)

Polarisation HH	Valid Grazing Angle Ranges [degrees]								
	Terrain Types								
Radar Bands	Soil & Rock	Trees	Grasses	Shrubs	Short Veg	Road Surfaces	Urban	Dry Snow	Wet Snow
L	40-90	-	10-90	10-90	10-90	-	-	20-90	20-90
S	40-90	-	10-90	10-90	10-90	-	-	20-90	20-90
C	40-90	-	10-90	10-90	10-90	-	-	20-90	20-90
X	10-90	10-90	10-90	10-90	10-90	20-80	-	15-90	20-90
K_u	10-30	10-90	10-90	10-90	10-90	20-80	-	15-90	15-90
K_a	-	-	20-80	20-70	10-90	20-80	-	15-90	20-90
W	-	-	-	-	-	-	-	-	-

(b)

Polarisation HV	Valid Grazing Angle Ranges [degrees]								
	Terrain Types								
Radar Bands	Soil & Rock	Trees	Grasses	Shrubs	Short Veg	Road Surfaces	Urban	Dry Snow	Wet Snow
L	40-90		10-90	10-90	10-90	-	-	20-90	20-90
S	50-90		10-90	10-90	10-90	-	-	20-90	20-90
C	40-90		10-90	10-90	10-90	-	-	20-90	20-90
X	20-90	10-90	20-70	20-70	20-80	-	-	15-70	15-90
K_u	30-80	10-90	20-50	20-50	20-90	-	-	15-90	15-90
K_a	-	-	-	-	-	-	-	-	-
W	-	-	-	-	-	-	-	-	-

(c)

Polarisation VV	Valid Grazing Angle Ranges [degrees]								
	Terrain Types								
Radar Bands	Soil & Rock	Trees	Grasses	Shrubs	Short Veg	Road Surfaces	Urban	Dry Snow	Wet Snow
L	40-90	-	10-90	10-90	10-90	-	-	20-90	20-90
S	50-90	-	10-90	10-90	10-90	-	-	20-90	20-90
C	40-90	-	10-90	10-90	10-90	-	-	20-90	20-90
X	20-80	10-90	10-90	10-90	10-90	20-80	-	20-90	20-90
K_u	30-90	10-90	10-90	10-90	10-90	20-80	-	20-90	20-90
K_a	-	-	20-80	20-70	10-80	20-80	-	20-90	20-90
W	-	-	-	-	-	-	-	15-90	15-50

the plateau region.

3.1.7 σ° Generating Function Land Clutter Model

Often backscatter coefficient models are developed that are described by a set of equations which yields a constant given a fixed set of measurement conditions. Due to the nature of these models, they therefore lack randomness of true σ°observations. Mediavalli and Connor [18], realised that in order to develop a land clutter model that produces backscatter values that reflect the randomness of true σ° observations, it should be based upon real world backscatter characteristics. There are two possibilities to develop such a model, firstly a complicated electromagnetic model could be used that calculates the scattering of various terrain types in a Monte Carlo fashion, or to develop a generating function model

that returns values similar to those of measured terrain reflection coefficients. They argued that all the previous models would be generally unacceptable to use for model validation as they were deterministic in nature and repeatedly produced identical backscatter values, for a given category [64].

The data that they decided to base their model on was the Ulaby and Dobson set of radar scattering statistics for terrain. The data presented by Ulaby and Dobson does not represent the actual backscatter numbers, but rather data of the statistical properties of the backscatter numbers and their frequency of occurrence in histogram form. The data reflects the reality in which σ° from different terrain types is determined by the actual properties of the terrain.

The requirements for the generator were that the attributes of the coefficients in this generator need to behave in a certain way. The mean and standard deviation of the generated distributions of σ° need to approach those of the measured data, and the frequency of occurrence must be similar to the original data. The generator was thus designed such that it returns values that are similar to the observed measurement terrain scattering data found in [17]. The generator should output values for all terrain types, polarisations, and radar bands associated with the Ulaby and Dobson datasets.

They developed a probabilistic land clutter model (i.e. a model that does not repeatedly produce identical backscatter values for a given category setup, but produces results of varying values that conform to the statistical nature of real world measurements for a given category setup), that returns the σ° for any combination of terrain type, frequency band, polarisation and grazing angle that would be similar to, and have similar statistical properties as the observed data by Ulaby and Dobson. Thus instead of using Ulaby and Dobson's empirical model that only provides a deterministic answer, use the statistical data gathered by Ulaby and Dobson to develop a probabilistic σ° generating land clutter model. Thus being able to obtain any percentile statistic and statistical properties rather than only the mean values.

The generating function is defined by Equation 3.10 [18].

$$\sigma^\circ = \beta(-\ln(U)^\alpha) + \gamma \tag{3.10}$$

where β is the amplitude term, α is the skewness parameter and γ is the distribution adjustment term. These model parameters are chosen in such a way that they produce backscatter values that form a set of combinations that yield the required mean and standard deviation values for each category. An optimisation algorithm is used to correctly choose values for α and β for a fixed γ value, such that it generates the desired mean and standard deviation values with minimum error (i.e. the aim is to minimise the error between the generated standard deviation and mean values and those from the measured data determined by Ulaby and Dobson). If the algorithm rejects the distribution, the γ term either increases or decreases until the output of mean and standard deviation is acceptable [18].

As with the Ulaby and Dobson land clutter model, this generator is limited to the categories of data sets where sufficient data exists. The categories with insufficient data thus corresponds with the null areas shown in Table 3.6. For conditions of low grazing angle, an adapted version of the GTRI sea clutter model was used. The use of the GTRI sea clutter model for determining reflectivity from low angle land clutter is discussed in section 3.1.8.

Figure 3.6 shows the mean reflected energy σ° in dBs for the various terrain types at 10 GHz, polarisation HH, using the generating function developed by Mediavalli and Conner. The number of samples used to generate the below plot was $N = 1000000$.

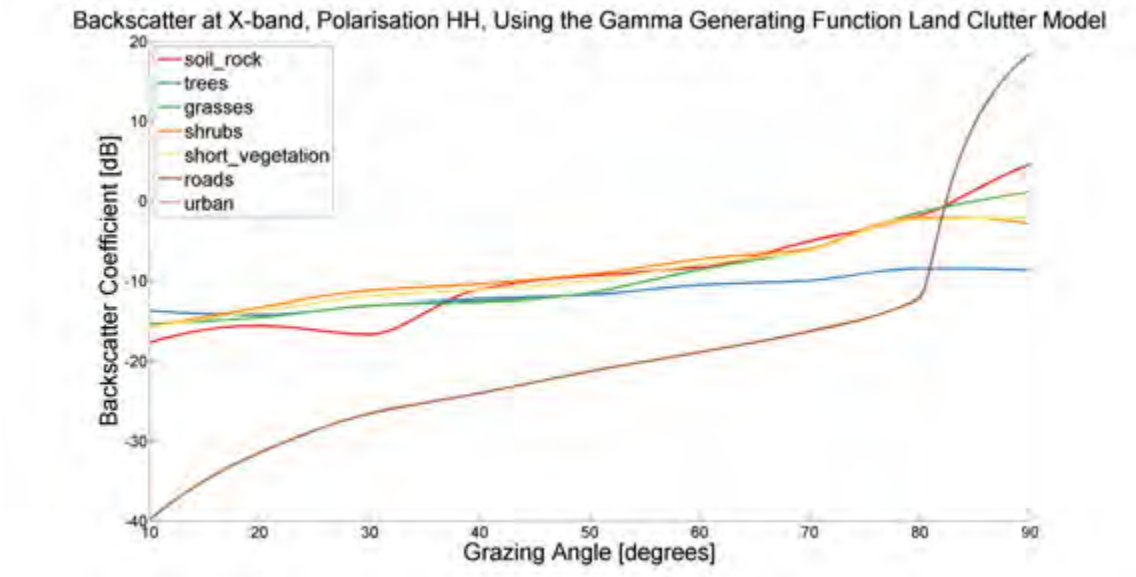

Figure 3.6: Mean reflected energy σ^0 in dBs for the various terrain types at 10 GHz, polarisation HH, using the generating function developed by Mediavalli and Connor.

Due to the fact that this model is based upon datasets by Ulaby and Dobson, it represents the same advantages as well as disadvantages and limitations. However the gamma generating function generates a probabilistic output instead of deterministic at a better angular resolution than the standard Ulaby and Dobson model [18]. The probabilistic nature makes it suitable for validation purposes. This is an excellent model to use to simulate any percentile statistic and backscatter characteristics that behaves in a similar way to real world observed data. The model does however use more computing resources than the Ulaby and Dobson model due to its probabilistic nature. The σ° generating function land clutter model would in general be classified as an excellent model to use for site specific radar land clutter modelling for grazing angles ranging in the plateau region.

3.1.8 Adapted GTRI Sea Clutter Model

The GTRI sea state clutter model provides mean clutter strength predictions for land clutter in low grazing angle range, or where no available measurements are given for a particular angular extent of the generating function model by Mediavalli and Conner. This model is used due to the scarcity of measured data in the low grazing angle range (0°to 15°) .

Mediavalli and Connor decided that for cases of low grazing angle regions (0°to 15°), where there is a scarcity of measured data, they would adapt and use the GTRI sea clutter model. The adaptation to the model allows the surface roughness to be changed from very smooth to very high by changing certain descriptors of the GTRI model. They argued that the shapes of different sea states in the low grazing angle region is similar to different surface roughness terrain types producing different shapes for σ°. The adaptation uses the different sea state models to relate to different terrain types of different surface roughness [19]. The GTRI sea state model equations are shown below [2].

For 1 to 10 GHz

$$\sigma^{\circ}_{HH} = 10\log[3.9 \times 10^{-6} \lambda \delta^{0.4} A_i A_u A_w] \tag{3.11}$$

For 1 to 3 GHz

$$\sigma^{\circ}_{VV} = \sigma^{\circ}_{HH} - 1.73\ln(h_{av} + 0.015) + 3.76\ln(\lambda) + 2.46\ln(\delta + 0.0001) + 222 \quad (3.12)$$

$$\sigma_{\phi} = (14.5\lambda + 5.5)\delta h_{av}/\lambda \quad (3.13)$$

$$A_i = \sigma^4_{\phi}/(1 + \sigma^4_{\phi}) \quad (3.14)$$

$$A_u = \exp[0.2\cos\phi(1 - 2.8\delta)(\lambda + 0.015)^{-0.4} \quad (3.15)$$

$$qw = 1.1(\lambda + 0.015)^{0.4} \quad (3.16)$$

$$V_w = 8.67h^{0.4}_{av} \quad (3.17)$$

$$A_w = [1.94V_w/(1 + V_w/15.4]^{qw} \quad (3.18)$$

where λ is the radar wavelength, δ is the grazing angle, ϕ is the angle between antenna boresight and wind direction, h_{av} is the average wave height, A_i is the interference factor, A_u is the upwind-downwind factor, A_w is the wind speed factor, V_w is the velocity of the wind, qw is the power factor and σ°_{ϕ} is the calculated backscatter. These sea state descriptor values are shown in Table 3.7.

The decisions made as to which sea state to assign to a particular terrain type is as follows. Firstly it compares the number of facets available, and the average slope of the facets. In the cases where there is data available, the sea state to use is experimentally determined by matching the roughness of the terrain type with the roughness of the equivalent sea state model. In the cases where no data is available, terrain types with smooth surfaces such as snow is given smaller sea states, and terrain types with rough surfaces such as trees is given larger sea state values [19].

Table 3.7: GTRI sea state for wind speed and wave height descriptor values [19].

Sea state	**Wind speed** [ms^{-1}]	**Wave height** [m]
smooth	<3.5	<0.3
slight	3.5-6.2	0.3-0.9
moderate	6.2-8.2	0.9-1.5
rough	8.2-9.8	1.5-2.4
very rough	9.8-11.8	2.4-3.7
high	11.8-15.4	3.7-6
very high	15.4-23.2	6-12.2

Figure 3.7 shows the reflected energy σ° in dBs for the various terrain types at 10 GHz using the adapted GTRI sea clutter model.

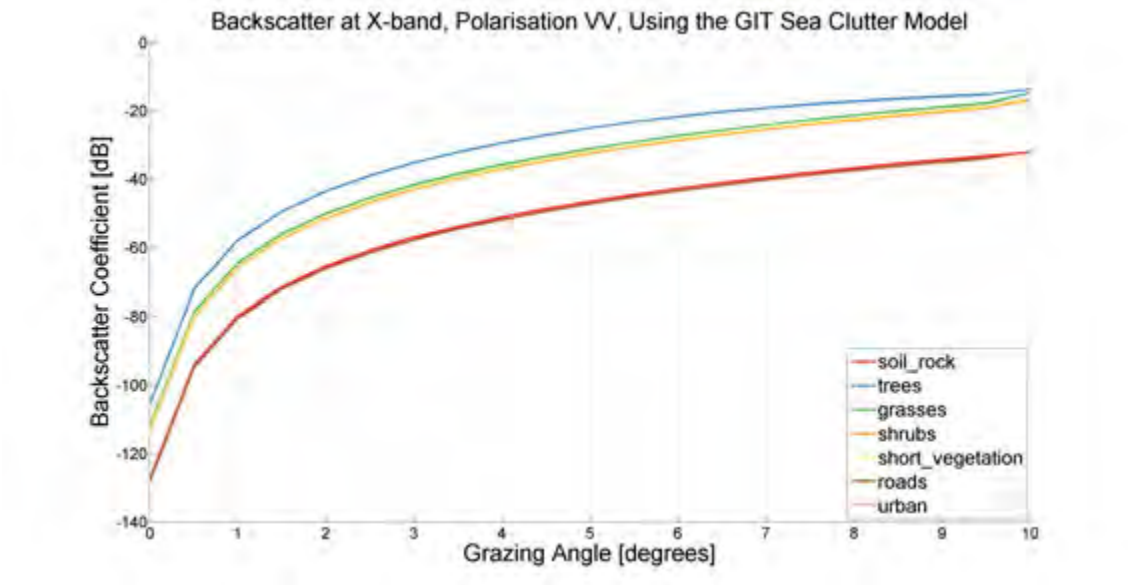

Figure 3.7: Backscatter at X-band, Polarisation HH, Using the Adapted GTRI Sea Clutter Model.

The adapted GTRI sea state model can be used to model reflectivity in the low grazing angle region, due to the similarities of the shapes of σ° between different sea states, and those related to terrain type surface roughness. However, it should be noted that this model does not reflect the true complex nature of σ° at low grazing angles and should be used with caution. Due to the limitations of this model, the adapted GTRI sea clutter model would in general be considered a weak model to use for site specific radar land clutter modelling in the low grazing angle region.

3.1.9 Billingsley Land Clutter Model

The text by Billingsley [6], provides an extremely comprehensive set of models that specifically focuses on low grazing angle land clutter. Most of these models and current information available on low angle land clutter characteristics was uncovered by Billingsley during his time at Massachusetts Institute of technology/Lincoln Labs (MIT/LL). Some of the important conclusions made by Billingsley on low angle clutter are:

1. Land clutter at low grazing angles are characterised by patchiness / lack of uniformity in spatial extent, due to shadowing and due to extreme resolution dependencies leading to large resolution cell-to-cell variability.

   (a) Higher radar spatial resolution leads to less averaging and therefore more variability.

   (b) Note that resolution changes the shape of the whole spatial amplitude distribution (PDF), not just the tails.

2. Clutter amplitude statistics in the low-grazing angle region are characterised by distributions with long tails (spiky clutter), making Weibull and Log-Normal distributions suitable choices to model their probability density functions (PDFs).

3. The long tails of the distributions are due to the prevalence of terrain shadowing and multipath at these low grazing angles.

4. In general, rough surfaces have a larger σ° than smooth surfaces for low grazing angles (conversely, at very high grazing angles (near 90°), smooth surfaces exhibit a higher σ° than rough ones).

Billingsley's land clutter models are unconventional compared to other models that focus on clutter in the plateau and high grazing angle region. Firstly, Billingsley notes that at low-grazing angles, it is not practical to take grazing angle into consideration in the conventional sense on a micro facet grazing angle level. He reasons that digital elevation model (DEM) data is just not at a high enough resolution to sensibly incorporate into low-angle clutter models. In addition he mentions that DEM data also does not take into account the discrete elements that dominate scintillation of land clutter at low angles. He mentions that all attempts to this extent have failed. Thus instead of grazing

angle, Billingsley classifies his models in terms of the depression angle, which is relatively simple and unambiguous quantity to determine. The differences between depression angle, and grazing angle are shown in section 2.4.3.2.

Secondly, Billingsley notes that at low depression angles, the effective F^4 term is different in each resolution cell and thus can significantly affect the clutter strength measurement (i.e. greater significance as compared to those from higher grazing angles). The effect of F^4 is thus much more of a concern at low depression / grazing angles. Billingsley also uses the standard $\frac{4}{3}$ Earth Model to account for effects of earth curvature and atmospheric refraction. Thus at short range where effects of refraction are negligible, grazing angle and depression angle are assumed to be equal.

For smaller depression angles, the standard deviations from measurements are much larger than for a Rayleigh distribution. For decreasing depression angles, the ratio of the average to median σ° values increase substantially. This indicates that there is a large increase in the standard deviation with decreasing depression angles. At low angles, F increases rapidly and thus backscatter strength from scatterers increase rapidly as well with height above the ground. Land objects, even at small heights can cause considerable shadowing effects. Thus changes in F^4 are exaggerated at smaller depression angles. According to Billingsley, for farmlands at low depression angles, there is a large increase in spread when the resolution cell size is decreased, this is due to strong dominating discrete scatterers. However, for forests at low depression angles, less spread occurs when the resolution cell size is decreased, because the forest is a more homogeneous surface. For forests at high depression angles, even less spread is seen as a result of improved illumination. Urban terrain also show decreasing spread with increasing angle, but with a much stronger average backscatter than for corresponding rural / low relief terrain distributions [10].

Thirdly, due to the nature of F at low depression angles, Billingsley places a strong dependence of the spread of land clutter distributions on spatial resolution.The spatial resolution or cell size A in m^2 is defined by Equation 3.19,

$$A = r \times \triangle r \times \triangle \theta \tag{3.19}$$

where r is the range, $\triangle r$ is the range resolution, and $\triangle \theta$ is the beamwidth. The spatial

resolution cell area, A, from the geometry of land clutter for a surface radar is shown in Figure 3.8.

From various land clutter measurement campaigns during Billingsley's time at MIT/LL, he developed an angle specific land clutter model for the prediction of ground clutter amplitude statistics of directly visible terrain at low depression angles. The model provides the amplitude statistics for various terrain types and frequencies, as shown in Table 3.8. The model is provided within a context of Weibull statistics, where $\overline{\sigma_W^\circ}$ is the Weibull mean strength and a_w is the Weibull shape parameter. The model is dependent on frequency due to individual scatterers within a resolution cell that are frequency dependent. There is however a stronger dependence on the a_w weibull parameter on spatial resolution. Each $\overline{\sigma_W^\circ}(dB)$ is a mean of $\sigma^0 F^4$ values calculated from the Weibull equation 2.15, by using the associated a_w value and the measured median of $\sigma^\circ F^4$. The terrain descriptor classifies terrain in terms of its roughness or relief (slope), and its land cover. The Billingsley angle specific land clutter model is shown in Table 3.8.

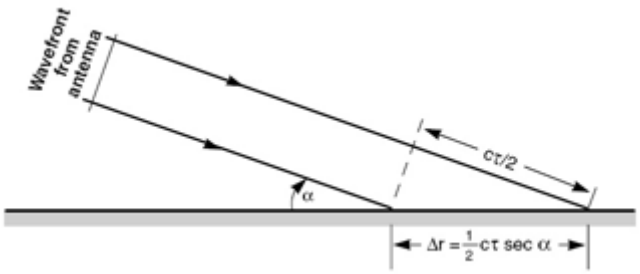

(a)

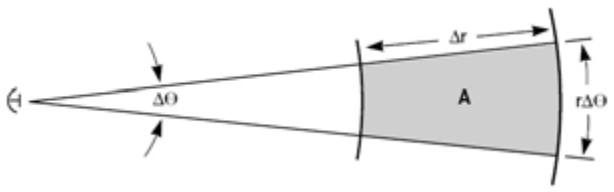

(b)

Figure 3.8: Spatial resolution cell area, A, from the geometry of land clutter for a surface radar: (a) elevation view, (b) plan view [6].

Table 3.8: Billingsley's angle specific land clutter model [6].

Terrain Type	Depression Angle (deg)	$\overline{\sigma_w^\circ}$ (dB) Frequency Band					a_w Resolution(m^2)	
		VHF	UHF	L-	S-	X-Band	10^3	10^6
Rural/Low-Relief								
a) General rural	0.00 to 0.25	-33	-33	-33	-33	-33	3.8	2.5
	0.25 to 0.75	-32	-32	-32	-32	-32	3.5	2.2
	0.75 to 1.50	-30	-30	-30	-30	-30	3.0	1.8
	1.50 to 4.00	-27	-27	-27	-27	-27	2.7	1.6
	> 4.00	-25	-25	-25	-25	-25	2.6	1.5
b) Continuous forest	0.00 to 0.30	-45	-42	-40	-39	-37	3.2	1.8
	0.30 to 1.00	-30	-30	-30	-30	-30	2.7	1.6
	> 1.00	-15	-19	-22	-24	-26	2.0	1.3
c) Open farmland	0.00 to 0.40	-51	-39	-30	-30	-30	5.4	2.8
	0.40 to 0.75	-30	-30	-30	-30	-30	4.0	2.6
	0.75 to 1.50	-30	-30	-30	-30	-30	3.3	2.4
d) Desert, marsh, or grassland (few discretes)	0.00 to 0.25	-68	-74	-68	-51	-42	3.8	1.8
	0.25 to 0.75	-56	-58	-46	-41	-36	2.7	1.6
	> 0.75	-38	-40	-40	-38	-26	2.0	1.3
Rural/High-Relief								
a) General rural	0 to 2	-27	-27	-27	-27	-27	2.2	1.4
	2 to 4	-24	-24	-24	-24	-24	1.8	1.3
	4 to 6	-21	-21	-21	-21	-21	1.6	1.2
	> 6	-19	-19	-19	-19	-19	1.5	1.1
b) Continuous forest	any	-15	-19	-22	-22	-22	1.8	1.3
c) Mountains	any	-8	-11	-18	-20	-20	2.8	1.6
Urban								
a) General urban	0.00 to 0.25	-20	-20	-20	-20	-20	4.3	2.8
	0.25 to 0.75	-20	-20	-20	-20	-20	3.7	2.4
	> 0.75	-20	-20	-20	-20	-20	3.0	2.0
b) Urban, observed on open low-relief terrain	0.00 to 0.25	-32	-24	-15	-10	-10	4.3	2.8
Negative Depression Angle								
a) All, except mountains and high-relief continuous forest	0.00 to -0.25	-31	-31	-31	-31	-31	3.4	2.0
	-0.25 to -0.75	-27	-27	-27	-27	-27	3.3	1.9
	< -0.75	-26	-26	-26	-26	-26	2.3	1.7

The model thus provides, per terrain type, the Weibull mean clutter strength $\overline{\sigma_W^0}$ as a function of frequency (VHF through to X-band), and the Weibull shape parameter a_w as a function of the spatial resolution A. The shape parameter spans over a range between 10^3 and 10^6 m^2. The shape parameter for a certain spatial resolution is thus obtained from linear interpolation on $\log(A)$ between the values that are provided for $A = 10^3$ m^2 and

$A = 10^6\ m^2$.

Figure 3.9 shows the reflected mean energy $\sigma^\circ F^4$ in decibels for the various terrain types at 10 GHz using the Billingsley angle specific land clutter model.

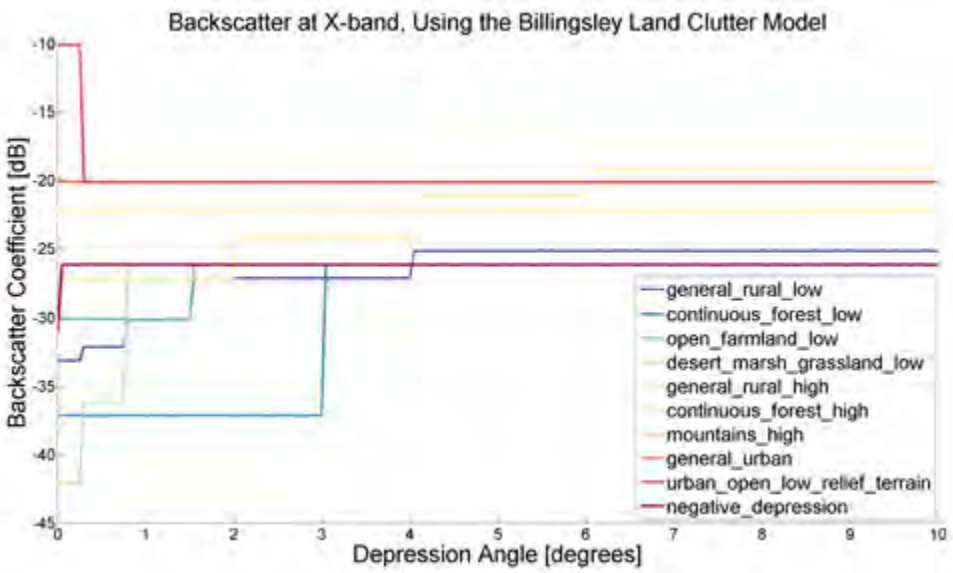

Figure 3.9: Reflected energy $\sigma^0 F^4$ in dBs for the various terrain types at 10 GHz using the Billingsley angle specific land clutter model.

$\sigma^\circ F^4$ is not a constant value over time and space, as shown in Figure 2.13. From this figure it can be seen that there is wide scatter at VHF, and less scatter as the frequency increases. The standard deviation thus decreases with increasing frequency from 16.6 dB at VHF, to 5.8 dB at X-band. Billingsley also reports that the differences in mean clutter levels for HH and VV polarisations are small, and thus do not need to be taken into account, as well as for changes in weather and season. Figure 3.10 shows how the mean ground clutter strength can vary with frequency as a function of terrain type [10].

It is clear that Billingsley is the authoritative model to use for low angle land clutter and it is strongly recommended that Billingsley's models be used at low angle clutter regions, supplemented by DEM data to determine terrain visibility and mean depression angle. This is also one of the only models to take into account terrain relief as well as VHF and UHF frequency bands. For geometries involved with ground radar, especially at low grazing angles, the surface slope is a significant factor to define the clutter environment. The model is given in terms of Weibull statistics thus any percentile clutter statistic can be determined. One of the drawbacks of the Billingsley land clutter models is that it does not take into account frequencies higher than X-band, as well as C-band. Due to the many

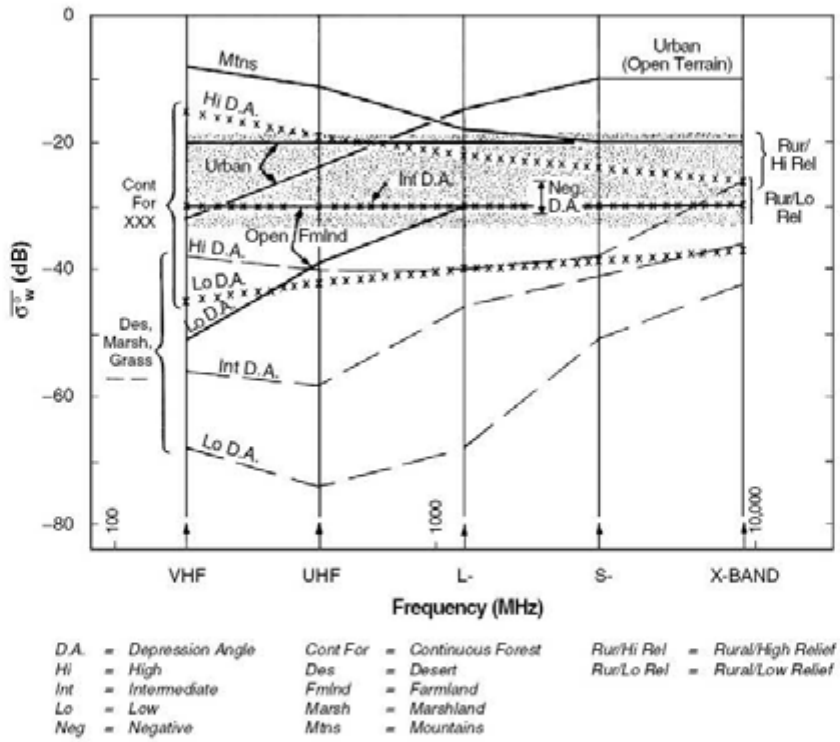

Figure 3.10: Mean clutter strength versus frequency for all measured terrain types [47].

advantages and information provided by Billingsley on low angle radar land clutter, the angle specific land clutter model by Billingsley would be considered an excellent model to use for site specific radar land clutter modelling in the low grazing angle region.

3.1.10 Land Clutter Models Discussion and Summary

System engineers have been using land clutter models for years to estimate the average σ° vs grazing angle δ. Basic models such as the constant gamma model, where σ° varies in direct proportion to δ, have been commonly used to estimate σ° and grazing angle dependence in the plateau region.

The range of grazing angles that is applicable to a model changes and depends on a number of factors, such as the surface roughness in terms of the radar wavelength and surface contour. Shadowing by hills, mountains and man made structures can limit the range of grazing angles that simple models such as the constant gamma model can be used for. Most models however do not consider terrain relief. The intensity of the clutter depends on terrain topography, terrain type, and radar operating parameters.

Due to repeated measurement campaigns both for radar and remote sensing research over

the years, there is a considerable amount of knowledge available for σ° from L through to K_a bands for the plateau and high grazing angle regions. There is also a comprehensive set of average σ° data as a function of radar frequency and terrain type in these grazing angle regions. Empirical land clutter models were developed from measured data using regression methods to estimate model parameters. There is however few sources of data available for low grazing angle regions. The only source that has comprehensively studied reflectivity from land in the low grazing angle region is Billingsley, whom has provided datasets for VHF through to X-band frequencies for low grazing angle regions. Generally for the plateau and high grazing angle regions, σ° decreases with decreasing grazing angle, but Billingsley has shown that at very low grazing angles this is untrue. He found that the median of average values of $\sigma^\circ F^4$ over the five considered radar bands was roughly the same ($\approx$ -30 dB for terrain type "general rural"), also that the spread of $\sigma^\circ F^4$ increases with decreasing frequencies. Thus $\sigma^\circ F^4$ can either be much larger or much smaller at lower frequency bands than at higher ones. However for smoother land surfaces with a few discretes, it was found that the median of average values for $\sigma^\circ F^4$ generally decreases with decreasing frequency.

In terms of polarisations, most of the available data are for HH and VV polarisations, or an average of the two. Few data sources are available for HV and VH polarisations and none for circular polarisation in terms of terrain backscatter [10]. Currently only the Ulaby and Dobson and Generating Function Land Clutter models take into account polarisation.

The types of clutter models that were presented were, basic and simple mathematical land clutter models, semi-empirical land clutter models, and empirical land clutter models which describe statistical behaviour. The simple models are based upon mathematical formulas that provide an estimation to the the general shape of the backscatter coefficient for different terrain types and frequencies, at grazing angles in the plateau region.

Semi-empirical models are based upon fitting model equations to observed data using the polynomial fit algorithms such as the least squares. These models thus output the backscatter coefficient that has the same mean value as the observed data, for different terrain types and frequencies at different grazing angles. Most semi-empirical models average out HH and VV polarisations, however there are a few that take polarisation into account as well. It is important to note that these models are deterministic in nature and do not represent the true statistical nature of σ^0 for different terrains.

The empirical models presented are based upon using observed terrain datasets as a reference to develop a probabilistic model that can be used to generate σ° values that behave in the same statistical nature as the statistics of the observed data. They use typical PDF models in which the corresponding PDF parameters are empirically derived. Any percentile statistic can be determined and not only a deterministic average value. These models inherently require more computer resources.

These empirical land clutter models are good for providing non-site specific clutter maps that describe the statistical properties of the clutter strength for different radars. These are thus mostly used to model the patchiness of clutter and not relevant for specific regions, terrain features and radar position. Site specific clutter models however represent the clutter intensity over a particular radar operation site of interest [63]. These models are dependent upon detailed information about the site.

A summary of the land clutter models discussed in this dissertation is shown in Table 3.9. Further analysis and comparisons of the listed land clutter models are investigated in section 4.1. Results obtained from this investigation further justifies the 'Model Validity / Compatibility' parameter seen in Table 3.9.

Table 3.9: Land clutter models summary.

Land Clutter Model	Type of Model	Terrain Types		Dependencies	Frequency Range	Grazing Angle Range	Polarisation Range	Type of Output	Validity / Model Strength
Constant Gamma	Mathematical	• Sea state 3 • Sea state 5 • Woods • Metropolitan	• Rugged mountain • Farmland • Wooded hill • Flatland	• Frequency • Grazing angle • Terrain type (based on Y constant)	3 – 10 GHz	20º - 60º	N/A	• Deterministic output • Mean (average) backscatter coefficient σº (dB)	• Medium validity • Strong model
Morchin	Mathematical	• Desert • Farmland • Woodland • Mountain		• Frequency • Grazing angle • Critical angle • surface roughness • Terrain type (based on model constants)	3 – 100 GHz	70º - 90º	N/A	• Deterministic output • Mean (average) backscatter coefficient σº (dB)	• Low validity • Weak model
Kulemin	Semi-Emiprical	• Concrete • Arable land • Snow • Deciduous and coniferous forest in summer	• Deciduous and coniferous forest in winter • Grass height more than 0.5m • Grass height less than 0.5m • Urban territories	• Frequency • Grazing angle • Terrain type (based on model constants)	3 – 100 GHz	15º - 30º	N/A	• Deterministic output • Mean (average) backscatter coefficient σº (dB)	• Low validity • Weak model
Nathanson	Semi-Emiprical	• Deserts • Farmlands • Heavy woods • Urban		• Frequency • Grazing angle • Terrain type	• 1 – 18 GHz • 27 – 40 GHz	• 15º - 30º • 3º • 10º • 30º • 60º	N/A	• Deterministic output • Mean (average) backscatter coefficient σº (dB) • Indication on whether values can be approximated by Rayleigh statistics	• Low validity • Weak model
GTRI	Semi-Emiprical	• Soil, sand and rocks • Grass • Tall grass crops • Trees	• Urban • Wet snow • Dry snow	• Frequency • Grazing angle • Surface roughness • Terrain type (based on model constants)	• 2 – 18 GHz • 27 – 40 GHz • 75 – 100 GHz	20º - 65º	N/A	• Deterministic output • Mean (average) backscatter coefficient σº (dB)	• Medium validity • Strong model

Ulaby and Dobson	Semi-Emiprical	• Soil and rock surfaces • Trees • Grasses	• Shrubs • Short vegetation • Urban areas • Snow dry • Snow wet	• Frequency • Incidence angle (Grazing angle) • Polarisation • Terrain type (based on model constants)	• 2 – 18 GHz • 27 – 40 GHz • 75 – 100 GHz	10º - 90º	• HH • HV • VV	• Deterministic output • Mean (average) backscatter coefficient (dB) • Standar deviation • 5^{th} percentile backscatter coefficient (dB) • 95^{th} percentile backscatter coefficient (dB)	• High validity between 20º and 70º • Low validity elsewhere • Excellent model
Gamma Generating Function	Emperical / Probabalistic	• Soil and rock surfaces • Trees • Grasses • Shrubs	• Short vegetation • Urban areas • Snow dry • Snow wet	• Frequency • Incidence angle (Grazing angle) • Polarisation • Terrain type (based on model constants)	• 2 – 18 GHz • 27 – 40 GHz • 75 – 100 GHz	10º - 90º	• HH • HV • VV	• Probabilistic output • Mean (average) backscatter coefficient (dB) • Standard deviation • Any percentile backscatter coefficient (dB)	• High validity between 20º and 70º • Low validity elsewhere • Excellent model
Adapted GTRI Sea Clutter Model	Semi-Empirical	For any terrain type. Based on the surface roughness of the terrain.		• Frequency •Grazing angle • Polarisation • Terrain type (based on model constants)	3 – 100 GHz	0º - 10º	N/A	• Deterministic output • Mean (average) backscatter coefficient σ^{0} (dB)	• Low validity • Weak model
Billingsley	Emperical / Probabalistic	• High or Low Relief: General Rural • High or Low Relief: Continuous forest • High or Low Relief: Desert • High or Low Relief: Marsh	• High or Low Relief: Grassland • High or Low Relief: Open farmland • High or Low Relief: Urban • Low relief negative depression angle	• Frequency • Deperession angle • Terrain type • Weibull shape parameter (dependent on spatial resolution). • Weibull scale parameter (dependent on mean values).	• 0.03 – 4 GHz • 8 – 12 GHz	• 0º - 10º • Negative depression angles	N/A	• Probabilistic output • Mean (average) backscatter coefficient (dB) • Standard deviation • Any percentile backscatter coefficient (dB)	• High validity • Excellent model

3.2 GIS Data

A fundamental procedure required in developing a site specific radar coverage and land clutter modelling tool, is the creation of the radar observed environment. Inputs that are required are DEM data, as well as land cover data for particular areas of interest. For the purpose of this dissertation, the focus of the simulation area will be the SADC region. Site specific clutter models are thus dependent upon detailed information of the radar observed environment. This information can be provided by DEM and Land Cover data [63].

3.2.1 Digital Elevation Model Data

DEM data is required to model the topography of the land for the simulated area of interest. The data is also required in a site specific radar coverage and land clutter modelling tool to determine facets, surface contours (slopes) and terrain shadowing regions. Several sources of DEM data are proposed and discussed. These are:

1. Shuttle Radar Topography Mission (SRTM) Digital Elevation Model Data.
2. Advanced Spaceborne Thermal Emission and Reflection Radiometer (ASTER) Global Digital Elevation Model (GDEM) Data.
3. Digital Terrain Elevation Data (DTED).
4. Astrium Digital Elevation Model Data.

Based on the information gathered, the above DEM's will be classified as either a weak, strong, or excellent DEM dataset to use for site specific radar coverage and land clutter modelling purposes. The classification will be based upon the model's validity, availability, resolution, accuracy, parameters taken into account, terrain classes covered and cover over SADC region.

3.2.1.1 Shuttle Radar Topography Mission (SRTM) Digital Elevation Model Data

SRTM datasets are remote sensed data that were obtained during an eleven day flight of the space shuttle endeavour and operated by NASA, DLR, and others in the U.S. The

Shuttle Radar Topography Mission (SRTM) was flown from 11/02/2000 to 22/02/2000. NASA and NGA worked together to acquire radar data from this mission that was used to create the first near-global set of land elevations [65].

Two radars were used for this process: a C-band Spaceborne Imaging Radar and a X-band Synthetic Aperture Radar (X-SAR). The shuttle flew at an altitude of 233 km, transmitting 1700 microwave pulses per second. These signals were reflected by the earth's surface and detected as radar echoes. The two radars were used to collect interferometric data, which is the comparison of two radar images or signals taken at slightly different angles. The mission used single pass interferometry, which acquired two sets of signals at the same time by using two different radar antennas [65]. One antenna was located on board the space shuttle and another was placed at the end of a 60 m mast that was extended from the shuttle, as shown in Figure 3.11.

Figure 3.11: Interferometric process from the SRTM space shuttle [65].

The SRTM mission successfully collected radar data over more than 80% of the earth's land surface between 60° north and 56° south latitude with data points that were sampled at every 1 arc second ($\approx$ 30 m). Post processing of the data was completed and resulted in three types of datasets, namely SRTM non-void filled, SRTM void filled and SRTM 1 arc second global. A description of the SRTM datasets is shown below:

1. **SRTM Non-Void Filled** datasets were processed from raw C-band SRTM data at NASA's Jet Propulsion Laboratory (JPL). These datasets were processed at a post spacing resolution of 1 arc second ($\approx$ 30 m) for areas within the US. For areas outside the US, the datasets were processed at a post spacing resolution of 3 arc seconds ($\approx$ 90 m).

2. **SRTM Void Filled** datasets are a result of additional processing done to the SRTM non-void filled dataset to address areas that have missing data or voids. These voids were a result of processing that did not meet quality specifications. The voids were filled using interpolation algorithms and other sources of elevation data. This dataset is available at a a post spacing resolution of 1 arc second ($\approx$ 30 m) for areas within the US and 3 arc seconds ($\approx$ 90 m) for areas outside the US.

3. **SRTM 1 Arc Second Global** datasets offer a worldwide coverage of the void filled SRTM data at a post spacing resolution of 1 arc second ($\approx$ 30 m).

All three datasets are available in three file formats, namely Digital Terrain Elevation Data (DTED), Band Interleaved by Line (BIL), and Georeferenced Tagged Image File Format (GeoTIFF). A summary of these datasets and formats is shown in Table 3.10.

Table 3.10: SRTM dataset characteristics.

Dataset type	Resolution	Vertical accuracy [m]	File formats	Projection	Raster size	Voids filled
SRTM Non-Void Filled	1 arc second US coverage 3 arc seconds global	$\approx +-5$	DTED, BIL or GeoTIFF	Geographic WGS84	1×1 degree tiles	No
SRTM Void Filled	1 arc second US coverage 3 arc seconds global	$\approx +-5$	DTED, BIL or GeoTIFF	Geographic WGS84	1×1 degree tiles	Yes
SRTM 1 Arc Second Global	1 arc second global	$\approx +-5$	DTED, BIL or GeoTIFF	Geographic WGS84	1×1 degree tiles	Yes

All versions and formats of the SRTM datasets are freely available, and currently being distributed for download from [66]. The SRTM 30 m dataset is currently the highest quality, resolution and accuracy DEM data that is freely available for download for the intended SADC region of interest. Due to this, SRTM 30 m would be classified as an excellent DEM dataset to use for use in a site specific radar coverage and land clutter modelling tool.

3.2.1.2 Advanced Spaceborne Thermal Emission and Reflection Radiometer (ASTER) Global Digital Elevation Model (GDEM) Data

ASTER GDEM is a set of digital elevation data covering most of land on earth, specifically land surfaces between $83°N$ and $83°S$. This was produced by the Japanese Ministry of Economy Trade and Industry (METI) in collaboration with the US National Aeronautics and Space Administration (NASA) using multispectral imaging data collected by the ASTER radiometer on board the Terra satellite.

There are two versions of the ASTER GDEM data available, version 1 and version 2. The files are available for download in Geotiff signed 16 bits format which includes a header file that provides all necessary geo-referencing information needed. Each tile is 1 degree latitude by 1 degree longitude cell in size consisting of 3601 by 3601 pixels. The data files are referenced to WGS84 ellipsoid and not the EGM96 geoid such as DTED data files [67]. A summary of the format information is shown in Table 3.11.

Table 3.11: Format information for ASTER GDEM DEM and QA files [67].

File information	DEM file and QA plane file
Output format	Geotiff, signed 16 bits
Geographic coordinates	Geographic latitude and longitude. WGS84 geodetic system
Tile size	3601×3601 pixels (1×1 degree)
Posting interval (resolution)	1 arc second (30 m)
Vertical accuracy [m]	$\approx +- (7-9)$
Coverage	North 83 degrees to South 83 degrees, 22600 tiles

Both versions have a resolution of 30 m (1 arc second sampling intervals). Version 2 is the improved dataset with higher quality and accuracy than version 1. Version 2 has enhanced accuracy due to the use of multiple images over the same area. For each GDEM tile, a quality assessment file QA of the same tile size is included as well. This file represents the number of scene based DEM's (number of images) that has contributed to the final DEM value at each pixel in the DEM file. It also provides the location of data anomalies that have been corrected and the data source used for the correction [68]. ASTER GDEM data files are available for download freely over the internet from the ASTER GDEM website at [67].

The ASTER GDEM solution provides a high resolution (1 arc second post interval spacing) elevation dataset in Geotiff format for the required SADC region of interest that is suitable for use in a site specific radar coverage and land clutter modelling tool. It should be noted that through inspection of the dataset for the SADC region, it was found that this data has some remaining artefacts that cause artificial hills, ridges and surface roughness that do not exist in reality. The dataset should thus be used with caution. Due to this, ASTER GDEM version 2 dataset would be classified as a good DEM dataset to use for use in a site specific radar coverage and land clutter modelling tool.

3.2.1.3 Digital Terrain Elevation Data (DTED)

Digital terrain elevation data (DTED) [69], is a standard of digital elevation datasets which is a uniform matrix of terrain elevation values that provide basic data for systems and applications that require terrain elevation, slope or surface roughness information. The dataset was developed by the National Imagery and Mapping Agency (NIMA) funded by the U.S. Department of Defence. These datasets were developed in support of U.S. military operations. The first set was originally developed in the 1970's for the purpose of supporting aircraft radar simulation and prediction modelling .

All DTED datasets are described as the height above the EGM96 Geoid reference and not above the WGS84 ellipsoid. DTED data are available in three levels of resolution i.e. level 0, 1 and 2. Each DTED file contains elevation data for a 1 degree latitude by 1 degree longitude cell. These levels are described in Table 3.12. DTED datasets has the format/file extension .dt0, .dt1 or .dt2 depending on the DTED level chosen. All DTED dataset files contain a header file which provides the geo-referencing information [70].

Table 3.12: DTED levels description.

DTED Level	Resolution [arc second]	Vertical accuracy [m]	Row×Column [N×M]	Tile Size [N×S]
0	30	$\approx +-(10-100)$	1200×1200	1×1
1	3	$\approx +-(10-30)$	2400×2400	1×1
2	1	$\approx +-(10-20)$	3600×3600	1×1

DTED level 0 has a resolution of 30 arc seconds ($\approx$ 900 m). This DTED level is considered cartographic DTED, meaning that the DTED datasets were derived from existing charts and manually entered into a computer to create the DTED file. DTED level 0 datasets thus are known to have varying levels of quality and accuracy. DTED level 1 has

a resolution of 3 arc seconds ($\approx$ 90 m), and considered to be a basic medium resolution dataset. DTED level 1 has a resolution of 1 arc second ($\approx$ 30 m), and considered to be a basic high resolution dataset. DTED level 1 datasets has a quality measurement of less than 90% confidence of a linear error of less than 30 m, and a horizontal error of less than 50 m. DTED level 2 datasets has a 90% confidence of less than 18 m and a horizontal error of less than 23 m. This means that 9 out of 10 measurements should be less than the spacing value listed but potentially the tenth value could have an error greater than that spacing value [70].

The distribution and availability of DTED products is authorised by the U.S Department of Defence. DTED level 0 is freely available for download through the internet within copyright restrictions, however level 1 and 2 DTED datasets are not freely available for download. DTED level 1 and 2 are specifically suited for military activities.

The DTED solution provides a high to low resolution (1-30 arc second post interval spacing) elevation dataset in Geotiff format for the required SADC region of interest. However only the low level dataset is freely available for download. The low level dataset can be used to provide a rough idea of terrain shadowing effects but would not be sufficient to use in a site specific radar coverage and land clutter modelling tool. DTED 30 m (level 2) would be classified as an excellent dataset for use in a site specific radar coverage and land clutter modelling tool.

3.2.1.4 Astrium Data

Astrium Geo-Information Services is a European company generating one of the best digital elevation data sets currently available. They provide a dataset for any land area in the world with various resolutions ranging from 30 m down to 1 m. The dataset has a vertical accuracy of 2 m relative and 4 m absolute, which is significantly better than any DTED, ASTER GDEM or STRM datasets. All datasets are based upon optical and radar technologies. The quality and accuracy is achieved from extensive post processing of the data to conform to the true nature of the land. Astrium offers a solution of highest data quality and accuracy compared to DTED or ASTER GDEM sources, however this data is not freely available. Astrium's standard offerings and prices are available on their website at [71]. A summary of the features of the available Astrium datasets are shown below in

Table 3.13.

Table 3.13: Elevation datasets currently available from Astrium [72].

Type of Dataset	Resolution (grid spacing) [m]	Vertical accuracy [m]	Coverage area	Date derived from
WorldDEM	12	2	Pole to pole coverage	TerraSAR-X and TanDEM-X radar satellite missions
Elevation 30	30	8	> 75 million km^2	SPOT 5 optical satellite data. Voids filled with TerraSAR-X data
Elevation 10	10	5	Regional coverage on request	TerraSAR-X radar satellite data
Elevation 8	8	3	Regional coverage on request	SPOT 6 stereo and tri stereo optical satellite data
Elevation 4	4	2	Regional coverage on request	Pleiades stereo and tri stereo optical satellite data
Elevation 1	1	1.5	Regional coverage on request	Pleiades stereo and tri stereo optical satellite data

DEM data from Astrium would be the ideal set to use for site specific radar land clutter modelling as it represents the most recent and true nature of land topography. The drawback is the cost as it would become extremely expensive to purchase all the datasets to cover the SADC region. For example, a 30 m resolution data set from Astrium for the whole of South Africa's land areas (about 1 214 000 sq. km), at the standard price of the Euro, at €2.3 per sq. km, this Astrium data would cost approximately €2.792 M or R36.149 M. Astrium data should be classified as an excellent dataset, however due to the financial constraints involved in acquiring this dataset, the Astrium solution would not be desirable to use for site specific radar coverage and land clutter modelling.

3.2.2 Land Cover Data

Land cover data is required to model the terrain cover for the simulated area of interest. Several sources of land cover data are proposed and discussed. These are:

1. Global Land Cover Data (GlobeLand 30).

2. South African National Land Cover Data (NLC) 1994, 2000, 2005, 2009.

3. Global Land Cover (GLC) 2000 Data.

4. Global Land Cover by National Mapping Organisations (GLCNMO)

5. Global Land Cover Share (GLC-Share)

Based on the information gathered, the above land cover datasets will be classified as either a weak, strong, or excellent land cover dataset to use for site specific radar land clutter modelling purposes. The classification will be based upon the model's validity, resolution, parameters taken into account, terrain classes covered and cover over SADC region.

3.2.2.1 Global Land Cover Data (GlobeLand30)

With the demand for improved global land cover data at higher spatial resolutions and accuracy, China embarked upon a global land cover mapping project in 2010. This project produced the first 30 m resolution global land cover dataset with 10 classes of terrain types. This dataset covers land cover of the earth between 80° N to 80° S longitude.

The data and images that were used for the development of GlobeLand30 were multispectral images from the US land resources satellite (Landsat), as well as multispectral images from China's Environmental Disaster Alleviation Satellite (HJ-1). Auxiliary data from existing land cover datasets and online resources were also used during the processing and development of GlobeLand 30.

GlobeLand30 includes 10 land cover types, namely, cultivated land, forest, grassland, shrubland, wetland, water bodies, tundra, artificial surfaces, bareland, permanent snow and ice. A description for each of these land types is shown below.

1. **Cultivated Land** includes land types that are used for agriculture, horticulture, gardens, paddy fields, irrigated and dry farmland, vegetation and fruit gardens, etc.

2. **Forest** includes land types that are covered with trees, with vegetation cover of more than 30%, as well as deciduous and coniferous forests and sparse woodland with cover of between 10 - 30%, etc.

3. **Grassland** include land types that are covered by natural grass with cover of more than 10 %.

4. **Shrubland** includes land types that are covered with shrubs with cover more than 30%, including deciduous and evergreen shrubs and desert steppe with cover more than 10%, etc.

5. **Water Bodies** includes land types that have water bodies in the area, including rivers, lakes, reservoirs, fish ponds, etc.

6. **Wetland** includes land types that are covered with wetland plants and water bodies, including inland marsh, lake marsh, river floodplain wetland, forest / shrub wetland, peat bogs, mangrove and salt marsh, etc.

7. **Tundra** includes land types that are covered by lichen, moss, hardy perennial herb and shrubs in the polar regions, including shrub tundra, herbaceous tundra, wet tundra and barren tundra, etc.

8. **Artificial Surfaces** includes land types that are modified by human activities, including all kinds of habitation, industrial and mining area, transportation facilities, and interior urban green zones and water bodies, etc.

9. **Barelands** includes land types that are covered with vegetation cover lower than 10%, including desert, sandy fields, Gobi, bare rocks, saline and alkaline lands, etc.

10. **Permanent Snow and Ice** includes land types that are covered by permanent snow, glacier and icecap.

GlobeLand30 adopts the geographic WGS84 coordinate system. The data is available in GeoTIFF file format and consists of five parts, namely, classification result file, coordinate information file, map setting file of classification image, metadata file and illustrative file. The overall accuracy of GlobeLand30 is approximately 80.33%. The dataset can be downloaded freely over the internet from the GlobeLand30 website at [73].

GlobeLand30 is currently the latest and most up to date freely available land cover dataset available for the SADC region. It takes into account terrain classes which can be related to land clutter models. It is also of a high resolution that can easily be integrated with current DEM data sources. GlobeLand30 would thus be classified as an excellent dataset to use for site specific radar coverage and land clutter modelling purposes.

3.2.2.2 South African National Land Cover 1994 (NLC 1994)

The South African National Land Cover 1994 (NLC 1994) is a land cover dataset that is based on Landsat imagery acquired from 1994 - 1995. The NLC 1994 was mapped manually from a 1:250000 scale of these Landsat image maps. The dataset contained 31 terrain types with a map accuracy of 79.4%. The map was further simplified into 5 terrain classes, namely, urban, forestry and plantations, mining and quarries, cultivation and agriculture and other [74]. The NLC 1994 five terrain class land cover map is shown in Figure 3.12.

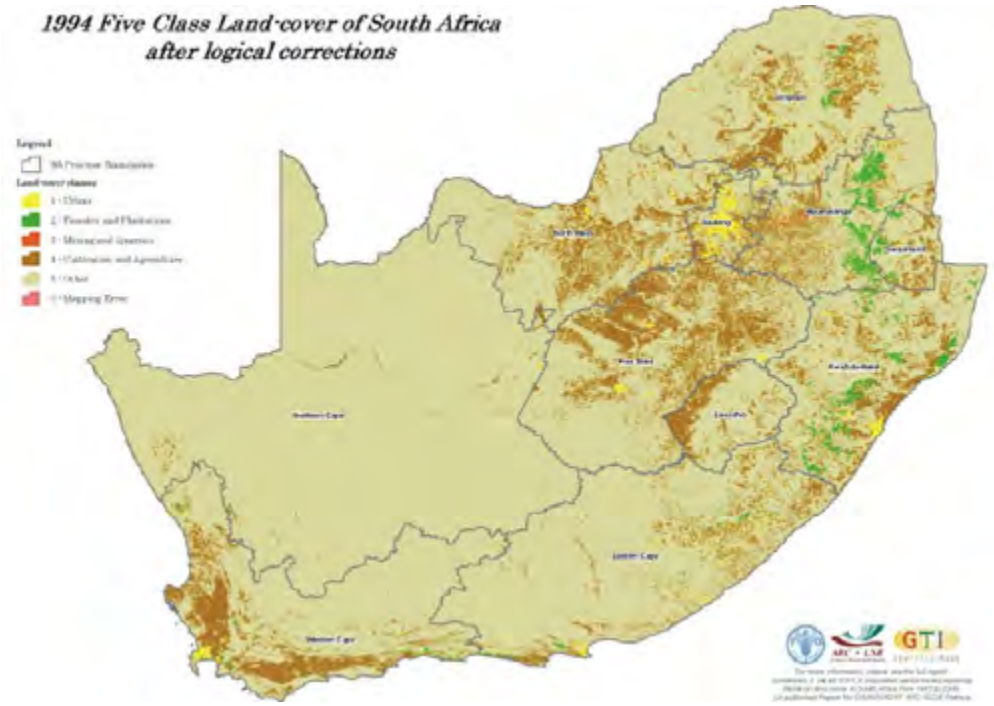

Figure 3.12: NLC 1994 five terrain class land cover map [74].

3.2.2.3 South African National Land Cover 2000 (NLC 2000)

The South African National Land Cover 2000 (NLC 2000) is a land cover dataset that is based on digital Landsat imagery acquired from 2000-2001. The dataset was developed from digital raster datasets and contained 45 terrain types with a map accuracy of 65.8%. The map was further simplified into five terrain classes, namely, urban, forestry and plantations, mining and quarries, cultivation and agriculture and other [74]. The NLC 2000 terrain class land cover map is shown in Figure 3.13.

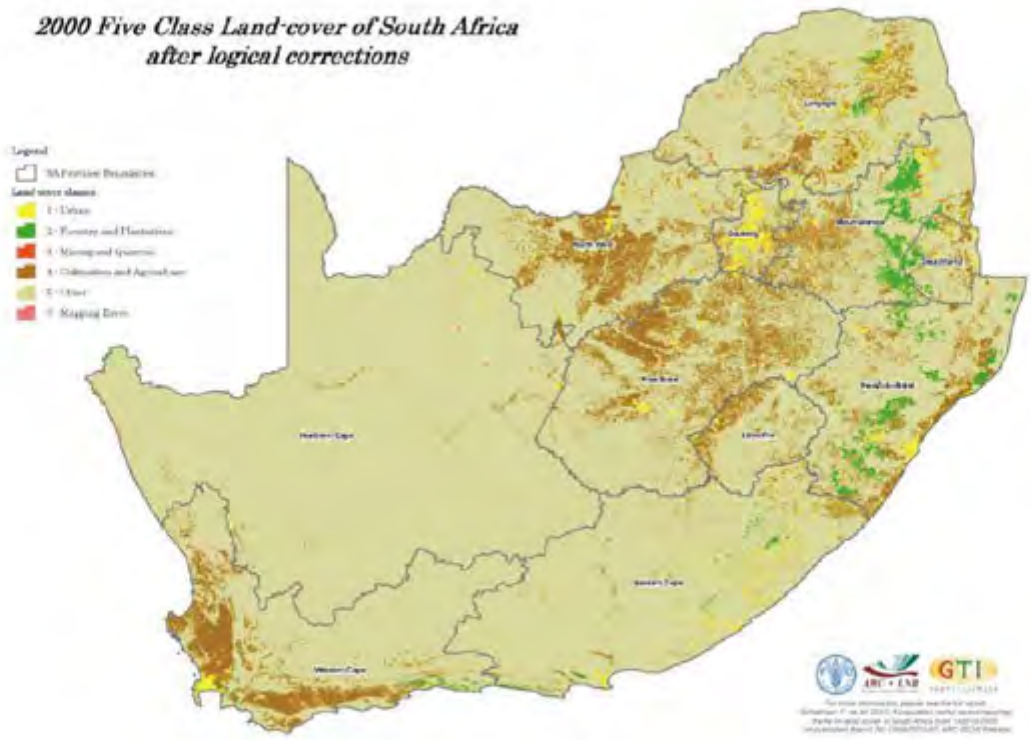

Figure 3.13: NLC 2000 five terrain class land cover map [74].

3.2.2.4 South African National Land Cover 2005 (NLC 2005)

The South African National Land Cover 2005 (NLC 2005) is a land cover dataset that was derived from a combination of existing land cover datasets which have been generated independently using SPOT satellite data. The processed map included five terrain classes, namely, urban, forestry and plantations, mining and quarries, cultivation and agriculture and other. The overall accuracy of NLC2005 was 80.37% [74]. The NLC 2005 five terrain class land cover map is shown in Figure 3.14.

3.2.2.5 South African National Land Cover 2009 (NLC 2009)

Most applications and projects relating to the use of land cover data in RSA have previously relied on the National Land Cover data map of 2000 and 2005. These datasets were clearly outdated for relevant use due to land cover change over time as they do not reflect the true nature of the current landscape. There was thus a high demand for improved land cover data maps on a national scale in RSA. Due to the demand, the South African National Biodiversity Institute (SANBI) embarked on a project to update the existing NLC dataset for South Africa. It should be noted that the project did not involve new radar data but rather involved using more recent data sources in conjunction with previous NLC data

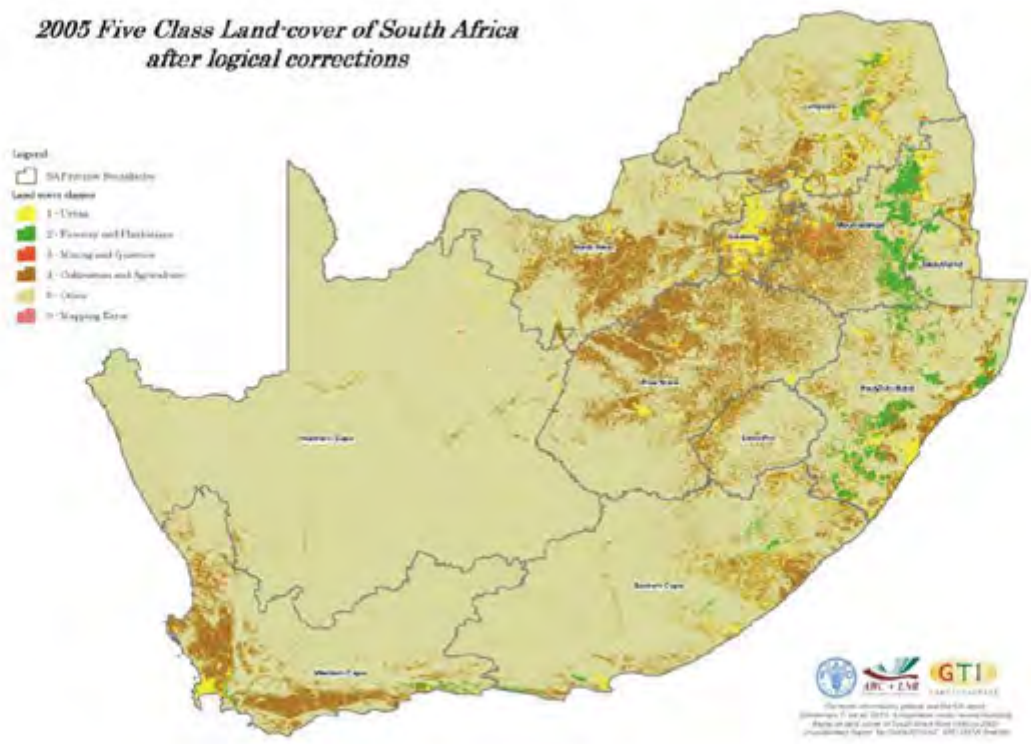

Figure 3.14: NLC 2005 five terrain class land cover map [74].

to create an improved national land cover data map for RSA. The data sources used in the development of NLC 2009 came from updated Eskom SPOT (2006-2007) imagery data [75].

The updated NLC 2009 land cover dataset included seven terrain types, namely, water-bodies, urban built up, plantations, natural, mines, degraded and cultivation. The dataset covers land cover in RSA with a spatial resolution of 30 m with geographic projection WGS84. The accuracy of NLC 2009 was not tested since there was no reference data to be used or ground control points. However, majority of the data in NLC 2009 came from the Eskom SPOT data which had an accuracy of 90%. It was assumed that NLC 2009 would have a similar accuracy. SANBI noted that the NLC 2009 land cover product should not be used as the new version of land cover map but this should be used as good indicator of land use changes over 10 years in South Africa [75]. The NLC 2009 seven terrain class land cover map is shown in Figure 3.15.

This product shows major land use in South Africa by using the best available data at the time. A drawback of all the NLC datasets are that it only covers the RSA region and not the SADC region of interest. The dataset is however of high resolution and suitable to use with DEM data. NLC 2009 is however outdated, as it was developed from land cover data sources from 2006 and 2007. Due to these drawbacks, the NLC 2009 land cover dataset

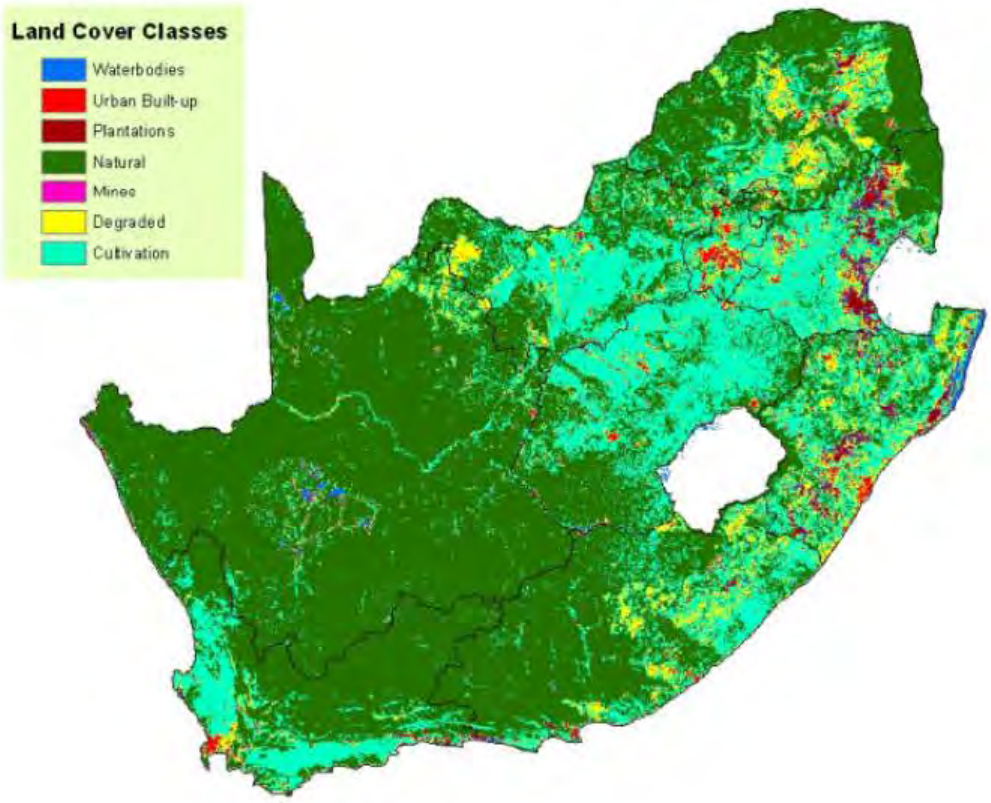

Figure 3.15: NLC 2009 five terrain class land cover map [75].

would be classified as a good dataset to use as compared to others, for site specific radar coverage and land clutter modelling within RSA.

3.2.2.6 Global Land Cover (GLC) 2000

The Global Land Cover (GLC) 2000 dataset is a land cover map that is based on land classifications that were produced by the Institute of Environment and Sustainability (IES) Global Vegetation Monitoring Unit. The dataset provides land cover for the entire earth and is available with a spatial resolution of 30 arc seconds (≈900 m). The projection the dataset is available in is geographic WGS84.

GLC 2000 is freely available for download from a number of sources. However the format of the files are in (.xtvm) which can only be opened and viewed using TerraViva Global Data Viewer software. The dataset includes 5 land cover types, namely, forests, woodlands shrublands and grasslands, agriculture, bare soil, and other land cover classes. A description for each of these land types is shown below.

1. **Forests** includes land types that are covered with closed evergreen lowland forest,

degraded evergreen lowland forest, montane evergreen forest (>1500 m), sub-montane forest (>900 m), swamp forest, mangrove, mosaic forest / croplands, mosaic forest / savanna, or closed deciduous forest (Miombo).

2. **Woodlands, Shrublands and Grasslands** includes land types that are covered with deciduous woodland, deciduous shrub land with sparse trees, open deciduous shrub land, closed grassland, open grassland with sparse shrubs, open grassland, sparse grassland, or swamp bushland and grassland.

3. **Agriculture** includes land types that are covered with croplands (> 50%), croplands with open woody vegetation, irrigated croplands and tree crops.

4. **Bare Soil** includes land types that are covered with bare rock, stony desert, sandy desert and dunes or salt hardpans.

5. **Other Land Cover Classes** includes land cover types that are made up of water-bodies or cities.

Due to the low resolution and limitations with the format of GLC 2000 data, this dataset would be classified as a weak dataset and not suitable for use in a site specific radar coverage and land clutter modelling tool.

3.2.2.7 Global Land Cover by National Mapping Organisations (GLCNMO)

The Global Land Cover by National Mapping Organisations (GLCNMO) is a global land cover dataset that was developed by the International Steering Committee for Global Mapping. This committee consists of various mapping organisations. The data was created using MODIS data that was observed upon the 2008 Terra and Aqua Satellites. The classification of terrain types was developed by the Food and Agriculture Organisation (FAO). The dataset includes twenty terrain types at a spatial resolution of either 30 arc seconds (≈900 m) for version 1 or 15 arc seconds (≈450 m) for version 2. GLCNMO covers 81.2% of the earth's land cover and is freely available over the internet from a number of mapping organisation sites. The geographic coordinate system used is WGS84 and the format of the files are in HDF-EOS. The twenty terrain types are namely, broadleaf evergreen forest, broadleaf deciduous forest, needleleaf evergreen forest, needleleaf deciduous forest, mixed forest, tree open, shrubs, herbaceous, herbaceous with sparse trees /

shrubs, sparse vegetation, cropland, paddy field, cropland / other vegetation mosaic, mangrove, wetland, bare area (gravel / rock), bare area (sand), urban, snow / ice and water bodies [76]. The GLCNMO version 2 is shown in Figure 3.16.

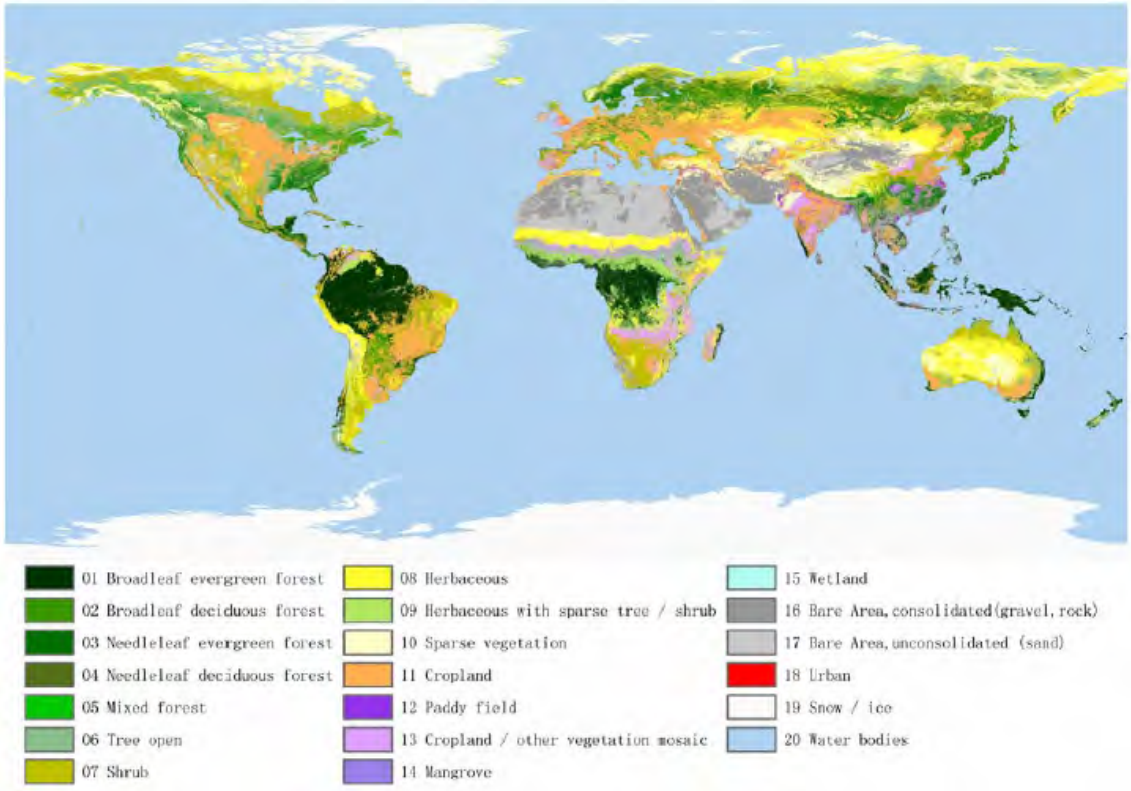

Figure 3.16: GLCNMO land cover map [76].

The GLCNMO dataset considers many different types of forest environments that is not entirely necessary for use in a site specific radar coverage and land clutter modelling tool. Due to this as well as the low resolution, GLCNMO would be classified as a weak dataset and not be suitable for use in a site specific radar coverage and land clutter modelling tool.

3.2.2.8 Global Land Cover Share (GLC-Share)

The Global Land Cover Share (GLC-Share) is a land cover data product that was developed by the FAO and released in 2014. This dataset aims to represent most land cover information from around the globe into one centralised database. The process involved in creating this dataset was to integrate the best land cover data available. The dataset is available with a spatial resolution of 30 arc seconds (≈900 m) for eleven terrain types, namely, artificial surfaces, cropland, grassland, tree covered areas, shrubs covered areas, herbaceous vegetation, mangroves, sparse vegetation, bare soil, snow and glaciers and

water bodies. The accuracy of this dataset is said to be 80.2 % [77]. GLC-Share is freely available for download in UML or raster format from [78]. The GLC-Share dataset is shown in Figure 3.17.

Figure 3.17: GLC-Share land cover map [77].

The GLC-Share land cover dataset would be ideally suited to use for clutter modelling in the SADC region, however the resolution of the current version is too low (900 m) for site specific clutter modelling purposes. The dataset should however be considered if future versions are of improved resolution. GLC-Share in it's current state would thus be classified as a weak dataset and not suitable for use in a site specific radar coverage and land clutter modelling tool.

3.2.3 GIS Data Discussion and Summary

Several DEM and LC data sources were investigated. It was found that many DEM data sources are of too low quality and resolution for use in a site specific radar coverage and land clutter modelling tool. Astrium provides one of the highest quality, accuracy and resolution DEM datasets currently available, however these are not freely available. Due to the large financial implication, the Astrium dataset is not suitable for use in the development of a site specific radar coverage and land clutter modelling tool. It was

found that the ASTER GDEM and SRTM 30 m DEM sources are currently the highest resolution datasets that are freely available and covers all the intended areas of interest. Even though these two datasets both have a resolution of 30 m, it was found that the ASTER GDEM data contained some remaining artefacts that cause artificial hills, ridges and surface roughness that do not exist in reality. The SRTM datasets therefore are more accurate. It is thus recommended that the SRTM 30 m DEM dataset be used in a site specific radar coverage and land clutter modelling tool.

Similarly, it was found that many LC data sources are either of too low quality, resolution or outdated for use in a site specific radar coverage and land clutter modelling tool. Two LC data sources can be considered, namely the NLC 2009 or GlobeLand30 m LC datasets. These are both at a high resolution of 30 m. The NLC 2009 dataset however only covers the RSA region, whereas the GlobeLand30 m covers the entire SADC region of interest. The GlobeLand30 m source is also a more current LC model than the NLC 2009 data source. The GlobeLand30 m dataset is therefore recommended for use in a site specific radar coverage and land clutter modelling tool.

Linking the appropriate land classes of these LC datasets to use with the various land clutter models is discussed in section 4.3.

A summary of the DEM and Land Cover data sources discussed above is shown in Table 3.14 and Table 3.15 respectively.

3.3 Simulating the Clutter Scene

3.3.1 Clutter Patch Grid Method

Once a DEM of the radar observed environment is loaded, it produces a $N \times M$ matrix model equally spaced in the x (longitude) and y (latitude) dimension. Each point represents a value corresponding to the terrain height information at the specified location. The effects of the earth's curvature and atmospheric refraction should be accounted for when simulating a radar observed environment covering large areas. The former will cause a blind area or dead zone as shown in Figure 2.4, and latter will curve the LOS of the radar, as seen in Figure 2.3. A close approximation to account for the effects of earth curvature

Table 3.14: Digital Elevation Model summary.

DEM Dataset	Versions	Resolution	Projection	Coverage Area	Format	Availability	Validity / Dataset Strength
SRTM	• SRTM Non-Void Filled • SRTM Void Filled • SRTM 1 Arc Second Global	• 30 m US, 90 m elsewhere • 30 m US, 90 m elsewhere • 30 m	WGS84	80 % earth landmass	• DTED • GeoTIFF • BIL	Freely available from online sources	High validity. Excellent dataset
ASTER GDEM	• Version 1 • Version 2	30 m	WGS84	Between 83° N and 83° S	GeoTIFF	Freely available from online sources	Medium validity. Good Dataset
DTED	• DTED 0 • DTED 1 • DTED 2	• 900 m • 90 m • 30 m	EGM96	• 50 % earth landmass • Worldwide landmass coverage • Worldwide landmass coverage	DTED	• Freely available from online sources • Upon request, not easily accesible	High validity. Excellent dataset
Astrium	• WorldDEM • Elevation 30 • Elevation 10 • Elevation 8 • Elevation 4 • Elevation 1	• 12 m • 30 m • 10 m • 8 m • 4 m • 1 m	WGS84	• Pole to pole coverage • > 75 million km^2 of earths surface • Regional coverage	Any raster or georeferenced image formats	Accesible from Astrium organistion at high prices	High validity. Excellent dataset

is to subtract from the original DEM data an effective elevation drop, $\triangle E$, as a function of distance from the radar. Equation 3.20 can be used to determine $\triangle E$ [79]. This drop in elevation effectively re-structures the DEM values such that the effects of earth curvature is negated. As discussed in section 2.1, to account for the refraction effects caused by the earth's atmosphere, a close approximation of $\frac{4}{3}$ of the earth's radius is used. This is known as the effective earth radius R_{eff}. This process to correct for earth curvature and atmospheric refraction effects is known as the $\frac{4}{3}$ Earth Model. This effectively in simulation replaces the actual atmosphere by a homogeneous atmosphere whereby the radar EM waves now propagate in straight lines.

$$\triangle E = R_{eff} - \sqrt{R_{eff}^2 - D_0^2} \tag{3.20}$$

where D_0 is the distance from the reference point, R_{eff} is the effective radius of the earth and $\triangle E$ is the change in elevation due to earth curvature.

Table 3.15: Land Cover data summary.

Land Cover Dataset	Versions	Resolution	Accuracy	Projection	Terrain Classes		Coverage Area	Format	Availability	Validity / Dataset Strength
GlobeLand30	Version 1	30 m	80.33%	WGS84	• Cultivated land • Forest • Grassland • Shrubland	• Water bodies • Wetland • Thundra • Artificial surfaces • Barelands	Global	GeoTIFF	Freely available from online sources	High validity. Excellent dataset
NLC	• NLC 1994 • NLC 2000 • NLC 2005 • NLC 2009	• 900 m • 900 m • 900 m • 30 m	>80%	WGS84	• Water bodies • Urban • Plantations	• Natural • Mines • Degraded • Cultivation	RSA region	GeoTIFF	Freely available from online sources	Medium validity. Good Dataset
GLC 2000	Version 1	900 m	Insufficient information	WGS84	• Forests • Woodlands, Shrublands	• Agriculture • Bare soil • Other	Global	GeoTIFF	Freely available from online sources	Low validity. Weak dataset
GLCNMO	Version 1	900 m	81.20%	WGS84	20 terrain classes, mostly vegetation and forests related		Global	GeoTIFF	Freely available from online sources	Low validity. Weak dataset
GLC-Share	Version 1	900 m	80.20%	WGS84	• Artificial surfaces • Cropland • Grassland • Tree	• Shrubs • Vegetation • Mangroves • Baresoil • Snow • Water bodies	Global	UML or Raster	Freely available from online sources	Low validity. Weak dataset

A DEM of a simulated mountainous terrain is shown in Figure 3.18a. The DEM was then corrected for earth curvature and refraction effects using the $\frac{4}{3}$ Earth Model, as shown in Figure 3.18b.

It should be noted that using a factor $k = \frac{4}{3}$ as is used in the above model, is merely a convenient approximation to account for atmospheric effects. The perfect value for k will change as a function of altitude, atmospheric conditions, frequency, etc [1]. According to Blake [27], the $\frac{4}{3}$ Earth Model is reasonably accurate up to altitudes of approximately 4 km, but at higher altitudes it predicts too much ray bending. Another limitation of assuming standard atmospheric refraction is that at small grazing angles, changes in the factor k can cause large percentage changes in the angle (see Figure 2.5). For land clutter modelling, the clutter returns of interest are those from land terrain which is within the range of altitude heights where the $\frac{4}{3}$ Earth Model is most accurate. Regardless of the $\frac{4}{3}$ earth models limitations, the model is an accepted model to use to account for atmospheric refraction in computations due to its simplicity and effectiveness [10, 1, 26, 27]. The $\frac{4}{3}$ Earth Model is therefore deemed a sufficient model to be used in a site specific radar coverage and land clutter modelling tool to account for the effects of earth's curvature and atmosphere.

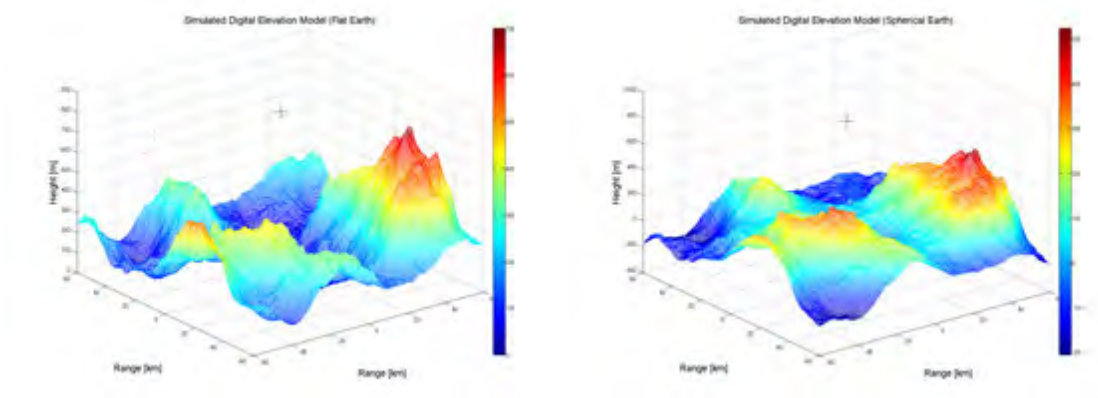

(a) (b)

Figure 3.18: DEM for simulated mountainous terrain: (a) uncorrected DEM, i.e. curvature of earth and refraction not taken into account, (b) corrected DEM, i.e. curvature of the earth and refraction taken into account.

Once a DEM is loaded and corrected for earth curvature and atmospheric refraction, it produces a $N \times M$ matrix model equally spaced in the x (longitude) and y (latitude) dimension. Each point represents now a value corresponding to the corrected terrain height information. These points can not be used as simulated clutter patches as they do not represent a surface. Instead, the DEM can be broken up into a number of small triangles in which each triangle represents a sample point with a certain area. Each of these triangles can then be used as a small area clutter patch. Once this has been created, parameters such as distance to each patch, angle of incidence, grazing angle and surface normal can be calculated through relevant linear algebraic equations. This method of meshing was implemented on the simulated DEM data shown in Figure 3.18b data and is described as follows.

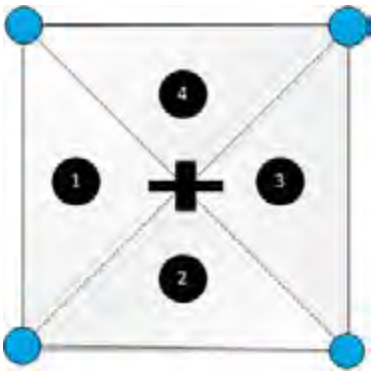

Figure 3.19: Triangulation process.

An example of the DEM data representation is shown above in Figure 3.19. The blue dots represent the height points of the corrected DEM. The meshing algorithm reduces

each block of four DEM points into four triangles, each triangle sharing a common point shown by the centre of the block. This centre point is an average height of the four corresponding heights that make up the original block. The algorithm then finds the centre of each triangle and assigns an average height to that centre point from the three given heights of each triangle end points. The centre of each triangle now becomes the new simulation point, as indicated by the black dots. The normal of each triangle surface can then be determined using the dot product manipulation of the given triangle end point vectors. From the surface normal and using the vector between the centre point of each triangle and the radar location point, the grazing angle, incidence angle, and depression angle can be computed. This information as well as the area of each triangle is important parameters required for clutter calculations.

3.3.2 Radar Coverage

Terrain masking can be determined by calculating the LOS coverage of the loaded DEM from the radar location reference point. A method that can be used to calculate LOS coverage is by using Ray Tracing algorithms.

The Nvidia Optixray engine is a programmable ray tracing engine that can be implemented to perform ray tracing applications. This method uses a ray tracing algorithm in order to determine visibility. Ray tracing is a technique that generates an image by tracing a path of light through pixels in an image plane, and simulates the effects that the ray encounters with virtual objects. The ray tracer works as follows. A ray is shot out to each sample point from the radar location, the ray tracer then determines the intensity or closest point in that ray, and every point the ray hits following the first one is considered hidden. This method aims to provide a fast and accurate visibility result. An example of this process is shown in Figure 3.20. The white areas represent masked terrain areas.

3.3.3 Clutter Cell Size, DEM Resolution, and DEM Height Accuracy

The accuracy and fidelity of the calculated grazing angles and visibilities are dependent upon the DEM arc spacing resolution and to a lesser extent on DEM height accuracy.

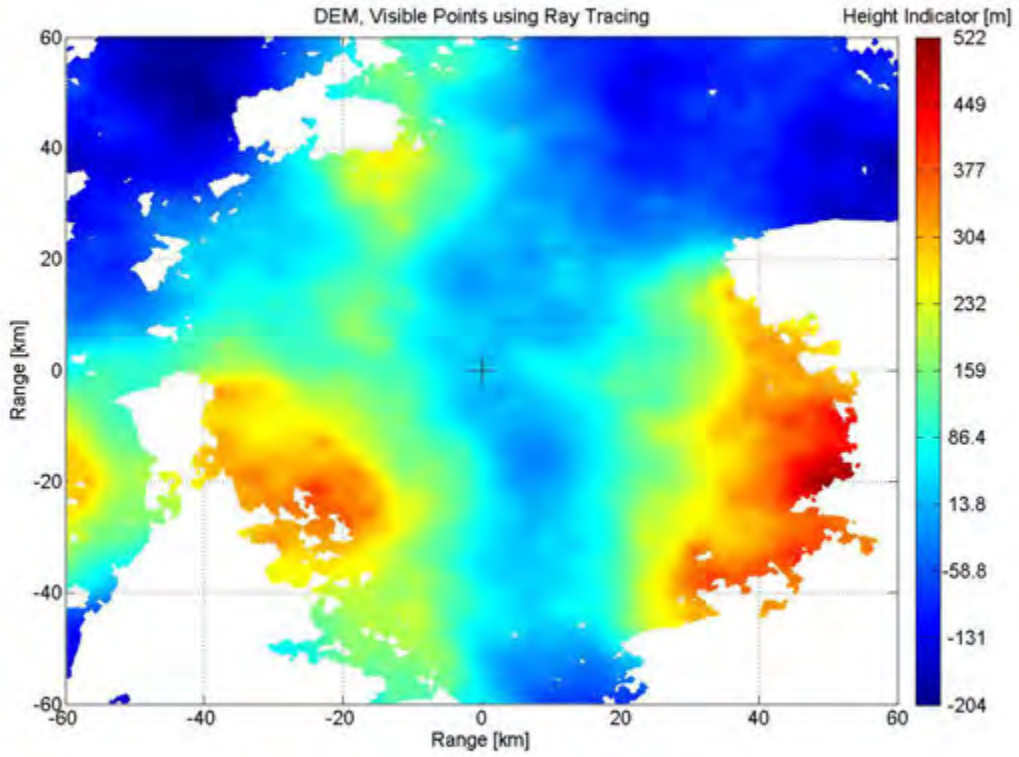

Figure 3.20: Radar coverage using ray tracing process.

DEM arc spacing resolution determines the distance between height points. The less this distance is (higher the resolution), the more data points are available to model land topography. Effectively increasing the fidelity of the simulated DEM. The purpose of using DEM data is to simulate land topography (to determine grazing angle) as well as to determine LOS visibilities.

The size of the simulated clutter patches as well as computation time is directly dependent upon the arc spacing resolution of DEM data used. The above simulation steps were followed when simulating five different data sets each of the same location and coverage extent but different resolutions. The resolutions were for 90 m , 30 m, 10 m, and 5 m respectively, each for an area coverage spanning out to 9 km radius. Due to the non availability of freely available DEM data at resolutions higher than 30 m, the 5 m and 10 m datasets were developed from the 30 m dataset using bicubic interpolation methods. This was done to determine the effects of clutter cell size and computation time for higher resolution datasets. The results for the number of DEM points after meshing, average clutter cell sizes and computation time for each resolution set is shown in Table 3.16.

The average clutter cell size for 30 m DEM data is ~253.04 m^2. From Table 3.16, it can

Table 3.16: Clutter cell sizes and computation times for different DEM data resolutions for 9 km radius coverage area.

DEM Resolution	Number of DEM points after meshing	Average clutter cell size [m^2]	Computation time [s]
900 m	1600	~238990	~0.5504
90 m	153664	~2269.5	~0.6185
30 m	1364224	~253.04	~0.7909
10 m	12960000	~26.25	~2.9006
5 m	51782416	~9.58	~25.0224

be seen that there is an exponential increase in the number of DEM data points as well as computation time as the resolution of DEM data used is increased. As the resolution increases, the clutter cell size decreases which would improve upon the accuracy of the simulated clutter measurement. However, a trade off needs to be made as higher resolution would require significantly more computer resources. This is especially true for resolutions higher than 30 m as shown in 3.16. As discussed in section 3.2, the highest resolution DEM data that is freely available for the intended areas of interest are 30 m. This fact as well as the exponential increase in computer resources required for DEM resolutions higher than 30 m justifies the decision to use 30 m DEM data for use in a site specific radar coverage and land clutter modelling tool.

From the nature of how DEM data is produced, DEM height measurement errors are inevitable. These errors can be due to quantisation, discrete measurement or magnitude errors. Height errors in DEM data can be distributed randomly or systematically. The height accuracy of a DEM dataset is usually represented by a RMSE value. It is thus important to consider what RMSE height accuracy would be required for this particular application. A 10 km radius DEM was simulated, and randomly distributed errors applied to the dataset. The RMSE of these errors were 0 m, 5 m, 10 m and 15 m respectively. These simulated DEM's were then used to simulated clutter patches, to determine grazing angles and LOS visibilities as in the process described above. Statistics of the calculated grazing angle and percentage of calculated non visible DEM points for each set is shown in Table 3.17.

Table 3.17: Statistics of the calculated grazing angle for each DEM set of different RMSE values.

Calculated Statistics	RMSE = 0 m	RMSE = 5 m	RMSE = 10 m	RMSE = 15 m
non visible DEM points []	44.7	46	50.2	55
grazing angle mean [°]	4.7	4.8	5.2	5.8
grazing angle standard deviation [°]	2.5	2.6	2.9	3.4

From Table 3.17, it is shown that with an increase in RMSE, there is a general increase in the percentage of non visible DEM points, as well as an increase in the mean grazing angle, and grazing angle standard deviation. The grazing angle mean only changes by 0.1° with an injected RMSE of 5 m, and by 0.5° and 1.1° with an injected RMSE of 10 m and 15 m. These changes are fairly insignificant given that in most cases a change of 1° in grazing angle, changes the calculated backscatter coefficient value by less than 0.1 dBs for the plateau grazing angle region. This increases for low and high grazing angle regions. A more significant effect that increasing RMSE has is the percentage change in calculation of DEM visibilities. The percentage of non visible DEM points changes by 1.3% with an injected RMSE of 5 m, but increases to to 5.5% and 10.3% with an injected RMSE of 10 m and 15 m. The change in visibilities with RMSE of 5 m is fairly insignificant and considered acceptable in terms of the purpose of using DEM data for site specific radar coverage and land clutter modelling.

The above discussion on DEM resolution and height accuracy further justifies the recommendation to use the SRTM 30 m DEM dataset in a site specific radar coverage and land clutter modelling tool, which has a arc spacing resolution of 30 m, and an associated height accuracy RMSE of ~5 m.

3.3.4 Simulating Coherent Radar Returns

The above steps are necessary to obtain a clutter scene relative to the position of a radar system. The data is thus representative of the radar observed environment information (environment model) which includes the clutter patches, each with an associated LOS visibility from the radar, height, area, distance from the radar, grazing angle (including incidence and depression angles), and the terrain class that the patch matches to the closest (based on the Land Cover data chosen). Using environment model information, land clutter models can be used to provide a backscatter coefficient value for each visible clutter patch. The reflectivity (including the inherent pattern propagation factor F^4) for each clutter patch can be determined to create the land clutter model characteristics of the scene.

This only represents the radar observed environment, LOS coverage, and the reflectivity. The objective of simulating site specific radar land clutter returns can not be achieved

without the application of a radar sensor model, including the antenna beam pattern. The radar sensor contains information about the radar characteristics including but not limited to, radar operating frequency, waveform, radar resolution and range limits, antenna pattern, transmit and receive gains, radar position, height, and orientation, radar system losses etc. The mapping of the radar antenna beam pattern onto the scene and coherent addition of returns from the clutter patches would be the next step.

The modelling of coherent radar returns would firstly require the radar observed environment and land clutter model that was developed. The radar antenna beam pattern is modelled in both azimuth and elevation. The visible terrain data that is within the radar antenna beamwidth would be computed. Range traces are then formed at closely spaced azimuth angles which is based on the radar antenna beamwidth, scan rate, and pulse repetition frequency (PRF). The azimuth spacing needs to be chosen such that it provides adequate fidelity. The range samples are then calculated and spaced according the radar range resolution. Area sampling is performed for each range trace. For each range trace, all samples within the radar range bin is summed to simulate coherent radar return. The returns are modified by the attenuation relative to the antenna peak gain at boresight as a function of the off boresight sample angle. The land clutter power at the receiver for each range bin is then calculated using the radar equation.

3.4 Chapter Summary

In this chapter, several existing land clutter models, DEM and LC data sources were investigated.

A description and analysis of several existing land clutter models are presented in section 3.1. A summary of these land clutter models are presented in Table 3.9 above. Further analysis and comparisons of these land clutter models are investigated in section 4.1.

A description and analysis of several DEM and LC data sources are presented in section 3.2. It is recommended that the SRTM 30 m DEM dataset and the GlobeLand30 LC dataset should be used in a site specific radar coverage and land clutter modelling tool as they are currently the highest quality DEM and LC datasets that are freely available that covers all intended areas of interest. A summary of these DEM and LC data sources are

presented in Table 3.14 and Table 3.15 respectively.

Section 3.3 presents a meshing technique that can be used to simulate clutter patches in a site specific radar coverage and land clutter modelling tool. The process involves breaking up the DEM height points into triangular surface areas, each representing a clutter patch from which various calculations can be performed. Earth curvature and atmospheric refraction effects can be reduced by using the $\frac{4}{3}$ Earth Model. Section 3.3.2 presents a terrain LOS visualisation technique known as ray tracing that can be used in a site specific radar coverage and land clutter modelling tool to determine masked areas.

A discussion and brief analysis on the required simulated clutter cell size, DEM resolution, and DEM height accuracy. is given in section 3.3.3. This analysis further justified the recommendation to use the SRTM 30 m DEM dataset in a site specific radar coverage and land clutter modelling tool.

Furthermore, a process for simulating coherent radar clutter returns is given in section 3.3.4.

Chapter 4

Analysis and Results

This chapter provides a discussion of the land clutter / backscatter coefficient models in the context for use in a site specific radar coverage and land clutter modelling tool. It aims to determine which of the existing models are the most appropriate to use for the varying simulation cases, as well as to identify categories of land clutter models where little or insufficient models are available. It also aims to provide the link between the different terrain classes described in land cover data compared to those in land clutter / backscatter coefficient models. Land clutter and land cover link results will be illustrated and tabulated in aid of developing algorithms for use in a site specific radar coverage and land clutter modelling tool. It ends by proposing a guide on the process to follow for the development of a site specific radar coverage and land clutter modelling tool.

4.1 Analysis of Land Clutter Models

This section provides an analysis of the various land clutter models discussed in this dissertation. The aim is to determine how well site specific simulated clutter using the land clutter models agree with measured data, and which models are best suited to use for the various grazing angle regions. The process will be based on information gathered from literature for low grazing angles, and from comparing simulated clutter using the land clutter models with measured data for angles in the plateau and high grazing angle region. This information does not aim to fully validate the various land clutter models considered in this dissertation for all cases, but rather aims to determine whether the

assumptions made in section 3.1 about the compatibility (strength) and validity of these models are valid for a few cases.

4.1.1 Low Grazing Angle Region

As stated in previous sections, the text by Billingsley in [6], analyses low grazing angle clutter regions extensively. The analysis of results for low angle clutter modelling will be based upon Billingsley's finding's on simulated low angle land clutter using the land clutter model as described in section 3.1.9. It should be noted that the clutter map comparison described below are between a measured scene, and a simulated scene where the parameters that were used in the simulated land clutter model were derived from the scene. They are therefore likely to be similar, however the purpose for including this analysis was to identify important findings made by Billingsley with regard to the way in which he based his validation of the model, as well as the performance of LOS coverage obtained using 90 m DTED data.

In [6], Billingsley aims to validate his land clutter model with measured data. The process involved simulating the spatial variation of land clutter at Brazeau, a forested wilderness area in Alberta Canada using his proposed model. Firstly 90 m DEM data was used to determine the LOS terrain visibility, and surface slopes. Land cover data was then integrated to identify the different land cover types within the area of interest. The clutter strength for each visible cell was then calculated using Billingsley's land clutter model. An example of the outcome of this process is shown in Figure 4.1.

Figure 4.1 compares the simulated and measured clutter maps. The black regions in the simulated map represent the masked terrain regions. This corresponds reasonably well with the masked regions as shown in the measured data. The coloured regions represent the backscatter coefficient $\sigma^{\circ}F^4$ values for the measured and simulated maps. There is generally a good correlation between $\sigma^{\circ}F^4$ for the measured and simulated clutter maps. Billingsley however noted that the cell to cell spatial correlation of the measured map is not precisely followed by the simulated map.

Billingsley bases his validation on how the particular radar system performance measure computed from simulated clutter compares to the performance measure using measured clutter and not on how closely the simulated and measured clutter maps compare. By

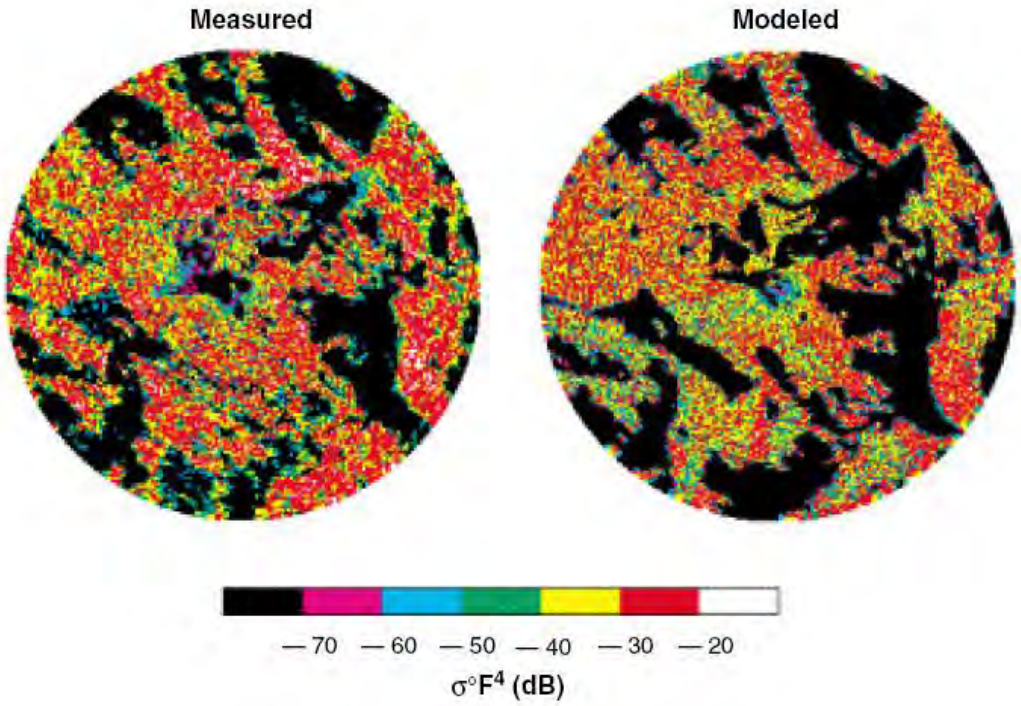

Figure 4.1: Comparison of measured and simulated land clutter map at Brazeau, Alberta Canada [6].

using this validation process, Billingsley determined that his land clutter model performs with highly satisfactory accuracy for computing clutter limited system performance [6]. The above comparison used 90 m resolution DEM data as it was the highest resolution available at the time. Billingsley noted that the fidelity of predicting the masked areas will significantly improve if higher quality DEM data of higher resolution is used. This further justifies the use of the currently available 30 m DEM data.

4.1.2 Plateau and High Grazing Angle Region

In 2013, radar engineers from the Council of Scientific and Industrial Research (CSIR) embarked on a radar clutter measurement campaign conducted from an airborne platform using an L-band radar [4]. This campaign was funded by the Armaments Corporation of South Africa (ARMSCOR). The campaign was conducted in the Western Cape region of South Africa. Measurements were taken of five terrain types, namely farmlands, fynbos, commercial urban, residential urban and informal urban areas. Permission was obtained from CSIR and ARMSCOR to be granted access to this measurement trial data to use for the purpose of this research study. The data collected from these measurements were

processed to determine the backscatter coefficient σ° in dBs as a function of grazing angle δ for the five terrain types. The range of measured angles are in the plateau and high grazing region. This is shown in Figure 4.2.

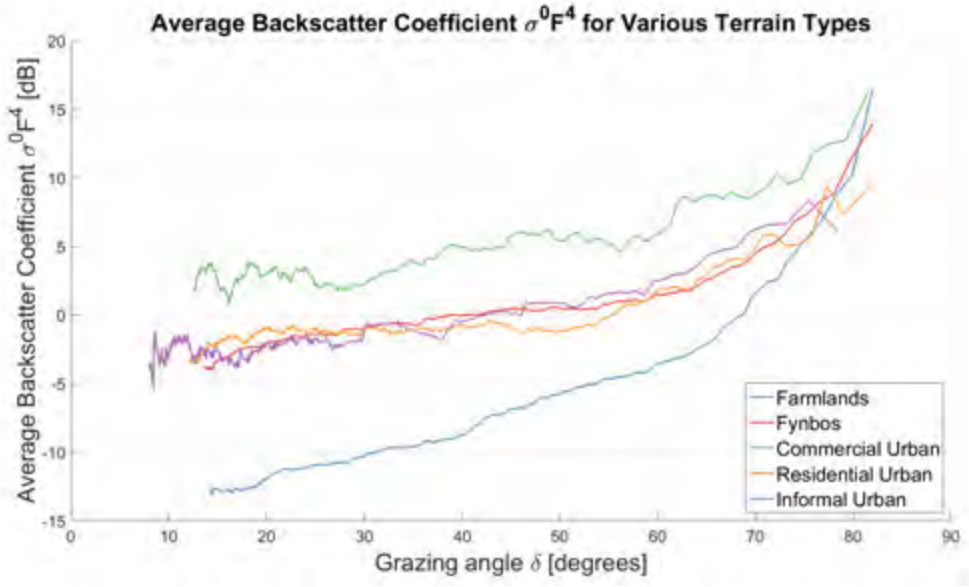

Figure 4.2: Average backscatter coefficient $\sigma^\circ F^4$ for various terrain types.

From Figure 4.2 it can be seen that there is general dependence of σ° on grazing angle in the plateau and high grazing region that agrees with literature. It also shows that urban terrains produce σ° values that are of an order of magnitude higher than farmlands or shrub like plantation terrain types. This is in agreement with the the list of given land clutter models, as shown in Figures 3.1, 3.2, 3.3, 3.4, 3.6 and 3.5.

Figures 4.3, and 4.4 show a comparison of the measured σ° values for different terrain types with σ° values simulated using the various land clutter models described in chapter 3 for plateau and high grazing angles. The measured data is compared to land clutter models terrain types that are the same or similar. Measured farmland and fynbos data is compared with land clutter model, Constant Gamma with terrain type 'farmland' and 'flatland', Morchin with terrain type 'farmland' and 'desert', Kulemin with terrain type 'arable land', GTRI with terrain type 'tall grass crops' and 'soil, sand and rocks', and Ulaby and Dobson or Generating Function with terrain type 'shrubs'. Similarly measured commercial urban, residential urban, and informal urban data is compared with land clutter model, Constant Gamma with terrain type 'metropolitan', Kulemin with terrain type 'urban territories', GTRI with terrain type 'urban' and 'soil' and Ulaby and Dobson or Generating Function with terrain type 'urban'.

The root mean squared error (RMSE) between the measured and simulated average backscatter ($\sigma^{\circ}F^4$) data for plateau and high grazing angle regions is shown in Figure 4.5.

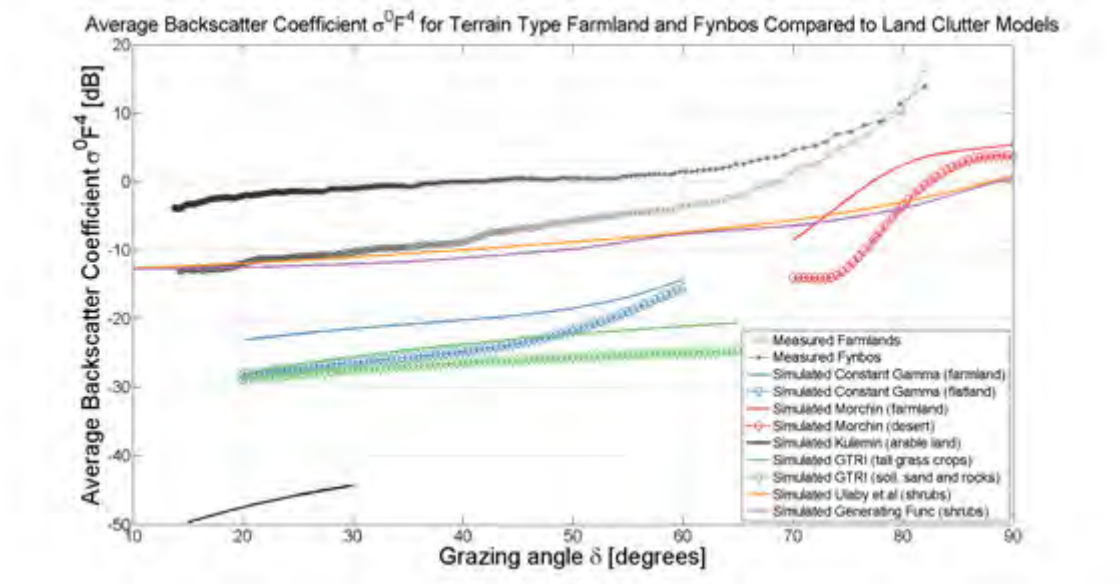

Figure 4.3: Average backscatter coefficient $\sigma^{\circ}F^4$ for terrain types farmland and fynbos compared to land clutter models.

From Figures 4.3 it can be seen that the measured data for farmlands is for most grazing angles larger than the simulated data from land clutter models. It is believed that this is due to discrete scatterers such as tree trunks interspersed in the homogeneous terrain. As expected, the land clutter model that closely agrees with the measured farmland data in the plateau grazing angle region is the Ulaby and Dobson and Generating Function land clutter models with terrain type (shrubs), with an associated RMSE of 1.4 dBs, and 2 dBs respectively. The backscatter from the measured fynbos data is significantly larger than the measured farmland data for the plateau grazing angle region and decreases in difference as the grazing angle moves towards the high grazing angle region. As with the farmland data, the land clutter model that is closest to the the measured fynbos data is the Ulaby and Dobson and Generating Function land clutter models with terrain type (shrubs). Even though fynbos is considered shrub-like terrain type, it produces a RMSE that is as much as 9.9 dBs, and 10.5 dBs for the simulated Ulaby and Dobson and Generating Function land clutter models respectively. This is again believed to be as a result of discrete scatterers. The land clutter model that produced the largest RMSE (larger than 34 dBs) relative to the measured data was for all cases the Kulemin land clutter model. This agrees with the assumption that Kulemin is a considered a weak and low validity

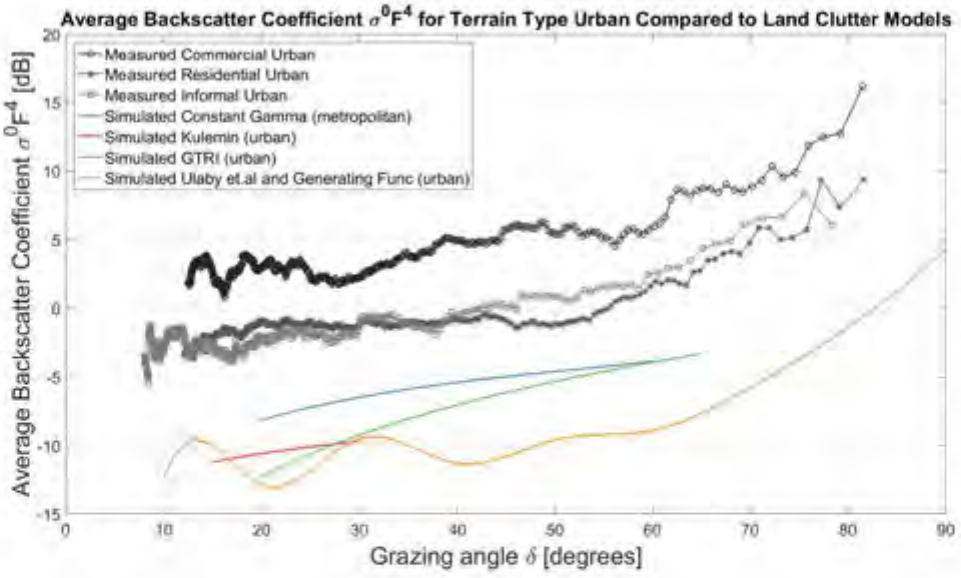

Figure 4.4: Average backscatter coefficient $\sigma^{\circ}F^4$ for all urban terrain types compared to land clutter models.

land clutter model. From literature it was believed that the GTRI land clutter model would be a more valid model to use for farmlands than the Constant Gamma land clutter model. However from these figures it is seen that the Constant Gamma land clutter model produces less of an RMSE (11.5 dBs against measured farmlands, and 20.3 dBs against measured fynbos) relative to the measured data than the GTRI land clutter model (RMSE of 15.8 dBs against measured farmlands, and a RMSE of 24.6 dBs against measured fynbos) for grazing angles in the plateau region. For high grazing angles, the Ulaby and Dobson and Generating Function land clutter models produces values that are closest to the measured data (RMSE of 7.8 dBs and 8.1 dBs against measured farmlands, and a RMSE of 10.4 dBs and 10.6 dBs against measured fynbos), followed by the Morchin land clutter model (RMSE of 8.9 dBs against measured farmlands, and a RMSE of 10.5 dBs against measured fynbos). However, for the limited grazing angle range between 70° and 90°, the Morchin land clutter model has the lowest RMSE (8.9 dBs against measured farmlands, and 10.5 dBs against measured fynbos) as compared to the Ulaby and Dobson and Generating Function land clutter models (RMSE of 11.1 dBs and 12.1 dBs against measured farmlands, and a RMSE of 11.8 dBs and 12.9 dBs against measured fynbos).

From Figure 4.4 it is seen that commercial urban terrains produces larger backscatter coefficient values than that of residential and informal urban terrains. This is due to the the large scattering sources such as tall buildings in commercial urban areas. The measured

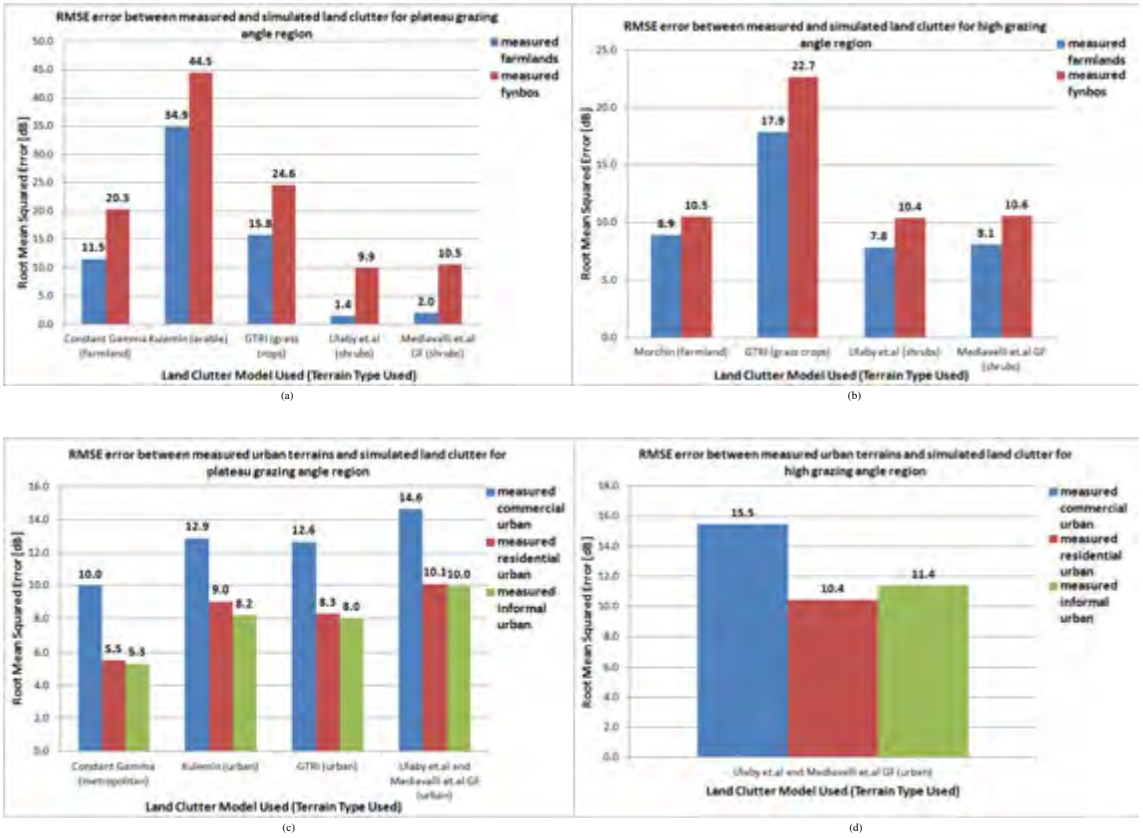

Figure 4.5: RMSE of the measured average backscatter $\sigma^{\circ}F^4$ for and simulated data from land clutter models : (a) RMSE error between measured and simulated land clutter for plateau grazing angle region , (b) RMSE error between measured and simulated land clutter for high grazing angle region , (c) RMSE error between measured urban terrains and simulated land clutter for plateau grazing angle region , (c) RMSE error between measured urban terrains and simulated land clutter for high grazing angle region.

urban data is as much as 10 dBs larger than that of the closest land clutter model. The land clutter model that produces values that are closest to the measured Urban terrain data is the Constant Gamma land clutter model for grazing angles in the plateau region, with an associated RMSE of 10 dBs, 5.5 dBs, and 5.3 dBs for commercial, residential and informal urban respectively). This is followed by GTRI, Ulaby and Dobson and Generating function, and Kulemin (limited grazing angle range for Kulemin model) land clutter models respectively. As with the measured farmland and fynbos data, the Constant Gamma land clutter model performs better than the GTRI land clutter model. The land clutter model that produced the largest RMSE relative to the measured urban data was the Ulaby and Dobson and Generating function land clutter model for grazing angles in the plateau region. This is due to the lack of sufficient data available for urban terrain in the Ulaby and Dobson and Generating Function land clutter models. Only the Ulaby and Dobson and Generating Function is valid for the high grazing angle region for urban

terrain. Care should be taken when modelling for urban terrain in the high grazing angle region as the RMSE is large (15.5 dBs, 10.4 dBs and 11.4 dBs for commercial, residential and informal urban respectively).

4.1.3 Discussion and Summary

As seen in chapter 3, it was found that only Billingsley's land clutter model and the adapted GTRI sea clutter model is valid for the entire low grazing angle region. Nathanson's land clutter model tables can be used as well but for only a few limited discrete grazing angles.

The adapted GTRI sea clutter model is based on linking sea states with various surface roughness of different terrain types. This provides the general and not true behaviour of σ° for varying terrains at low grazing angles. The adapted GTRI sea clutter model should thus be used with caution and thus classified as a weak and low validity model. It is clear that Billingsley is the authoritative land clutter model to use for low grazing angle regions specifically for the terrain classes that he has used to derive his model. Billingsley's validation process as discussed above further justifies the assumption that his model is considered an excellent and high validity model to use for low grazing angle regions specific to the terrain classes defined in the model.

For grazing angles in the plateau region, Ulaby and Dobson or Gamma Generating Function should be considered first as they produced backscatter values that produced the lowest RMSE to measured data as compared to the others. The Constant Gamma land clutter model performed better than the GTRI land clutter model for all cases. The Kulemin land clutter model produced the largest error and thus justifies the assumption made to classify it as a weak and low validity model.

For general high grazing angles, the Ulaby and Dobson and Generating Function land clutter models should be considered first, as they produced backscatter values that produced the lowest RMSE to measured data as compared to the others. Following these will be the Morchin and GTRI land clutter models respectively. However, for the limited grazing angle range between 70° and 90°, the Morchin land clutter model should be considered first as it produced the lowest RMSE in this region of angles.

As shown in the cases of urban terrain comparisons, it is further justified that the Ulaby and Dobson or Gamma Generating Function should be used with caution for cases where the model is based on insufficient data. Specifically for urban terrain, the Constant Gamma model should be considered first, followed by the GTRI and Kulemin land clutter models for plateau grazing angle regions respectively. For urban terrain at high grazing angles, only the Ulaby and Dobson or Gamma Generating Function is valid and can be considered, however this should be used with caution as the model for urban terrain is based on insufficient data. It should be noted that for urban areas, the land clutter can in most cases only be modelled in a general way as urban terrain is far too complex to be accurately statistically modelled.

Nathanson's tables provides average values for σ° for only a few discrete grazing angles and thus not suitable for use in site specific land clutter modelling where the dependence of σ° for a range of grazing angles would be required.

In general, and in order of models validity classification (weak, strong or excellent), Table 4.1a provides a list of land clutter models that can be used to simulate σ° for low, plateau and high grazing angle regions. Based on the foregoing results, Table 4.1b provides a list in order of preference of land clutter models to use specifically for urban terrains. The models in brackets are models that are not valid for the particular grazing angle region, but if required is able to produce σ° values for that region. It should be noted that models other than the top listed models should be used only if a higher listed model does not support a certain model dependent that is of interest to the researcher. Measured data of other terrain types and frequencies are required to properly compare and validate land clutter models for all terrain types and model dependencies. This is recommended for future work.

4.2 Grazing Angle and Frequency Ranges Considered by Land Clutter Models

A summary of the land clutter models discussed in this dissertation is shown in Figure 4.6. This figure shows the range of frequencies, and grazing angles that each model encompasses as a bounding box. Each model is represented by a different colour as

Table 4.1: Land clutter models to use for low, plateau and high grazing angle regions in order of model compatibility and validity.

(a) General land clutter model list.

Low grazing angle region	Plateau grazing angle region	High grazing angle region
1. Billingsley	1. Ulaby et.al / Generating Function	1. Ulaby et.al / Generating Function
2. Adapted GTRI Sea Clutter	2. Constant Gamma	2. Morchin
3. Nathanson	3. GTRI	3. (Constant Gamma)
4. (Constant Gamma)	4. Kulemin	4. (GTRI)
5. (GTRI)	5. Nathanson	-

(b) Land clutter model list specifically for urban terrain.

Low grazing angle region	Plateau grazing angle region	High grazing angle region
1. Billingsley	1. Constant Gamma	1. Ulaby et.al / Generating Function
2. Adapted GTRI Sea Clutter	2. GTRI	2. (Constant Gamma)
3. Nathanson	3. Kulemin	3. (GTRI)
4. (Constant Gamma)	4. Ulaby et.al / Generating Function	-
5. (GTRI)	5. Nathanson	-

shown in the legend. Furthermore the compatibility (strength) and validity of each model is shown by the corner marker symbols, as shown in the legend as well. A region enclosed by a bounding box with crosses (X) at each corner indicates high validity model (excellent model). Similarly circles (O) indicate a medium validity model (strong model) and an upward pointing triangle ($\triangle$) indicates a low validity model (weak model). Figure 4.7 shows this plot on a log scale to highlight the range of low frequencies considered as well.

4.2.1 Low Grazing Angle Region

From Figure 4.6 it can be seen that there exists land clutter models for all grazing angle regions and most radar frequencies. However the validity of these models in these angle and frequency ranges needs to be taken into consideration. As shown in Figure 4.6, Billingsley's land clutter model is the only high validity model in the low grazing angle region. Other models of lower validity in the low grazing angle region is the Adapted GTRI and Nathanson land clutter models. Billingsley's high validity model however is only valid for radar frequencies from VHF to X-band with the exception of S-band. The Adapted GTRI model can be used for other grazing angle and frequencies not considered by Billingsley but at a lower validity.

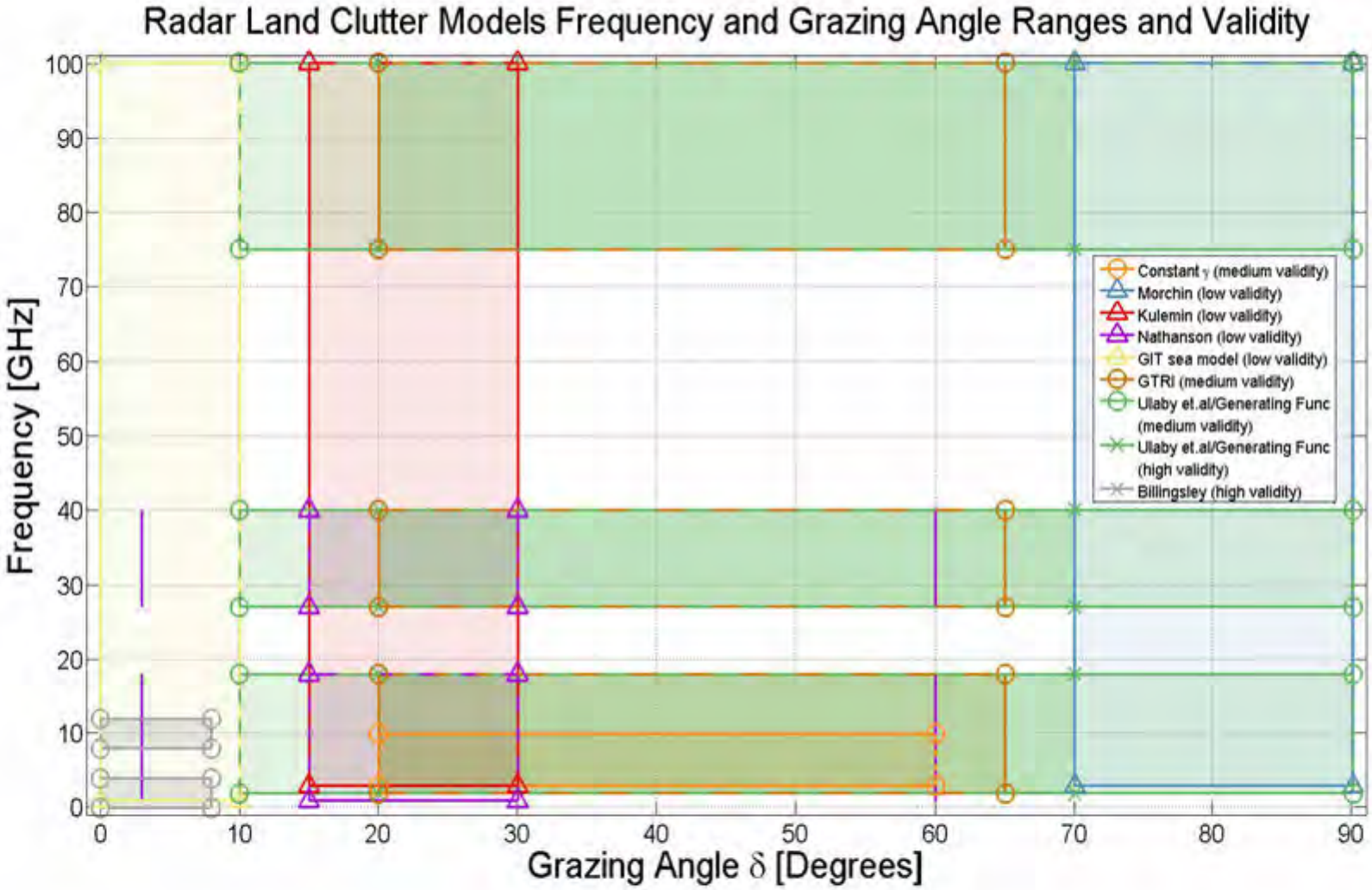

Figure 4.6: Radar land clutter models frequency and grazing angle ranges and validity.

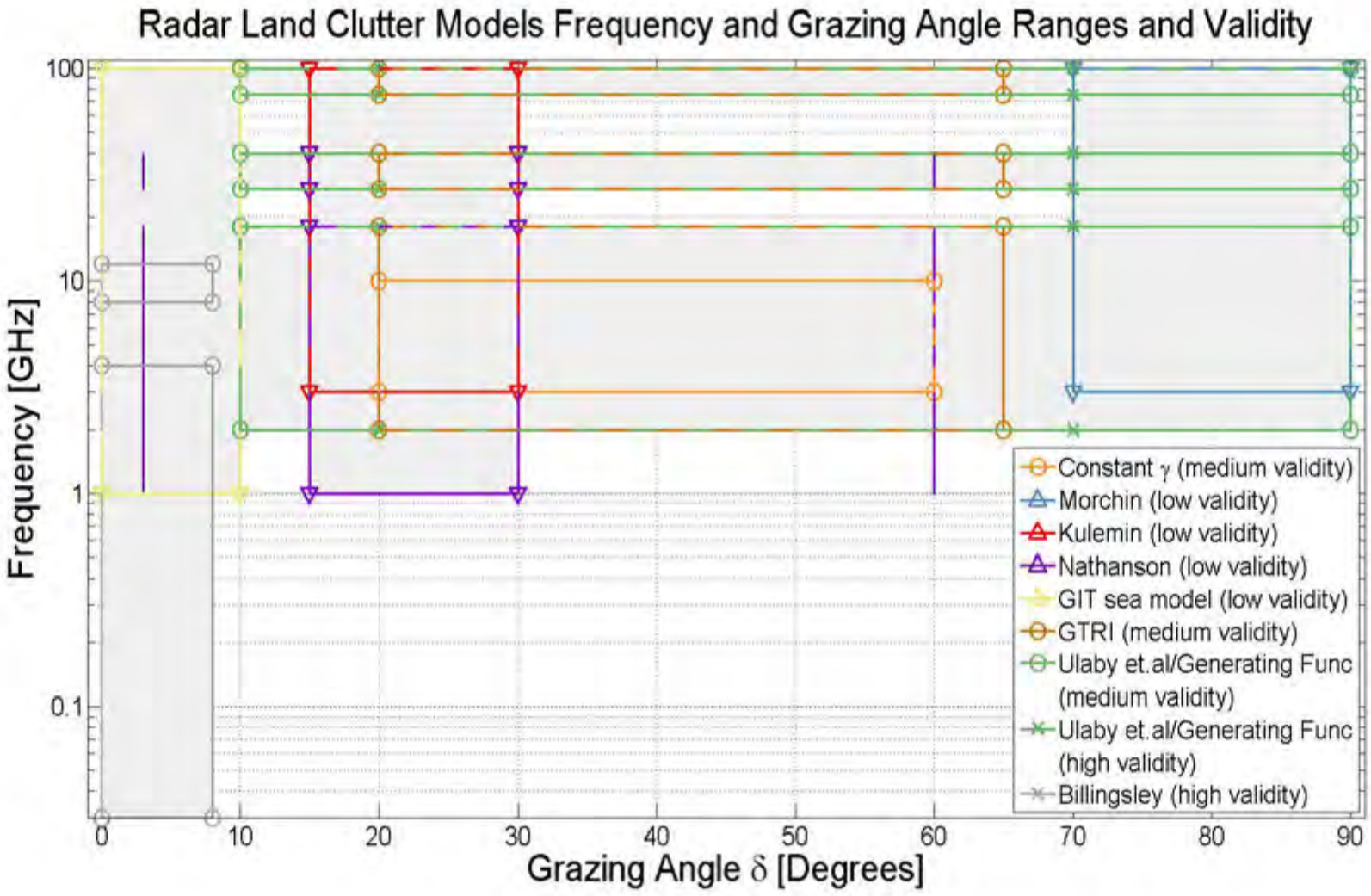

Figure 4.7: Radar land clutter models frequency and grazing angle ranges and validity (log scale).

4.2.2 Plateau Grazing Angle Region

For the plateau grazing angle region, the Ulaby and Dobson and Generating Function land clutter model is the only high validity models. Other models of lower validity in the plateau grazing angle region are the Constant Gamma and GTRI land clutter models (medium validity), followed by the Kulemin and Nathanson land clutter models (low validity). Ulaby and Dobson and the Generating Function model is valid for frequency bands from L to W, with the exception of K and V band. The Kulemin model can be used for other grazing angle and frequencies not considered by Ulaby and Dobson / Generating Function land clutter model, but at a lower validity.

4.2.3 High Grazing Angle Region

For high grazing angle regions, the Ulaby and Dobson and Generating Function model can be used, however it should be noted that for high grazing angles this model is considered medium validity. This is followed by the Morchin land clutter model. Thus no high validity model exists for high grazing angle region. The valid frequency bands range from L to W band.

4.2.4 Discussion and Summary

It is shown that high validity land clutter models only exist for a limited range of grazing angles and frequencies. Furthermore, no land clutter model exists for K and V frequency band in the plateau grazing angle region. This may be due to a lack of radars in the K and V frequency bands. This is believed to be due to the high attenuation that occurs in these regions as discussed in section 2.1.1, making these frequency bands unsuitable for general radar use. There also does not exist any land clutter models currently for low frequencies in the plateau and high grazing angle regions, as shown in Figure 4.7. Land clutter models other than high validity models should be used with caution for cases where no high validity model exists. As shown in section 4.1, these lower validity models can at times produce simulated values that are orders of magnitude different from measured data.

It is thus recommended that future research in land clutter modelling focus on developing

high validity models for all non-existing and lower validity regions that has been identified above.

4.3 Linking Land Clutter Models to Land Cover Data

Land cover data is required to determine the type of terrain cover of the simulated clutter patches. For all different simulated clutter patch terrain types, an appropriate land clutter model terrain type should be used that closely matches the clutter patch terrain type. The GlobeLand30 or NLC 2009 land cover datasets were identified as appropriate models to use to classify land cover within the SADC and RSA region of interest. Thus for each terrain type found in the GlobeLand30 or NLC 2009 datasets, a decision was made as to which of the terrain types for each land clutter model matches to the land cover data terrain type the closest. Either the land clutter model does or does not have a terrain type that matches with the land cover data terrain type. The decision can be classified in three ways, either the land clutter model with chosen terrain type fully agrees and matches with the land cover data terrain type, closely agrees and matches with it, or only partially agrees and matches with the land cover data terrain type. In some cases no land clutter model terrain type matches with the land cover data terrain type.

The process of linking the land cover data terrain types to land clutter model terrain types is shown in Table 4.2 for GlobeLand30 dataset and in Table 4.3 for NLC 2009 dataset.

4.4 Proposed Site Specific Radar Coverage and Land Clutter Modelling Tool Program Flow

As proposed, the site specific radar coverage and land clutter modelling tool can be executed according to the following steps.

1. **Load latitude and longitude location of site of interest.** This point will serve as the reference point where the simulated radar is located. All calculations are based on this reference point.

2. **Load simulated radar specific parameters.** Radar parameters required are the

Table 4.2: Linking GlobeLand30 terrain types to Land Clutter model terrain types.

GlobeLand30 Land Cover Dataset	Constant Gamma	Morchin	Kulemin	Nathanson	GTRI	Ulaby & Dobson / Generating Function	Adapted GTRI Sea	Billingsley
Cultivated Land	Farmland	Farmland	Arable Land	Farmland	• Tall grass crops • Soil, sand and rocks	• Shrubs • Trees	For any terrain type for low grazing angles less than 10°	**High or low relief:** • Open Farmland. • Low relief negative depression angle
Forest	Woods	Woodlands	• Decideous and coniferous forests • Grass both	Heavy woods / jungle	• Trees • Tall grass crops	Trees	For any terrain type for low grazing angles less than 10°	**High or low relief:** • Continuous forests • Open farmland • General rural
Grassland	Flatland	N/A	Grass (both heights)	N/A	Grass	• Grasses • Short vegetation	For any terrain type for low grazing angles less than 10°	**High or low relief:** • Grassland • General rural
Shrubland	Flatland	Desert	Arable Land	Deserts	Soil, sand and rocks	• Shrubs • Short vegetation	For any terrain type for low grazing angles less than 10°	**High or low relief:** • Marsh • General rural
Water bodies	N/A	N/A	N/A	N/A	N/A	Short Vegetation	For any terrain type for low grazing angles less than 10°	N/A
Wetland	N/A	N/A	N/A	N/A	N/A	Short Vegetation	For any terrain type for low grazing angles less than 10°	N/A
Tundra	Flatland	N/A	Arable Land	N/A	Soil, sand and rocks	• Shrubs • Short vegetation	For any terrain type for low grazing angles less than 10°	**High or low relief:** • Marsh • General rural
Artificial surfaces	Metropolitan	N/A	• Urban Territories • Concrete	Urban	Urban	Urban	For any terrain type for low grazing angles less than 10°	**High or low relief:** • Urban. •Low relief negative depression angle
Barelands	• Farmland • Flatland	• Desert • Farmland	Arable land	• Desert • Farmland	Soil, sand and rocks	Soil and rock surfaces	For any terrain type for low grazing angles less than 10°	**High or low relief:** • Marsh • General rural
Snow and Ice	N/A	N/A	Snow	N/A	Wet and Dry snow	Wet and Dry snow	For any terrain type for low grazing angles less than 10°	N/A
Missing data	Nearest classification	Nearest classification	Nearest classification	Nearest classification	Nearest classification	Nearest classification	Nearest classification	Nearest classification

Table Legend	
	• Model terrain type only partially agrees with land cover terrain type. •Low validity
	Model terrain type closely agrees with land cover terrain type. • Medium validity
	• Model terrain type fully agrees with land cover terrain type • High validity
	No model terrain type matches with land cover terrain type.

Table 4.3: Linking NLC 2009 terrain types to Land Clutter model terrain types.

NLC 2009	Constant Gamma	Morchin	Kulemin	Nathanson	GTRI	Ulaby & Dobson / Generating Function	Adapted GTRI Sea	Billingsley
Water Bodies	N/A	N/A	N/A	N/A	N/A	Short Vegetation	For any terrain type for low grazing angles less than 10°	N/A
Urban	Metropolitan	N/A	• Urban Territories. • Concrete	Urban	Urban	Urban	For any terrain type for low grazing angles less than 10°	**High or low relief:** • Urban. •Low relief negative depression angle
Plantations	Woods (for planted areas of wood)	Woodlands (planted tree areas)	• Decideous and coniferous forests • Grass both	Heavy woods / jungle	• Trees • Tall grass crops	Trees	For any terrain type for low grazing angles less than 10°	**High or low relief:** General rural. Open farmland
Natural	• Flatland • Woods • Wooded Hill	• Woodland. • Mountain for high slope areas	• Decideous and coniferous forests • Grass both heights	• Farmlands • Desert	• Soil, sand and rocks • Grass	• Soil and Rock Surfaces • Short Vegetation • Trees. • Grasses • Shrubs	For any terrain type for low grazing angles less than 10°	**High or Low relief:** • General rural • Continuous Forest • Desert, marsh or grassland • Low relief negative depressio angle • Mountains
Mines	Metropolitan	N/A	Concrete	Urban	Urban	Urban	For any terrain type for low grazing angles less than 10°	**High or low relief:** • Urban • Low relief negative depressio angle
Degraded	Flatlands (degraded flatland areas)	• Woodland. • Mountain for high slope areas	• Decideous and coniferous forests • Grass both heights	• Farmlands • Heavy woods	• Trees • Soil, sand and rocks	• Soil and Rock Surfaces • Short Vegetation • Grasses • Shrubs	For any terrain type for low grazing angles less than 10°	**High or Low relief:** • General rural • Continuous Forest • Desert, marsh or grassland • Low relief negative depressio angle • Mountains
Cultivation	Farmlands	Farmland	Arable Land	Farmland	• Tall grass crops • Soil, sand and rocks	• Shrubs • Trees	For any terrain type for low grazing angles less than 10°	**High or low relief:** • Open Farmland • Low relief negative depressio angle
Missing data	Nearest classification	Nearest classification	Nearest classification	Nearest classification	Nearest classification	Nearest classification	Nearest classification	Nearest classification

Table Legend	
	• Model terrain type only partially agrees with land cover terrain type. •Low validity
	Model terrain type closely agrees with land cover terrain type. • Medium validity
	• Model terrain type fully agrees with land cover terrain type • High validity
	No model terrain type matches with land cover terrain type.

radar tower height, radar operating frequency, range resolution, polarisation etc.

3. **Load DEM and Land Cover data for area of interest.** The DEM data will be used to identify masked areas within the radar observed environment and to determine the land topography and slopes. The land cover data will be used to determine the type of terrain cover for each simulated clutter patch.

4. **Account for earth curvature and atmospheric refraction.** The $\frac{4}{3}$ earth model will be used to distort the loaded DEM and Land Cover data in order to account for earth curvature and atmospheric refraction effects.

5. **Create simulated clutter patches.** Clutter patches will be created by breaking the DEM data up into triangular surfaces. A suitable meshing process will be used for this process. Each triangular surface will be a separate clutter patch.

6. **Determine masked areas.** By using Ray Tracing algorithms, the LOS from the reference point to each centre point of each clutter patch will be determined. All clutter patches that are not within LOS will be disregarded and not used further in the simulation. These will show the masked areas within the terrain.

7. **Determine data for each visible clutter patch.** For all visible clutter patches, the range to the clutter patch from reference point, clutter patch surface normal and area, grazing, incidence and depression angles, and type of terrain cover will be determined.

8. **Determine backscatter coefficient σ° for each visible clutter patch.** Based on each visible clutter patches grazing angle / incidence angle / depression angle, terrain type, terrain relief and slope, as well as the radar operating frequency, an appropriate land clutter model will be chosen to simulate a backscatter coefficient σ° value for the clutter patch. The land clutter model chosen will be based on the highest validity model that can be used that is valid for all the necessary input data. This decision should correspond with the proposed land clutter model to use for different situations as discussed in this dissertation.

9. **Determine RCS for each clutter patch.** Once σ° is calculated for each visible clutter patch, the RCS can be calculated by multiplying σ° with the area of the

clutter patch. At this point the radar observed environment model, LOS coverage and land clutter model of the scene is complete.

10. **Develop the radar sensor model.** As discussed in section 3.3.4, the radar sensor model needs to be developed. This shows the characteristics of the radar system and antenna beam pattern.

11. **Develop radar range traces.** As discussed in section 3.3.4, range traces are then formed at closely spaced azimuth angles which is based on the radar antenna beamwidth, scan rate, and pulse repetition frequency (PRF). The azimuth spacing needs to be chosen such that it provides adequate fidelity. The range samples are then calculated and spaced according the radar range resolution. Area sampling is performed for each range trace.

12. **Simulate coherent radar returns.** As discussed in section 3.3.4, for each range trace, all samples within the radar range bin is summed to simulate coherent radar return. The returns are modified by the attenuation relative to the antenna peak gain at boresight as a function of the off boresight sample angle. The land clutter power at the receiver for each range bin is calculated using the radar equation.

4.5 Chapter Summary

In this chapter, an analysis of the land clutter models, as well as the linking of land cover terrain classes with land clutter models terrain types were presented.

Section 4.1 presents a comparison of existing land clutter models with measured data. These comparisons justify the validity and compatibility for land clutter models in the low, plateau and high grazing angle regions. Conclusions drawn and recommendations made based on these comparisons are given in section 4.1.3 above.

Section 4.2 presents a view of the range of grazing angles, frequencies and validity for the existing land clutter models. Ranges that lack high validity land clutter models were identified. It is recommended that future land clutter model research be conducted in these identified ranges. Further conclusions and recommendations based on this analysis are given in section 4.2 above.

Linking of land cover terrain classes with the appropriate land clutter terrain types are presented in section 4.3. Recommendations made for this linking process is given in Table 4.2 for GlobeLand30 dataset and in Table 4.3 for NLC 2009 dataset.

A proposed program flow for a site specific radar coverage and land clutter modelling tool is presented in section 4.4.

Chapter 5

Conclusions, Recommendations and Future Work

This chapter provides conclusions and recommendations based on the foregoing information in the report and then ends by highlighting areas for future work.

5.1 Conclusions and Recommendations

The aim of this project was to bring together the models and processes required to start the development of a site specific radar coverage and land clutter modelling tool. The objectives were therefore to investigate the related theoretical information and intended models and processes required for the development of a site specific radar coverage and land clutter modelling tool. In order to complete this objective, a theoretical study with regards to elements that would influence the development of such a tool was done. These included topics covering radar propagation, radar coverage, geographic information systems (GIS) related data and radar land clutter / backscatter coefficient models. Different land clutter models can be used for different simulation and radar characteristics, thus existing land clutter model's validity are based on different underlying model assumptions and dependencies. The main focus of this investigation was thus to determine the most appropriate land clutter models to use for varying terrain types, range of frequencies and significant characteristics which affect clutter returns. This included a comparison of measured backscatter data with simulated backscatter data calculated from these land clut-

ter models. Furthermore to provide classification tables in terms of each model's validity for different grazing angles and frequency ranges. The purpose being to aid clutter model decisions required for the development of a site specific radar coverage and land clutter modelling tool, and to highlight grazing angle and frequency ranges where low validity or no land clutter models are available, such that recommendations can be made on where future studies on land clutter modelling can be focussed on.

Chapter 2 highlighted a number of important considerations with regards to developing a site specific radar coverage and land clutter modelling tool. It was shown that it is important to consider the effects that propagation, the atmosphere and curvature of the earth has on a propagating EM wave. The make up and concentration levels of water and oxygen in the different zones of the atmosphere can introduce signal attenuation and refraction effects. The curvature of the earth can limit the radar horizon. A simple method that was proposed that takes into account earth curvature and atmospheric refraction was the $\frac{4}{3}$ Earth Model. The model does however have limitations. The model assumes standard atmospheric conditions throughout altitudes and assumes constant ratio of actual to effective earth radius. In reality, this ratio will change as a function of altitude, atmospheric conditions and frequency. Because of it's simplicity and convenience, the $\frac{4}{3}$ Earth Model has been a trusted model to use to account for the effects of atmospheric refraction in simulation by various radar analysts and researchers.

It was found that the effects of the pattern propagation factor, F, should be noted when simulating or measuring radar land clutter. In all instances the author notes that F to the fourth power would be inherently included in the measurement and modelling of the backscatter coefficient, σ°. For the purposes of this research, no attempts are made to separate the effects of propagation (in terms of F^4), over the terrain, between the radar and the clutter cell from the intrinsic terrain backscatter σ°, from the clutter cell itself. This being for all measures of clutter strength, or measures of backscatter coefficient σ°, both in the representation of measured data as well as in predictive modelling of σ°. This separation is a complex task and in some cases not realisable, especially at lower grazing angles. Thus terms such as the clutter strength, σ or σ°, as used in this dissertation is defined as the product of the backscatter coefficient σ° and the pattern propagation factor to the fourth power, F^4 , where F is assumed to include all propagation effects, including multipath and diffraction, between the radar and the clutter cell.

In order to model the radar observed environment effectively, high quality digital elevation model (DEM) and land cover data is required. DEM data is used to model the terrain topography such that masked areas and terrain relief can be determined. Similarly for successful characterisation of the clutter performance, land cover data of the intended simulated area needs to be taken into account. Various sources of DEM and land cover data were investigated in this dissertation. It was found that the SRTM 30 m DEM data is currently the highest quality elevation dataset that is freely available and covers all intended areas of interest. Two land cover data sources can be considered, namely the NLC 2009 or GlobeLand30 m LC datasets. These are both at a high resolution of 30 m. The NLC 2009 dataset however only covers the RSA region, whereas the GlobeLand30 m covers the entire SADC region of interest. The GlobeLand30 m source is also a more current LC model than the NLC 2009 data source. The GlobeLand30 m dataset is therefore recommended for use in a site specific radar coverage and land clutter modelling tool.

The method proposed to create simulated clutter patches was by meshing processes. The method proposed to determine masked terrain and LOS radar coverage was by using ray tracing algorithms.

In order to estimate radar system performance in land clutter, clutter models are required. These land clutter models are generally described by the backscatter coefficient σ°. It was found that there are many radar and environment parameters that influence σ°. These are shown in Table 2.2. One of the factors that influences σ° and that was of interest in this dissertation was the grazing angle. It was found that σ° behaves differently in different grazing angle regions, namely the low, plateau, and high grazing angle regions. Standard probability density functions (PDF's) models can be used to describe the variation of different types of land clutter. From measurement data, statistical parameters required by these PDF models for different types of land clutter can be defined empirically. Empirical and semi-empirical models that describe the mean backscatter reflectivity σ° for various types of land terrain as a function of frequency, grazing angle and polarisation can also be developed from measurement data. Empirically derived PDF models would require large amounts of computer resources for use in a site specific radar coverage and land clutter modelling tool described in this study. Semi-empirical models describe the average backscatter coefficient given by simple formulas containing several parameters. These provide a quick and simple estimation of the backscatter coefficient and considered more

suited to be used for developing a site specific radar coverage and land clutter modelling tool. Mathematical models can also be developed that provide an estimation to the the general shape of the backscatter coefficient. Radar land clutter models are difficult to characterize with consistency and accuracy. This is due to the complex nature of clutter. No land clutter model will therefore represent the exact clutter returns from a specific site. However these models can be used to predict typical conditions. The nature of land clutter models can be determined from how they were derived, and their relationship with clutter returns seen on specific sites or trials. The nature of how a land clutter model was derived is thus an important factor to consider when determining the appropriate model to use for particular cases.

One of the main objectives was thus to identify and investigate existing land clutter models that can be used in a site specific radar coverage and land clutter modelling tool to predict typical conditions. The author notes that specific scene measurements will not coincide with modelling predictions exactly, however the purpose of this analysis was to identify which models would be best suited (or be the best fit model to use for specific scenes). Where a first order analysis of the simulated radar coverage and clutter performance would aid in the design and deployment of radar systems (especially where measurement data in the concept design phase is not possible or not feasible). The analysis as well as the comparison to measured data thus aims to identify not only the best fit models, but if the approach of using models is valid, and to what extent, which design consideration questions or trade-offs could it add value to.

Several mathematical, empirical, and semi-empirical land clutter models were considered. These land clutter models were:

1. Constant Gamma Land Clutter Model.
2. Morchin Land Clutter Model.
3. Kulemin Land Clutter Model.
4. Nathanson Land Clutter Model Tables.
5. Georgia Tech Research Institute (GTRI) Land Clutter Model.
6. Ulaby and Dobson Land Clutter Model.

7. σ° Generating Function Land Clutter Model.

8. Adapted Georgia Tech Research Institute (GTRI) Sea Clutter Model.

9. Billingsley Land Clutter Model.

It was found that only Billingsley's land clutter model and the adapted GTRI sea clutter model is valid for the entire low grazing angle region. Nathanson's land clutter model tables can be used as well but only for a few limited discrete grazing angles. It is clear that Billingsley is the authoritative land clutter model to use for low grazing angle regions. Billingsley's successful validation process further justifies the assumption that his model is considered an excellent and high validity model to use for low grazing angle regions.

For grazing angles in the plateau region, the Ulaby and Dobson or Gamma Generating Function model should be considered first as they produced backscatter values that were the closest and lowest RMSE relative to measured data as compared to the others. The Constant Gamma land clutter model performed better than the GTRI land clutter model for all cases. The Kulemin land clutter model produced the largest RMSE and thus justifies the assumption made to classify it as a weak and low validity model.

For general high grazing angles, the Ulaby and Dobson and Generating Function land clutter models should be considered first, as they produced backscatter values that produced the lowest RMSE to measured data as compared to the others. Following these will be the Morchin and GTRI land clutter models respectively. However, for the limited grazing angle range between 70° and 90°, the Morchin land clutter model should be considered first as it produced the lowest RMSE in this region of angles.

As shown in the cases of urban terrain comparisons, it is further justified that the Ulaby and Dobson or Gamma Generating Function should be used with caution for cases where the model is based on insufficient data. Specifically for urban terrain, the Constant Gamma model should be considered first, followed by GTRI and Kulemin land clutter models for plateau grazing angle regions respectively. For urban terrain at high grazing angles, only the Ulaby and Dobson or Gamma Generating Function is valid and can be considered, however this should be used with caution as the model for urban terrain is based on insufficient data. It should be noted that for urban areas, the land clutter can in most cases only be modelled in a general way as urban terrain is far too complex to be accurately statistically modelled.

Nathanson's tables provide average values for σ° for only a few discrete grazing angles and are therefore not suitable for use in site specific radar land clutter modelling where the dependence of σ^0 on a range of grazing angles would be required.

As it was shown when comparing simulated data to measured data, the presence of discrete scatterers interspersed can significantly increase the reflectivity measurement from homogeneous terrain. It is thus important to remove any sources of discrete scatterers when developing future land clutter models. These discrete scatterers are also important to consider when developing a site specific radar land clutter modelling tool to determine radar dynamic ranges, as their contribution can be orders of magnitude larger than the average backscatter values of the homogeneous terrain.

A classification table was presented indicating the appropriate land clutter models to use in order of validity (weak,strong or excellent) for different grazing angle regions. This table should be followed when developing algorithms for the site specific radar coverage and land clutter modelling tool. It was found that only Billingsley and Ulaby and Dobson / Generating Function land clutter model can be classified and used as a high validity model. It was also shown that for many grazing angle and frequency ranges of interest, only lower validity models exist, and in some cases no models exist. These were identified specifically for high frequencies in the low grazing angle region, low frequencies in the plateau grazing angle region, and the high grazing angle region for all frequencies.

For each terrain type found in the GlobeLand30 and NLC 2009 datasets, a decision was made as to which of the terrain types for each land clutter model matches to the land cover data terrain type the closest. This classification was presented in the form of a table. It was found that for some land cover classes, either none or low validity match is found with a land clutter model. This is also dependent on the grazing angle and frequency. It is thus recommended that future land clutter modelling work should be done in not only the missing grazing angle and frequency ranges identified, but for certain terrain classes identified by land cover data as well.

A proposed program flow for a site specific radar coverage and land clutter modelling tool was presented. The proposed classification tables (Tables 4.1a, 4.1b, 4.2 and 4.3) that show the appropriate models to use for different cases should be followed when developing algorithms for a site specific radar coverage and land clutter modelling tool.

This will ensure that an existing land clutter model with the highest validity available will be used to simulate σ° values.

It was concluded that the validity of the such a tool is highly dependent on the validity of the data and specifics of the land clutter model used. In some cases for specific frequencies and terrain types, the result from the land clutter model closely matches measured data, and in some cases it does not. A land clutter model may be classified as a high validity model in general, but for certain cases where insufficient data exists, the validity of the model can decrease significantly.

It was shown that high validity land clutter models only exist for a limited range of grazing angles and frequencies. Furthermore, no land clutter model exists for K and V frequency band in the plateau grazing angle region. This may be due to a lack of radars in the K and V frequency bands. This is believed to be due to the high attenuation that occurs in these regions, making these frequency bands unsuitable for general radar use. There also does not exist any land clutter models for low frequencies in the plateau and high grazing angle regions. Land clutter models other than high validity models should be used with caution for cases where no high validity model exists. Lower validity models can at times produce simulated values that are orders of magnitude different from measured data.

It is thus recommended that future research in land clutter modelling focus on developing high validity models for all non-existing and lower validity regions that have been identified. It is also recommended that measured data for all terrain types considered in the land cover data sources be conducted such that a full comparison and validation process can be performed for all land clutter models terrain types of interest.

5.2 Future Work

Based on the insights gained during this research study, the following proposed future works aims to extend and improve on the development of a site specific radar coverage and land clutter modelling tool:

1. This dissertation only focused on the spatial statistics and average values. Future work can aim to investigate simulating the temporal statistics of clutter as well.

2. Future studies can be conducted into implementing the insights gained into the development, testing and validation of such a tool.

3. Future studies can be conducted to develop new high validity land clutter models for grazing angles, frequencies and terrain types not represented by existing models.

4. All existing empirical land clutter models are based upon measured data from areas not within the SADC region. Future studies can be conducted to develop land clutter models that are based upon terrain and measurements taken from within the SADC region.

Appendix A

Source Code

All source code that the author has developed and used to generate simulations and analysis results as seen in this report has been included as an attachment to the submission. Subsequently it can also be obtained via the following link: *https://www.dropbox.com/sh/oopuav0gau0i7bx/AACZSvCGW78tuZKYppaM-qT5a?dl=0*

Bibliography

[1] M. Skolnik. *Introduction to Radar Systems*. McGraw-Hill Education, 2002.

[2] M A Richards et al. *Principles of modern radar*. Number v. 1 in Principles of Modern Radar. SciTech Publishing, Incorporated, 2010.

[3] The Institute of Electrical and Electronics Engineers. IEEE standard radar definitions. *IEEE Std 686-2008 (Revision of IEEE Std 686-1997)*, pages c1–41, May 2008.

[4] J.J. de Witt and J.J. Strydom. Analysis of measured l-band airborne land clutter from the western cape region of south africa. In *Radar Conference (Radar), 2014 International*, pages 1–6, Oct 2014.

[5] Juan Pablo Ardila Lopez. Assessment and modeling of angular backscattering variation in alos scansar images over tropical forest areas. 2008.

[6] J.B. Billingsley. *Low-angle Radar Land Clutter: Measurements and Empirical Models*. Radar, Sonar, Navigation and Avionics Bks. William Andrew Pub., 2002.

[7] N C Currie. *Radar reflectivity measurement: techniques & applications*. Artech house radar library. Artech House, 1989.

[8] S H Yueh. K-distribution and polarimetric terrain radar clutter. *Electromagnetic Waves and Applications*, 3:747–768, April 1989.

[9] GP Kulemin, EA Goroshko, and EV Tarnavsky. Land backscattering model for millimeter wave radar. In *Modern Problems of Radio Engineering, Telecommunications and Computer Science, 2004. Proceedings of the International Conference*, pages 138–141. IEEE, 2004.

[10] M Long. *Radar Reflectivity of Land and Sea*. Artech House radar library. Artech House, 2001.

[11] William Connor. Low grazing angle terrain backscattering coefficient generator. Masters thesis, Air Force Institute of Technology USA, Airforce Institute of Technology, 2950 P Street WPAFB, OH 45433-7765, March 1999.

[12] Christopher C Lin and J Patrick Reilly. A site-specific model of radar terrain backscatter and shadowing. *Johns Hopkins APL Technical Digest*, 18(3):433, 1997.

[13] G Rode. Radar clutter backscattering simulation for specific sites. *Frequenz*, 62(1-2):7–11, 2008.

[14] Roger E Clapp. *A theoretical and experimental study of radar ground return*. Radiation Laboratory, Massachusetts Institute of Technology, 1946.

[15] W.C. Morchin. *Airborne Early Warning Radar*. Artech House radar library. Artech House, 1990.

[16] Fred E Nathanson et al. *Radar Design Principles*, chapter 9, pages 247–282. SciTech Publishing, 1999.

[17] F.T. Ulaby and M.C. Dobson. *Handbook of Radar Scattering Statistics for Terrain*. Artech House remote sensing library. Artech House, 1989.

[18] R. Mediavilla, W. O'Connor, V. Pyati, and K. Wilson. Terrain backscattering coefficient generator. In *Geoscience and Remote Sensing Symposium, 1999. IGARSS '99 Proceedings. IEEE 1999 International*, volume 2, pages 1429–1431 vol.2, 1999.

[19] Kelce Wilson, Dale Patrick, and James Blair. Radar scattering statistics for digital terrain models, 2005.

[20] Donald E Kerr. *Propagation of short radio waves*, volume 24. IET, 1951.

[21] Khan Major Mohammad Ali, Rahman Afia Binte, Popy Jannatul Fardous, et al. *Effects of changing RCS and Antenna Array pattern Radar performance*. PhD thesis, Department of Electrical, Electronics and Communication Engineering (EECE), 2011.

[22] F.T. Ulaby, D.G. Long, W.J. Blackwell, C. Elachi, and K. Sarabandi. *Microwave Radar and Radiometric Remote Sensing*. University of Michigan Press, 2014.

[23] B.R. Mahafza. *Radar Systems Analysis and Design Using MATLAB*. CRC Press, 2002.

[24] Leslie W Barclay. *Propagation of radiowaves*, volume 502. Iet, 2003.

[25] D.K. Barton. *Modern Radar System Analysis*. Artech House Radar Library. Artech House, 1988.

[26] G.R. Curry. *Radar Essentials: A Concise Handbook for Radar Design and Performance*. Electromagnetics and Radar Series. Institution of Engineering and Technology, 2012.

[27] L.V. Blake. *Radar range-performance analysis*. LexingtonBooks, 1980.

[28] K.R. Noth. Modeling and simulation of a ground based sense and avoid architecture for unmanned aircraft system operations. In *Integrated Communications, Navigation and Surveilance Conference (ICNS), 2011*, pages O7–1–O7–9, May 2011.

[29] A.G. Huizing and A. Theil. *CARPET (Computer-aided Radar Performance Evaluation Tool): Radar Performance Analysis Software and User's Manual, Version 1.0: Buch*. Artech House, 1993.

[30] Wayne L Patterson. *Advanced Refractive Effects Prediction System*. Space and Naval Warfare Systems Center, Defense Technical Information Center 8725 John J. Kingman Road Ft. Belvoir, VA 22060-6218, 1 edition, April 1998.

[31] Yunhan Dong. Models of land clutter vs grazing angle, spatial distribution and temporal distribution-l-band vv polarisation perspective. Technical report, DTIC Document, 2004.

[32] Daniel Sabel, Marcela Doubkova, Wolfgang Wagner, Paul Snoeij, and Evert Attema. A global backscatter model for c-band sar. In *Proceedings of the ESA Living Planet Symposium, Bergen, Norway*, volume 28, 2010.

[33] Floyd M Henderson, Anthony J Lewis, et al. *Principles and applications of imaging radar. Manual of remote sensing, volume 2*. John Wiley and sons, 1998.

[34] E. V. Tarnavsky and G. P. Kulemin. Modeling of radar land clutter map for small grazing angles. In R. S. Romaniuk, editor, *Photonics Applications in Astronomy, Communications, Industry, and High-Energy Physics Experiments II*, volume 5484 of *Society of Photo-Optical Instrumentation Engineers (SPIE) Conference Series*, pages 702–706, July 2004.

[35] Abdenasser Djafri and Boualem Haddad. Mapping of weather radar ground clutter using the digital elevation model (srtm). *Signal & Image Processing: An International Journal (SIPIJ)*, 3:135–151, 2012.

[36] RA Kropfli, I Katz, TG Konrad, and EB Dobson. Simultaneous radar reflectivity measurements and refractive index spectra in the clear atmosphere. *Radio Science*, 3(10):991–994, 1968.

[37] Klett, Eberhard Witwe, Detleffsen, Christoph Peter, et al. *Photometria*. sumptibus viduae Eberhardi Klett, 1760.

[38] Benjamin Crowell. 2 simple nature an introduction to physics for engineering and physical science students. 2007.

[39] William M Haynes. *CRC handbook of chemistry and physics*. CRC press, 2014.

[40] Thomas Lillesand, Ralph W Kiefer, and Jonathan Chipman. *Remote sensing and image interpretation*. John Wiley & Sons, 2014.

[41] Kevin J Sangston and Kari R Gerlach. Coherent detection of radar targets in a non-gaussian background. *Aerospace and Electronic Systems, IEEE Transactions on*, 30(2):330–340, 1994.

[42] J.B. Billingsley, A. Farina, F. Gini, M.V. Greco, and L. Verrazzani. Statistical analyses of measured radar ground clutter data. *Aerospace and Electronic Systems, IEEE Transactions on*, 35(2):579–593, Apr 1999.

[43] Ulku Cilek Doyuran and Yalcin Tanik. Detection in range-heterogeneous weibull clutter. In *Radar Conference, 2007 IEEE*, pages 343–347. IEEE, 2007.

[44] M. Sekine and Y. Mao. *Weibull Radar Clutter*. Electromagnetics and Radar Series. P. Peregrinus Limited, 1990.

[45] HC Chan. Temporal statistics of low-angle ground clutter. Technical report, DTIC Document, 1989.

[46] Stephen O Rice. Mathematical analysis of random noise. *Bell System Technical Journal*, 23(3):282–332, 1944.

[47] J Barrie Billingsley and John F Larrabee. *Multifrequency measurements of radar ground clutter at 42 sites*. Massachusetts Institute of Technology, Lincoln Laboratory, 1991.

[48] KD Ward et al. Sea clutter: Scattering, the k distribution and radar performance. *IET Radar, Sonar and Navigation Series 20*, 22(1), January 2006.

[49] T.J. Nohara and S. Haykin. Canadian east coast radar trials and the k-distribution. *Radar and Signal Processing, IEE Proceedings F*, 138(2):80–88, Apr 1991.

[50] Eo Jakeman. On the statistics of k-distributed noise. *Journal of Physics A: Mathematical and General*, 13(1):31, 1980.

[51] Eo Jakeman and PN Pusey. A model for non-rayleigh sea echo. *Antennas and Propagation, IEEE Transactions on*, 24(6):806–814, 1976.

[52] G Sun et al. Terrain effect on forest radar backscatter: Modelling and correction. Number 01-074 in CEOS-SAR, 1 Department of Geography, University of Maryland, College Park, MD 20742 USA, 2001. Department of Geography, University of Maryland.

[53] J P Wilson et al. *Terrain Analysis: Principles and Applications*. New York: Wiley, 2000.

[54] Christine Mary Rutherford Fowler. *The solid earth: an introduction to global geophysics*. Cambridge University Press, 1990.

[55] Witold Fraczek. Mean sea level, gps, and the geoid. [Online] at: `http://www.esri.com/news/arcuser/0703/geoid1of3.html`, July 2003.

[56] Raytheon STX Williamson and RH Rapp. The development of the joint nasa gsfc and the national imagery and mapping agency (nima) geopotential model egm96. *NASA Technical Paper NASA/TP-1998-206861, Goddard Space Flight Center, Greenbelt*, 1998.

[57] Antonio Di Gregorio and Louisa JM Jansen. Land cover classification system (lccs): classification concepts and user manual. *FAO, Rome*, 1998.

[58] P Mayaux, E Bartholome, M Massart, C Van Cutsem, A Cabral, A Nonguierma, O Diallo, C Pretorius, M Thompson, M Cherlet, et al. A land cover map of africa. carte de occupation du sol de lafrique. *European Commission, Joint Research Center, EUR*, 20665, 2003.

[59] S Feng and J Chen. Low-angle reflectivity modeling of land clutter. *Geoscience and Remote Sensing Letters, IEEE*, 3(2):254–258, 2006.

[60] Frank Hanssen, Roel May, Yngve Steinheim, Roald Vang, et al. Gis-modeling of radar detection coverage and ground clutter within the complex environment of smøla wind-power plant. 2011.

[61] C Lin et al. Radar terrain clutter model with consideration of propagation effects. In *Microwave Conference, 1993. 23rd European*, pages 478–482, Sept 1993.

[62] Ramesh Nepal et al. A simulation study of the impact of surface clutter and space-borne precipitation radar sensor. *36th Conference on Radar Meteorology*, September 2013.

[63] Andriy Kurekin, Lik-Kwan Shark, Kenneth Lever, Darren Radford, and Dave Marshall. Site-specific land clutter modelling based on radar remote sensing images and digital terrain data. In *Remote Sensing*, pages 783013–783013. International Society for Optics and Photonics, 2010.

[64] Michael A Temple and Kelce S Wilson. Probabilistic backscatter coefficient generating function. In *AeroSense'99*, pages 644–649. International Society for Optics and Photonics, 1999.

[65] Digital Geography. Release of world-wide high resolution srtm data. [Online] at: `http://www.digital-geography.com/announcement-realease-worldwide-high-resultion-srtm-data-30m/#.VMJXaEeUePa`, September 2014.

[66] United States Department of the Interior. Shuttle radar topography mission (srtm) 1 arc-second global. [Online] at: `https://lta.cr.usgs.gov/SRTM1Arc`, January 2012.

[67] Jspace Systems. Aster global digital elevation model (gdem). [Online] at: https://www.jspacesystems.or.jp/ersdac/GDEM/E/4.html, October 2012.

[68] GDEM ASTER. Aster global dem validation summary report. [Online] at: http://www.ersdac.or.jp/GDEM/E/image/ASTERGDEM_ValidationSummaryReport_Ver1.pdf, 2009.

[69] Nicolas H. Durland. Defining mean sea level in military simulations with dted. In *Proceedings of the 2009 Spring Simulation Multiconference*, SpringSim '09, pages 115:1–115:3, San Diego, CA, USA, 2009. Society for Computer Simulation International.

[70] John Pike. Digital terrain elevation data [dted]. [Online] at: http://www.fas.org/irp/program/core/dted.htm, January 2009.

[71] Airbus Defence and Space. World dem from astrium. [Online] at: http://www.geo-airbusds.com/files/pmedia/public/r5434_9_geo_022_worlddem_en_low.pdf, 2014.

[72] Airbus Defence and Space:Geo-Intelligence. Terrain data - global to local. [Online] at: http://www.geo-airbusds.com/files/pmedia/public/r3181_9_geo_026_geoelevation_en_low.pdf, 2013.

[73] Open Land Service. Global land cover 2013. [Online] at: http://www.globallandcover.com/home/Enbackground.aspx, 2014.

[74] Fritz Schoeman, TS Newby, MW Thompson, and Elzie Catharina Van den Berg. South african national land-cover change map. *South African Journal of Geomatics*, 2(2):94–105, 2014.

[75] SANBI. Updating national land cover. Technical report, SANBI (South African National Biodiversity Institute), 2 Pretoria St, Pretoria, 0184 South Africa, October 2009.

[76] Ryutaro Tateishi et al. Global map-global land cover (glcnmo). Technical report, Chiba University, Center for Environmental Remote Sensing, Chiba University, Center for Environmental Remote Sensing, 1-33 Yayoi-cho, Inage-ku Chiba, 263-8522 Japan, November 2008.

[77] John Latham et al. Global land cover share. Technical report, Food and Agricultural Organisation of the United Nations (FAO), FAO, Viale delle Terme di Caracalla, 00100, Rome, Italy, 2014.

[78] Global Land Cover Network. Glc-share. [Online] at: `http://www.glcn.org/databases/lc_glcshare_en.jsp`, 2014.

[79] Lin-San Yang, Jia Xu, Xiao Gao, Xiu-Tan Wang, and Ying-Ning Peng. A novel three-dimensional coverage visualization system of netted radars based on arcobjects. In *Radar Conference, 2009 IET International*, pages 1–5, April 2009.

[80] George L Bair. Airborne radar simulation. *Camber Corporation, Dallas, Texas*, 1996.

[81] Jody L Kirtner and Harry R Anderson. The application of land use/land cover data to wireless communication system design. *EDX Engineering, Inc., http://proceedings. esri. com/library/userconf/proc98/PROCEED/TO550/PAP525 P*, 525:1–16.

[82] Sagi Katz, Ayellet Tal, and Ronen Basri. Direct visibility of point sets. *ACM Trans. Graph.*, 26(3), July 2007.

[83] W S Ament. Forward and backscattering by certain rough surfaces. *Antennas and Propagation*, 4:369–373, July 1956.

[84] Wm Randolph Franklin, Clark K Ray, and Shashank Mehta. Geometric algorithms for siting of air defense missile batteries. *A], Research Project for Battle*, (2756), 1994.

[85] Christelle Vancutsem, Eduardo Marinho, FranÃ§ois Kayitakire, Linda See, and Steffen Fritz. Harmonizing and combining existing land cover/land use datasets for cropland area monitoring at the african continental scale. *Remote Sensing*, 5(1):19, 2012.

[86] D Barton. Land clutter models for radar design and analysis. *Proceedings of the IEEE*, 73(2):198–204, Feb 1985.

[87] J P Reilly et al. A radar land clutter model and its verification. In *Geoscience and Remote Sensing Symposium, 1994. IGARSS '94. Surface and Atmospheric Remote*

Sensing: Technologies, Data Analysis and Interpretation., International, volume 4, pages 2319–2321, Aug 1994.

[88] Li Zhang et al. Airship radar system modeling and simulation. Progress In Electromagnetics Research Symposium, August 2012.

[89] Mark Thompson. Development of a new south african land cover dataset using automated mapping techniques. Pretoria South Africa, August 2013. GeoTerraImage Pty Ltd.

[90] Mike Hensel and Erik P Blasch. Fusion of distributions for radar clutter modeling. In *Fusion 2004: Seventh International Conference on Information Fusion*, 2004.

[91] G. Davidson, H.D. Griffiths, and S. Ablett. Statistical analysis of high resolution land clutter. In *RADAR 2002*, pages 434–438, Oct 2002.

[92] G. Davidson, H.D. Griffiths, and S. Ablett. Statistical analysis of high resolution land clutter. In *RADAR 2002*, pages 434–438, Oct 2002.

[93] Andrew J Gatesman, Thomas M Goyette, Jason C Dickinson, Jerry Waldman, Jim Neilson, and William E Nixon. Physical scale modeling the millimeter-wave backscattering behavior of ground clutter. In *Aerospace/Defense Sensing, Simulation, and Controls*, pages 141–151. International Society for Optics and Photonics, 2001.

[94] Antonio Di Gregorio et al. *Land Cover Classification System*. Food and Agriculture Organization of the United Nations, FAO Viale delle Terme di Caracalla 00100 Rome Italy, 2 edition, 2005.

[95] Ricardo Mediavilla. Terrain backscattering coefficient generator. Master's thesis, Air Force Institute of Technology USA, 2950 Hobson Way, Wright Ptrsn Afb, OH 45433, United States, 1999.

[96] Iulian Rosu. Basics of radio wave propagation. [Online] at: `http://www.qsl.net/va3iul/`.

[97] Tom Mahood. Radar ranges of the mojave desert. [Online] at: `http://www.thehowlandcompany.com/radar_stealth/Bluefire.htm`, June 2012.

[98] Canan OZGEN. *Spectral and Statistical Analyses of Experimental Radar Clutter Data*. PhD thesis, Middle East Technical University, 2010.

[99] Maria S Greco and Fulvio Gini. Radar clutter modelling, 2013.

[100] H Laur, P Bally, P Meadows, J SANCHEz, B Schaettler, and E Lopinto. Derivation of the backscatter coefficient sigma0 in esa ers sar pri products. esa document no. Technical report, ES-TN-RS-PM-HL09, 1997.

[101] GLCN Secretariat and Land Cover Topic Centre. Land cover activities in the sadc region. Technical report, Food and Agriculture Organization of the United Nations, NRC, Food and Agriculture Organization of the United Nations (FAO) Viale delle Terme di Caracalla Rome 00100, Italy, 2008.

[102] T Fawwaz et al. Millimeter wave measurement and modelling of terrain scattering. Technical Report 07040188, Radiation Laboratory, University of Michigan, Ann Arbor, Michigan 48109, February 1992.

[103] SANBI. Gis metadata : Detailed report. Technical report, South African National Biodiversity Institute, 2 Pretoria St, Pretoria, 0184, South Africa, January 2009.

EBE Faculty: Assessment of Ethics in Research Projects

Any person planning to undertake research in the Faculty of Engineering and the Built Environment at the University of Cape Town is required to complete this form before collecting or analysing data. When completed it should be submitted to the supervisor (where applicable) and from there to the Head of Department.
If any of the questions below have been answered YES, and the applicant is NOT a fourth year student, the Head should forward this form for approval by the Faculty EIR committee: submit to Ms Zulpha Geyer - Zulpha.Geyer@uct.ac.za; Chemical Engineering Building, Upper Campus, UCT, (Ph 021 650 4791).
NB: A copy of this completed form must be included with the thesis/dissertation/report when it is submitted for examination.

Name of Principal Researcher/Student: **Sulayman Salie** Department: **Electrical Engineering**

Preferred email address of applicant: **ssalie@ska.ac.za**

If a Student: Degree: **MEng Electrical Engineering** Supervisor: **Professor Michael Raymond Inggs**

If a Research Contract indicate source of funding/sponsorship: **Council of Scientific and Industrial Research**

Research Project Title: **Site Specific Radar Coverage and Land Clutter Modelling**

Overview of ethics issues in your research project:

Question 1: Is there a possibility that your research could cause harm to a third party (i.e. a person not involved in your project)?	YES	NO
Question 2: Is your research making use of human subjects as sources of data? If your answer is YES, please complete Addendum 2.	YES	NO
Question 3: Does your research involve the participation of or provision of services to communities? If your answer is YES, please complete Addendum 3.	YES	NO
Question 4: If your research is sponsored, is there any potential for conflicts of interest? If your answer is YES, please complete Addendum 4.	YES	NO

If you have answered YES to any of the above questions, please append a copy of your research proposal, as well as any interview schedules or questionnaires (Addendum 1) and please complete further addenda as appropriate.

I hereby undertake to carry out my research in such a way that

- there is no apparent legal objection to the nature or the method of research; and
- the research will not compromise staff or students or the other responsibilities of the University;
- the stated objective will be achieved, and the findings will have a high degree of validity;
- limitations and alternative interpretations will be considered;
- the findings could be subject to peer review and publicly available; and
- I will comply with the conventions of copyright and avoid any practice that would constitute plagiarism.

Signed by:	Full name and signature	Date
Principal Researcher/Student: signature removed	SULAYMAN SALIE	18/04/2016

This application is approved by:

Supervisor (if applicable):	Daniel O'Hagan	22/04/2016
HOD (or delegated nominee): Final authority for all assessments with NO to all questions and for all undergraduate research.	signature removed	25/4/16
Chair : Faculty EIR Committee For applicants other than undergraduate students who have answered YES to any of the above questions.		